Quantum many-particle electron transport in time-dependent systems with Bohmian trajectories

by
Alfonso Alarcón Pardo

B.S. in Physics, 2007
M.S. in Nanoelectronics 2009

Submitted to the
Departament d'Enginyeria Electrònica
in partial fulfillment of the requirements for the degree of
PhD in Electronic Engineering
at the
Universitat Autònoma de Barcelona

Thesis supervisor: Xavier Oriols Pladevall

Date of defense: April 2011

Summary

It is known that at nanoscale regime we must deal with the many-particle problem in order to study electronic devices. In this scenario, the time-dependent many-particle Schrödinger equation is only directly solvable for very few degrees of freedom. However, there are many electrons (degrees of freedom) in any electron device. In this sense, many-particle quantum electron formalisms (such as time-dependent Density Functional Theory, Green's functions techniques or Quantum Monte Carlo techniques) have been developed in the literature to provide reasonable approximations to model many-particle electron transport. An alternative proposal has been developed by Dr. Oriols to decompose the N-particle Schrödinger equation into a N-single particle Schrödinger equation using Bohmian trajectories. Based on this proposal a general, versatile and time-dependent $3D$ electron transport simulator for nanoelectronic devices, named *BITLLES (Bohmian Interacting Transport for non-equiLibrium eLEctronic Structures)* is presented.

The novelty of the *BITLLES* simulator is based on two points. First, it presents a many-particle quantum electron transport model taking into account explicitly the Coulomb and exchange correlations among electrons using Bohmian trajectories. Second, it provides a full information of the all current distribution moments (i.e. DC, AC fluctuations and even higher moments).

We summarize the important contributions of this thesis to the development of *BITLLES* simulator. Thus, we introduce explicitly the exchange correlations among electrons. In this context, we show how exchange interaction is the final responsible for determining the total current across the system. We also present a new approximation to study many-particle systems with spin of different orientations. Some practical examples are studied taking into account the exchange interaction. To the best of our knowledge, it is the first time that the exchange interaction is introduced explicitly (imposing the exchange symmetry properties directly into the many-particle wavefunction) in practical electron transport simulators.

We present the computation of the time-dependent total current in the high-frequency regime where one has to compute time-dependent variations of the electric field (i.e. the displacement current) to assure current conservation. We discuss the computation of the total (conduction plus displacement) current using Bohmian trajectories and the Ramo-Shockley-Pellegrini theorems. Different capabilities of *BITLLES* simulator such as AC and fluctuations are presented for *Resonant Tunneling Devices*.

We have used the *BITLLES* simulator to test a new type of nanoelectronic device designed to process signals at THz regime named *Driven Tunneling Device*. It is a three terminal device where the drain-source conductance is controlled by a gate terminal that can oscillate at THz frequencies. We also present practical examples on the functionality of this device such as rectifier and frequency multiplier.

Finally, we have developed a numerical approximation to solve the Schrödinger equation using tight-binding model to improve the band structure description of the *BITLLES* simulator.

Esta tesis esta dedicada a mis padres Mayte y Alfonso

Un camino de mil kilómetros se hace dando un paso detrás de otro.
(Proverbio Japonés)

Acknowledgements

Mi primer agradecimiento es para Xavier Oriols por haberme dado la oportunidad de comenzar en el mundo de la investigación. Agradecer su paciencia y el aprendizaje recibido durante estos años de relación académica.

También quiero dar las gracias a los compañeros (presentes y pasados) del *departamento de Ingeniería electrónica*: Guillem, Fabio, Abdelilah, Emmanuela, Gerard, Fito, Hender, Núria, Ferran, Javi, Fran, Marta, Miguel, Gabriel, Jordi Selga y Eloy. A mis amigos del *CIN2*: Joan, Irene, Carlos, Míriam y Lorena. También quiero agradecer a Laura, Jorge y Amanda por todos esos momentos inolvidable vividos durante los viajes y congresos. Gracias a todos por los ratos agradables que hemos pasado juntos.

Finalmente quiero dar las gracias a mi familia, a mis padres, a quienes debo mis primeras motivaciones en el campo de la ciéncia, por su infinita paciencia y por todos estos años de apoyo incondicional, sin ellos nada de esto hubiera sido posible. Por último un beso muy fuerte a mi hermana Mayte y a mis sobrinas Gemma y Estela.

Alfonso Alarcón Pardo

Marzo del 2011

Contents

List of Figures

Chapter 1

Introduction

Electronic devices have a great impact on our lives so much that it is imposible to imagine our present society without them. For example, they are the essential elements of computers that we use to work or of mobile phones that we use in our personal communication. In the last 50 years the electronics industry has been characterized by a progressive decrease in the dimensions of these electronic devices. This decrease in dimensions follows the so-called *Moore's law* which says that the number of transistors that can be implemented on a chip doubles roughly every two years. This simple rule has dominated the electronics industry since the second half of the twentieth century, the so-called microelectronics, Nowadays, the dimensions of the new commercial electron devices will attain few nanometers, so that we are now leaving the mentioned microelectronic era to enter into the new nanoelectronic era. However, at this atomic scales, electrons devices can no longer be described by classical mechanics and must be understood with quantum mechanics.

Theoretical approaches to treat electron transport constitute today a necessary tool to guide the continuous progress of the electronic industry. Electron transport theory and its application to electron device modeling has matured into a well-established field with active research, intensive software development, and vast commercial applications. The most successful technique to simulate electron devices has been the *Monte Carlo* technique based on *Boltzmann transport equation*. The Monte Carlo solution of the semiclassical Boltzmann transport equation has been extensively employed as a versatile, intuitive and realistic tool for nanoelectronics. However, it does not permit to study nanoelectronics devices with quantum effects (like tunneling or exchange interaction) and it must be replaced by others techniques based on the solution of the Schrödinger equation.

In the quantum regime we must treat with the many-particle problem to solve the time-dependent many-particle Schrödinger equation. However, it is well-known that the many-particle Schrödinger equation can be solved for very few degrees of freedom (two, three,...). Therefore, many-particle quantum electron techniques (such as time-dependent Density Functional Theory, Green's functions techniques or Quantum Monte Carlo techniques) have been developed to provide reasonable approximations to treat with this problem.

Alternatively, Dr. Oriols Group is developing a general, versatile and time-dependent $3D$ electron transport simulator for nanoelectronic devices, named *BITLLES (Bohmian Interacting Transport for non-equiLibrium eLEctronic Structures)* based on Bohmian mechanics.

Today, the Bohmian mechanics is starting to leave behind the original controversies that have accompanied it during the last decades. Now, it is well accepted that Bohmian mechanics can reproduce all experimental results as Copenhagen formulism. Even, when the Copenhagen mathematical machinery is used to compute observable results, the Bohmian interpretation can offer better interpretational tools. In many textbooks, we can find descriptions of electron dynamics as *"an electron crosses a resonant tunneling barrier and interacts with another electron inside the well"*. However, an electron crossing a tunneling region is not rigourously supported within orthodox quantum mechanics, but it is within the Bohmian picture. In some systems, the Bohmian equations might provide better computational tools than the ones obtained from the orthodox formalism, resulting in a reduction of the computational time and a better treatment of the number of degrees of freedom directly simulated.

In particular the *BITLLES* simulator is based on a novel algorithm for solving the many-particle Schrödinger equation with Bohmian mechanics. This algorithm is based on the work of reference [1] developed by Dr. Oriols, my thesis supervisor. It can include explicitly the Coulomb and exchange correlations (at a level comparable to the time-dependent Density Functional Theory) among electrons. The *BITLLES* simulator solves the many-particle correlations introduced by the Coulomb interaction among electrons by solving the time-dependent Poisson equation self-consistently with the time-dependent many-particle Schrödinger equation. This procedure provides a self-consistent solution of the Poisson and the many-particle Schrödinger equations beyond the mean field approximation [2–4].

The treatment of the Coulomb correlations has been investigated in detail by others members of the Dr. Oriols's group, [5]. However, the investigation of the exchange correlation is one of the milestone of this thesis. Electrons are fermions (spin 1/2) and, therefore, suffer from this exchange interaction. In a very simple picture, following Pauli exclusion principle, on can say that electrons with identical spin repel each other when they try to occupy the same regions of the phase-space. This interaction is not classical and we cannot find a term in the potential energies of the many-particle Schrödinger equation that accounts for it. This interaction is introduced in the *shape* of the wavefunction, through the requirement of providing anti-symmetrical wavefunctions. We say that a many-particle wavefunction is anti-symmetrical when the interchange of the degrees of freedom associated to two different electrons (positions and spin) provides a global change of the sign of the wavefunction.

An another relevant point of this thesis is the computation of electrical characteristics of nanoelectronics devices in a high-frequency regime such as AC and fluctuations. In these scenarios one has to compute time-dependent variations of the electric field (i.e. the displacement current) to assure that the total time-dependent current computed in a surface of the device active region is equal to that measured by an ammeter, i.e. *current conservation* [3, 4]. Therefore, the computation of the total (conduction plus displacement) current in *BITLLES* simulator is made by means of an algorithm based on the Ramo-Shockley-Pellegrini theorems [6–10] to compute the total current from the knowledge of the Bohmian particle dynamics in a $3D$ volume and the time-dependent variations of the electric field on the boundaries of that volume.

After this introduction we briefly explain the outline of this thesis. We divide its contents in the next chapters.

We begin the ***chapter 2*** with a brief explanation on the birth of the electronics and its

evolution towards nanoelectronics. Next, we introduce some revelent simulators of electronic devices and we explain the theoretical approaches that support them. We can divide these approaches into classical and quantum simulators. The first one are mainly solutions based on the Boltzmann transport equation using Monte Carlo technique. The second, are based on full quantum mechanics treatments, emphasizing the wave-like nature od electrons either for single-particle formalisms, as *Landauer-Büttiker formalism*, or many-particle formalisms such as *Density Functional Theory*, *Time-Dependent Density Functional Theory*, or *Quantum Monte Carlo* techniques.

In ***chapter 3***, we introduce the main concepts on Bohmian mechanics. First, we develop a historical overview about Bohmian mechanics. Next, we present the theoretical basis that describes Bohmian mechanics for both single and many-particle quantum systems, respectively. At the end of each of both sections we summarize the main ideas and equations in the form of few postulates. Finally, we explain the measurement process with Bohmian mechanics.

In ***chapter 4***, we explain the exchange interaction and its role in determining the total current across the system. In this sense, we present how exchange interaction determines the maximum number of electrons in the device active region. This limitation results from the huge energy that is needed to put two electrons very close. We also present an approximation to study many-particle system with spin of different orientations and an numerical example to test the mentioned approximation.

In the ***chapter 5***, we explain the main characteristics of our simulator named *BITLLES* (Bohmian Interacting Transport for non-equiLibrium eLEctronic Structures) developed by Dr. Oriols group. We present the algorithm to solve the many-particle time-dependent Schrödinger equation using Bohmian mechanics that explicitly includes the Coulomb and exchange correlation. We also explain how the Poisson equation and its boundary condition are implemented. Finally, we present the computation of the time-dependent current based on the quantum version of the Ramo-Shockley-Pellegrini theorems.

The ***chapter 6*** is devoted to present the numerical results. Here, we validate the functionality of *BITLLES* simulator with some examples. The first example is a *Resonant Tunneling Diode* (*RTD*) device. We comment the main functionalities of this device and next we present a serie of electrical applications (DC, AC and noise). The second, is a new type of device patented by our group, which we have called *Driven Tunneling Device* (*DTD*). This device is specially designed to model characteristic of high frequency such as AC or noise. A serie of electrical applications such as frequency rectifier and frequency multiplier for *DTD* devices are presented. Finally, we apply the concepts on exchange interaction introduced in *chapter 4* to study a nano-resistor using *BITLLES* simulator.

We end this work summarizing in ***chapter 7*** the main contributions of this thesis in the conclusions. And with an appendix where we present the application of tight-binding techniques for *BITLLES* simulator.

Chapter 2

An overview about simulation techniques

2.1 Introduction

In order to introduce the reader into the topic of this thesis, in Sec. 2.2, we explain briefly the birth of the electronics and its evolution towards nanoelectronics.

Next, in Sec. 2.3, we present a set of approaches to model electron devices. We can divide this approaches into classical and quantum. The first one are mainly solutions based on the Boltzmann transport equation using Monte Carlo technique often incorporating detailed descriptions of semiconductor properties such as band structures and scattering rates. The second, are based on full quantum mechanics treatments, emphasizing the wave-like nature either for single-particle scenarios, as *Landauer-Büttiker formalism*, or many-particle formalism such as *Density Functional Theory*, *time-dependent Density Functional Theory*, or quantum Monte Carlo techniques.

2.2 From electronics to nanoelectronics

Electronics as a scientific discipline was born around 1897, when Thomson showed that cathode rays were composed by a negatively charged particle, named the electron[1]. Later, in 1904, Fleming discovered that placing an electrode (a *metallic* material with lots of *unbounded* electrons inside) close to the filament of an incandescent bulb, was enough to established a net flow of electrons from the filament to the new electrode. This electronic device was called a diode. De Forest improved Fleming's original invention by creating the triode with an additional third terminal, the grid. The flux of electrons from the filament to the electrode was controlled by the voltage applied in the grid [11]. A particular voltage was used to defined an *On* state with a net current through the triode and another voltage for the *Off* state without current.

During half a century, spectacular electronic applications were developed with these vacuum valve tubes (diodes and triodes). However, the short life and high power consumption of

[1]In fact, the name electron was first used by the Greeks, *elecktron*, to refer to amber, which acquires the property of attracting other objects when it is rubbed. This process is called *frictional electrification* [12]

the vacuum tubes made the Bell laboratories to establish a research group focused on investigating the possibility of using semiconductor solid-state electron devices. In 1947, Bardeen, Brattain and Shockley created the first solid-state transistor at Bell laboratories. Although the functionality of the solid-state transistor was quite similar to that of the triode, the former was much smaller, faster, cheaper and more reliable. Thus, it became the fundamental element of the electronic technology in the second half of the 20th century. In the 60's, the previous solid-state transistor was improved by using a Metal-Oxide-Semiconductor (MOS) solid-state capacitor. A third terminal, the (metal) gate, separated from the (semiconductor) channel by an (oxide) dielectric, controlled the *On* and *Off* states of the transistor by means of a simple electrostatic force between gate and channel electrons. Because the importance of the electric field in defining the behavior of such MOS transistor, it was also called Field-Effect-Transistor (FET)[2].

In the near future, the development of electronics is expected to follow the Moore's law[3]. The International Technology Roadmap for Semiconductors (ITRS) [13], points to the improvement of the FET transistor as the best strategy to be followed. Nonetheless, the scientific community is looking for completely different alternatives to the FET transistors because of the mid-term scaling required by Moore's law (4 nm channel length transistors predicted for 2022 [13]) will be technologically and economically unattainable with the present FET technology. It is, however, still not clear which proposals will replace the present FET transistors in the mid-term future. Some works suggest that a *revolution* (similar to the substitution of vacuum tubes by solid state transistor) is awaiting for the electronic industry. Others affirm that such *revolution* will not take place, but we will see just an *evolution* of present FET transistors into smaller structures.

In any case, what is unquestionable is that the dimensions of the new commercial electron devices will attain few nanometers, so that we are now leaving the microelectronic era to enter into the new nanoelectronic era. Electrons devices can no longer be described by classical laws and must be understood with quantum laws. Therefore, theoretical approaches to treat quantum electron transport constitute today a necessary tool to guide the continuous breakthroughs of the electronic industry. We dedicated the next section to describe several simulation techniques developed for electron devices.

2.3 An overview about electron transport formalisms for nanoelectronics devices simulators

In the next subsections we summarize briefly the main theoretical tools developed to model electron transport and we present a set of highlight simulators related with these formalisms.

[2]It was also named MOSFET by combining both previous acronyms.

[3]In 1958, with the invention of the integrated circuit, i.e. the chip, a race for chip miniaturization started that lead to an empirical law known as Moore's Law: *"The number of transistors that can be implemented in a chip doubles approximately every 2 years"*. The increase in the number of transistors in a chip, offers more functions per chip with much lower cost per function, which gives as a result smaller electron devices, higher performance and greater energy efficiency.

2.3.1 Boltzmann transport equation

In this formulism we consider that particles behave classically and that we can know the position and the momentum of each particle as a function of time. The probability of finding a carrier distribution with momentums centered at $(\vec{p}_1, \ldots, \vec{p}_N, t)$ and with positions located at $(\vec{r}_1, \ldots, \vec{r}_N)$, and time t is the many-particle distribution function:

$$f(\vec{r}_1, \ldots, \vec{r}_N, \vec{p}_1, \ldots, \vec{p}_N, t)d\Omega, \tag{2.1}$$

where $d\Omega$ is an infinitesimal element of the phase-space spanned by the coordinates and momentum of all carrier.

However, the many-particle distribution function $f(\vec{r}_1, \ldots, \vec{r}_N, \vec{p}_1, \ldots, \vec{p}_N, t)$ is too difficult to be determined since it contains all possible correlations among particles (each particle motion depends on the other particles). A simplified distribution function is the one-particle distribution function:

$$f(\vec{r}, \vec{p}, t) \propto \int \Pi_{i=2}^{N} d\vec{r}_i d\vec{p}_i f(\vec{r}, \vec{p}; \vec{r}_2, \ldots, \vec{r}_N, \vec{p}_2, \ldots, \vec{p}_N, t), \tag{2.2}$$

where $f(\vec{r}, \vec{p}, t)d\vec{r}d\vec{p}$ is the average number of particles that at time t is found in a phase volume $d\vec{r}d\vec{p}$, around the phase-space point $(\vec{r}, \vec{p})$ [5, 14].

The Boltzmann transport equation is precisely a semiclassical equation of motion for a single-particle distribution function, also know as the Boltzmann distribution function:

$$\frac{\partial f(\vec{r}, \vec{p}, t)}{\partial t} + \frac{\vec{p}}{m}\vec{\nabla}_r f(\vec{r}, \vec{p}, t) + F\vec{\nabla}_p f(\vec{r}, \vec{p}, t) = \left(\frac{\partial f(\vec{r}, \vec{p}, t)}{\partial t}\right)_{coll}, \tag{2.3}$$

where $\vec{F}$ is an external force, m is the electron mass and $\left(\frac{\partial f(\vec{r},\vec{p},t)}{\partial t}\right)_{coll}$ is the so-called collision integral that includes, in principle, all scattering processes such as electron-electron scattering, generation and recombination precesses, the interaction with phonon and impurity [5, 15], etc.

2.3.1.1 Monte Carlo solution of the Boltzmann transport equation

The Monte Carlo[4] technique, applied to the solution of the Boltzmann equation, has been the most successful tool chosen for the international scientific community to simulate electron devices because it provides a strictly accurate solution of the Boltzmann equation through an intuitive picture of the dynamics of electrons by using trajectories. The Monte Carlo technique allows us to obtain the I-V characteristics of electron devices and other relevant information such as the local velocity distribution or the local electric field. It is a very versatile technique used as a *simulated experiment* to save costs and efforts in the development prototypes.

Although the Boltzmann transport equation (and the Monte Carlo method) accounts for far from equilibrium conditions, its fundamental limitation it is not able to directly include quantum effects.

[4]This technique is based on using *random* numbers hence the name of *Monte Carlo*.

2.3.1.2 MONACO simulator

The Monte Carlo code named *MONACO* is based on solve the semiclassical Boltzmann transport equation self-consistently with $1D$, $2D$ or $3D$ Poisson's equation.

This software has been developed in the *CMO* (Composants pour la Microelectronique et l'Optoelectronique) department at the Institut d'Electronique Fondamentale (IEF), Paris-Sud University [16].

This simulator has been used to study electron transport in advanced semiconductor devices but also for spin polarized transport in III-V heterostructures, and has been extended to carbon nanotubes transistors. Among the characteristics included in the code, one can mentioned the full-band description by coupling with k.p calculation, the multisubband transport in FET by self-consistent coupling with the Schrödinger equation, and the Monte Carlo solution of the Wigner quantum transport equation for RTDs, MOSFETs and CNTFETs.

2.3.1.3 DAMOCLES simulator

DAMOCLES are the acronym for *Device Analysis using MOnte CarLo Et PoiSson solver* [17]. The code of *DAMOCLES* was developed in 1987 by M.V. Fischetti and S.E. Laux to provide predictions for prototypes of the IBM company. This program combines a self-consistent solution, via a Monte Carlo technique, to the Boltzmann transport equation and the Poisson equation. Conditionally, the Schrödinger equation can also be coupled into the self-consistent solution, which allows *DAMOCLES* to model quantization in inversion layers and quantum wells. *DAMOCLES* uses the full band structure of the semiconductor with consistently calculated scattering rates in pursuit of physical accuracy and rigor.

2.3.2 Landauer-Büttiker formulism

2.3.2.1 Landauer formulism

The Landauer approach probably constitutes the simplest quantum description of electron transport. The description of the transport with this formalism is strictly based on the quantum nature of the electrons and it supposes that the current through a conductor is only expressed in terms of the quantum transmission probability of carriers injected from the external contacts.

In Landauer approach, in order to model the I-V characteristics, we consider a one-dimensional structure under an applied source-drain bias, V_{sd}, for various gate bias (that determines the barrier height) conditions. For a finite temperature the Landauer formula [18] is:

$$I_{V_{sd}} = \frac{2q}{h} \int_0^\infty dE \sum_{n,m=1}^{\infty} T_{n,m}(E) \left[f(E) - f(E + qV_{sd}) \right], \tag{2.4}$$

where q is the electron charge, h is the Planck's constant, $f(E)$ and $f(E + qV_{sd})$ are the Fermi-Dirac distributions of source and drain reservoir respectively, and $T_{n,m}(E)$ is the transmission coefficient that depends on the detailed shape that define the potential. Also, $T_{n,m}(E)$ depends on the electron conduction channels that can be defined through the use of

the indexes, n and m, that accounts for the electron energy confinement in the two lateral dimensions.

Probably, most relevant and successful result of the Landauer theory is the conductance formula [19, 20] which constitutes one of the most important achievements in quantum electron transport theory. In particular, the two-terminal version is:

$$G^{2t} = I/V^{2t} = 2q^2/hT. \tag{2.5}$$

Equation (2.5) relates the macroscopic conductance G with the microscopic total transmission coefficient T (T is the sum of the $T_{n,m}$ terms corresponding to different energies levels of the system) of the electron device, and provides a conceptual framework of thinking about conductance.

The original formulation of the Landauer approach is a single-particle model and it neglects electron-electron interaction, i.e. it assumes that the systems behaves as a Fermi liquid [21]. The popularity and the main virtues of the Landauer approach are due to its simplicity, the relatively low computational requirements and its rather intuitive picture of quantum electron transport. However, since continuous particles (scattering states) are assumed throughout the system, transient simulations are difficult or impossible to implement using the Landauer approach, i.e. it is a *steady-state formalism*.

2.3.2.2 Büttiker formulism

For predicting AC (also DC and fluctuation) properties of mesoscopic systems, important contributions were made by Büttiker and co-workers within the scattering matrix formalism. The main contribution of Büttiker was the development of the Landauer ideas within a second quantization formulation that allows the creation or annihilation of electrons. This extension does also take into account, somehow, the exchange interaction between electrons. They do also applied different many-body approximations (a simple one potential per conductor [22], a ThomasFermi screening potential [23], a Hartree-like approximation [24], a treatment of the electronelectron interactions on the level of a HartreeFock approach [25] and also a generalization of the scattering matrix to deal with Coulomb blockade [26]) to provide self-consistent theories for the AC conductance of mesoscopic systems with overall charge neutrality and total current conservation in the whole system plus reservoirs region.

2.3.3 Wigner function model

The quantum analogous of the classical many-particle distribution function of Eq. (2.1), is the *generalized Wigner pseudo-distribution*, also called Wigner function. It was introduced by Eugene Wigner in 1932 to study quantum corrections to classical statistical mechanics [27]. The goal was to link the wave function that appears in the Schödinger equation to a probability distribution in phase space.

It was firstly introduced by Wigner as:

$$f_w\left(\vec{r}_1,...,\vec{r}_N,\vec{k}_1,...,\vec{k}_N,t\right) \propto \sum_j \int_{-\infty}^{+\infty} \Psi_j\left(\vec{r}_1+\vec{y}_1,...,\vec{r}_N+\vec{y}_N,t\right)\cdot$$
$$\cdot\,\Psi_j^*\left(\vec{r}_1-\vec{y}_1,...,\vec{r}_N-\vec{y}_N,t\right)\cdot\prod_{k=2}^{N} d\vec{y}_k e^{2i\vec{k}_i\vec{y}_i}. \quad (2.6)$$

Analogously to the deduction of the one-particle distribution function $f\left(\vec{r},\vec{p},t\right)$ from the classical *many-particle distribution function* $f\left(\vec{r}_1,...,\vec{r}_N(t),\vec{p}_1,...,\vec{p}_N(t),t\right)$, we can obtain a *reduced density matrix* as follows:

$$\rho\left(\vec{r},\vec{r}',t\right) \propto \sum_j \int \Psi_j\left(\vec{r},\vec{r}_2,...,\vec{r}_N,t\right)\Psi_j^*\left(\vec{r}',\vec{r}_2,...,\vec{r}_N,t\right)\prod_{i=2}^{N} d\vec{r}_i. \quad (2.7)$$

The *Wigner function*, can be then calculated from the *reduced density matrix* as:

$$f_w\left(\vec{r},\vec{k},t\right) \propto \int_{-\infty}^{+\infty} \rho\left(\vec{r}+\vec{y},\vec{r}-\vec{y},t\right) d\vec{y} e^{2i\vec{k}\vec{y}}. \quad (2.8)$$

The kinetic equation for the Wigner function, reads very similar to the Boltzmann [28]:

$$\frac{\partial f_w\left(\vec{r},\vec{k},t\right)}{\partial t} + \frac{\hbar\vec{k}}{m}\vec{\nabla}_r f_w\left(\vec{r},\vec{k},t\right) + \frac{1}{2\pi\hbar}\int d\vec{k} V_w\left(\vec{r},\vec{k}-\vec{k}'\right) f_w\left(\vec{r},\vec{k}',t\right) =$$
$$= \left(\frac{\partial f_w\left(\vec{r},\vec{k},t\right)}{\partial t}\right)_{coll}, \quad (2.9)$$

where the Wigner potential V_w is defined as:

$$V_w\left(\vec{r},\vec{k}\right) = \frac{1}{i\hbar\left(2\pi\right)^3}\int \left(V\left(\vec{r}-\vec{y}\right)-V\left(\vec{r}+\vec{y}\right)\right)\exp\left(-i\vec{k}\vec{y}\right) d\vec{y}. \quad (2.10)$$

The Wigner formalism has several virtues. It constitutes a time-dependent approach to electrical transport accounting for far from equilibrium conditions in a rather natural way. In the same way as the collision integral in the Boltzmann transport equation, the Wigner's one can account, in principle, for all the many-body interactions. Unfortunately, obtaining analytical expressions for the collision integral is a very complicate job, and in practice, interactions are included just at a two-particle level. In this sense, the Wigner function constitutes in practice a *mean-field* approach to quantum electron transport without explicitly considering exchange interaction. In addition, Wigner function model have some difficulties to deal with time-dependent correlations, limiting thus their capabilities to predict AC or noise properties of electron devices.

2.3.4 Non-equilibrium Green's functions (NEGF)

Non-equilibrium Green's functions (NEGF), also referred as *Keldysh formalism* [29, 30], constitutes perse a many-body technique which allows us, at least in principle, to solve exactly the time-dependent Schrödinger equation for an interacting many-body system. The NEGF, are used into non-lineal systems under non-equilibrium conditions. This is done by solving equations of motion for specific time-dependent single-particle Green's functions [15]. However, NEGF are deduced from perturbation theory[5], so they can be strictly applied only to those systems where many-body perturbation theory holds[6] [14].

A rigorous introduction of the basis of *NEGF* requires a basic knowledge on the second quantization formalism [14, 31], so it becomes difficult to introduce them in a self-contained way without introducing some concepts that would extend unnecessarily this rather informal summary.

Despite the powerful and rigorous character of non-equilibrium Green's functions, they are in general accompanied by a rather nonintuitive and hard mathematical formulation. Even more, although electron-electron interactions beyond the mean-field approximation can be introduced throughout the self-energies, using them, except for simple model systems, it is a huge computationally demanding task, and most of the time outright impossible.

2.3.4.1 NEMO simulator

The *NEMO* (NanoElectronic MOdeling tool) software, was designed initially by S. Datta, R. Lake and G. Klimeck to study *High speed electronics* for *RTD's* devices at the Texas Instruments company, and subsequently evolved into a general-purpose nanoelectronic simulator used by Intel, Motorola, HP, Texas Instruments and many universities. The *NEMO* software is divided into two alternatives simulators: *NEMO-1D* and *NEMO-3D*.

The primary objective of *NEMO-1D* [32] tool was the quantitative modeling of high performance *RTD's*. This simulation tool is based on the *NEGF* that includes proper treatment of materials band structure.

On the other hand, *NEMO-3D* [33] calculates eigenstates in arbitrarily shaped semiconductor structures in the typical column IV and III-V materials. Atoms are represented by the empirical tight-binding model using s, sp3s* or sp3d5s* models with or without spin.

NEMO-3D is capable to compute the electronic structure within an empirical tight-binding model for quantum dots (3-D confinement), nanowires (2-D confinement), quantum wells (1-D) confinement, and bulk (no confinement) under limited crystal distortions.

2.3.5 Density functional theory (DFT)

The Density Functional Theory technique (DFT) was proposed by Dr. W. Kohn in 1964 [34] (which received the Nobel Prize in Chemistry in 1998 "for his development of the density-functional theory") to calculate equilibrium ground states (i.e. minimum energy).

[5]NEGF formalism follows steps similar to those of the kubo approach to determine the response of a closed system to an external time-dependent perturbation. However, the major difference with the Kubo approach is that it do not limits to weak perturbations.

[6]Examples of problems beyond standard many-body perturbation techniques are the Kondo effect [35] or the Luttinger liquid [36].

Starting from a N-electron Hamiltonian:

$$\hat{H}\left(\vec{r}_1, ..., \vec{r}_N, \vec{p}_1, ..., \vec{p}_N\right) = \hat{T} + \hat{W} + \hat{V}, \tag{2.11}$$

where $\hat{T}$ is the kinetic energy operator and $\hat{W}$ is the electron-electron interaction operator and $\hat{V}$ is the potential energy operator. Defining the density operator n as the reduced density operator of Eq. (2.7) evaluated at $\vec{r}' = \vec{r}$:

$$n\left(\vec{r}\right) = N \int \left|\Psi\left(\vec{r}, \vec{r}_2, ..., \vec{r}_N, t\right)\right|^2 \prod_{i=2}^{N} d\vec{r}_i, \tag{2.12}$$

and satisfying,

$$\int n\left(\vec{r}\right) d\vec{r} = N, \tag{2.13}$$

then, the operator $\hat{V}$, describing a local static potential (like the electron-ion potential), can be written as:

$$\hat{V} = \int d\vec{r} V\left(\vec{r}\right) n\left(\vec{r}\right). \tag{2.14}$$

The Hohemberg-Kohn theorem states that two external potentials, which differ by more than a constant, cannot give the same ground-state density. This establishes a one-to-one correspondence between the external potential and the ground-state density [37].

Inspired on the above theorem, Kohn and Sham deduced in 1965 their famous equations [38]:

$$\left[-\frac{\hbar^2}{2m}\vec{\nabla}^2 + V_H\left(\vec{r}\right) + V_{xc}\left(\vec{r}\right) + V\left(\vec{r}\right)\right] \phi_k^{KS}\left(\vec{r}\right) = \varepsilon_k \phi_k^{KS}\left(\vec{r}\right), \tag{2.15}$$

corresponding to the solution of the time-independent Schrödinger equation of auxiliary non-interacting electrons in the presence of the potential $V_{KS}\left(\vec{r}\right) = V_H\left(\vec{r}\right) + V_{xc}\left(\vec{r}\right) + V\left(\vec{r}\right)$, where:

$$V_H\left(\vec{r}\right) = e^2 \int d\vec{r}' \frac{n\left(\vec{r}'\right)}{\left|\vec{r} - \vec{r}'\right|}, \tag{2.16}$$

is the Hartree potential, and $V_{xc}\left(\vec{r}\right)$ is the *unknown exchange-correlation* potential including all the many-body correlation effects. We emphasize that exchange interaction is not directly considered.

Solving the above equations yields the wavefunctions $\phi_k^{KS}\left(\vec{r}\right)$, from which the ground-state density is:

$$n\left(\vec{r}\right) = \sum_{k=1}^{N} \left|\phi_k^{KS}\left(\vec{r}\right)\right|. \tag{2.17}$$

All properties of the ground-state system can be then extracted from Eq. (2.17). Unfortunately, since the exchange-correlation potential is unknown, some kind of educated guess must be formulated.

Despite its undeniable success for qualitative DC predictions obtaining information about the device frequency behavior is not possible. In summary, the main limitation of the ground-state Density Functional Theory in order to describe electron transport, is precisely its ground-state nature. In other words, such a theory assumes that the system under study occupies a *time-independent equilibrium state*.

2.3.5.1 SIESTA simulator

SIESTA (Spanish Initiative for Electronic Simulations with Thousands of Atoms) was born in 1996 to implement, in self consistent *DFT*, the order-N techniques developed for tight-binding in the early 1990s. *SIESTA* is both a method and its computer program implementation, to perform electronic structure calculations and ab initio molecular dynamics simulations of molecules and solids [39].

2.3.5.2 TRANSIESTA simulator

TRANSIESTA project [41] (which has generated the Danish spin-off company Atomistix) was originally developed by Mads Brandbyge, José Luis Mozos, Pablo Ordejón, Jeremy Taylor and Kurt Stokbro. *TRANSIESTA* is a procedure to solve the electronic structure of an open system formed by a finite structure sandwiched between two semi-infinite metallic leads. A finite bias can be applied between both leads, to drive a finite current. Using *TRANSIESTA* one can compute electronic transport properties, such as the zero bias conductance and the I-V characteristic, of a nanoscale system in contact with two electrodes at different electrochemical potentials. The method is based on using *NEGF*, that are constructed using the Density Functional Theory Hamiltonian obtained from a given electron density. A new density is computed using the *NEGF* formalism, which closes the *DFT-NEGF* self consistent cycle.

2.3.5.3 Gaussian simulator

The *Gaussian* [42] is a computational chemistry software program initially released in 1970 by John Pople and his research group at Carnegie-Mellon University as *Gaussian 70*. It has been continuously updated since then. The name originates from Pople's use of Gaussian orbitals to speed up calculations compared to those using Slater-type orbitals, a choice made to improve performance on the limited computing capacities of then-current computer hardware for Hartree-Fock calculations. The current version of the program is *Gaussian 09*. The *Gaussian* simulator has a rigorous treatment of quantum correlations and it is designed solely for physical-chemical studies, but they are far from the possible application to estimate the time-dependent current in electronic devices.

2.3.6 Time-Dependent Density Functional Theory (TDDFT)

In 1984, Runge and Gross generalized *DFT* to its time-dependent version [43]. Time-Dependent Density Functional Theory (TDDFT) includes time in the results of Sec. 2.3.5 in a very natural way, and more importantly, it is capable of describing *non-equilibrium* scenarios. Including a time-dependence into the Kohn-Sham potential, i.e. $V_{KS}(\vec{r},t) = V_H(\vec{r},t) + V_{xc}(\vec{r},t) + V(\vec{r},t)$, the time-dependent version of the Kohn-Sham equations becomes:

$$\left[i\hbar\frac{\partial}{\partial t} + \frac{\hbar^2}{2m}\vec{\nabla}^2 - V_H(\vec{r},t) - V_{xc}(\vec{r},t) - V(\vec{r},t)\right]\phi_k^{KS}(\vec{r},t) = 0. \tag{2.18}$$

And the charge density is then:

$$n\left(\vec{r},t\right)=\sum_{k=1}^{N}\left|\phi_{k}^{KS}\left(\vec{r},t\right)\right|. \tag{2.19}$$

TDDFT is in principle capable of accounting for both, far from equilibrium conditions and many-body phenomena. There exist, too, a series of theorems based on some reformulations of the *TDDFT*[7] guaranteeing that, if we know the exact dynamical functional $V_{xc}\left(\vec{r},t\right)$, all many-body dynamical effects can be evaluated using effective single-particle equations. We emphasize that the exchange interaction is not directly considered [14]. *TDDFT* [43] is an excited state theory, enabling the rigorous analysis of out of equilibrium systems.

2.3.6.1 Octopus simulator

The Octopus simulator [44], developed by the group of A. Rubio belonging to the *Nano-Bio Spectroscopy Group* of San Sebastián, is designed for a future implementation of methods to estimate the current in electronic systems, although their main activity is the study of temporal dynamics of more basic physical-chemical phenomena.

Octopus is a pseudo-potential real-space package aimed at the simulation of the electron-ion dynamics of $1D$, $2D$, and $3D$ finite systems subject to time-dependent electromagnetic fields. The program is based on *TDDFT* in the Kohn-Sham scheme. All quantities are expanded in a regular mesh in real space, and the simulations are performed in real time. The program has been successfully used to calculate linear and non-linear absorption spectra, harmonic spectra, laser induced fragmentation, etc. of a variety of systems. In *Octopus*, nuclei are described classically as point particles. Electron-nucleus interaction is described within the pseudo-potential approximation.

2.3.7 Monte-Carlo solution of many-particle Schrödinger equation

In Sec. 2.3.1.1 we applied Monte Carlo techniques to classical many-particle systems, here, we use this random techniques for studying quantum systems. Quantum Monte Carlo (QMC) techniques is a large class of computer algorithms to simulate quantum systems with the idea of solving the non-relativistic many-particle Schrödinger equation directly. It is an explicitly many-body method which takes into account electron correlation.

Among the quantum Monte Carlo methods that we can find in the literature [45–47] we emphasize the following:

Variational Monte Carlo: in this method we use Monte Carlo techniques to calculate for the quantum mechanical expectation value of the ground state energy. Also, it is used in order to optimize this expectation value by adjusting a trial wave function in a variational type of approach.

Diffusion Monte Carlo: this method employ the similarity between the Schrödinger equation and the diffusion equation in order to calculate the properties of a collection of interacting mechanical particles by simulating a diffusion process of the particles involved.

[7] There exist two modifications of the *TDDFT* called Time-Dependent Current Density Functional Theory, TDCDFT [48], and stochastic time-dependent current Density Functional Theory, STDCDFT [49].

Path integral Monte Carlo Method: this method describes a path-integral formalism of quantum mechanics which is a formulation elaborated by Feynman, based on ideas put forward by Dirac in which a quantum mechanical problem is mapped onto a classical mechanical system.

There are others quantum Monte Carlo methods, each of which uses the intrinsic randomness of the Monte Carlo concepts in different ways to solve the many-body problem. We can find an extensive description of these method in the references [45, 46].

2.3.7.1 CASINO simulator

CASINO is a code for performing quantum Monte Carlo (QMC) electronic structure calculations for finite and periodic systems. This code was written in the early 1990s in Cambridge by Richard Needs and Guna Rajagopal, assisted by many helpful discussions with Matthew Foulkes. This was later extended by Andrew Williamson up to 1995 and then by Paul Kent and Mike Towler up to 1998. *CASINO* is based on variational Monte Carlo and diffusion Monte Carlo techniques. It is applicable to finite systems such as atoms and molecules and also to systems with periodic boundary conditions in 1, 2 or 3 dimensions (polymers, slabs/surfaces, crystalline solids) with any crystal structure.

Chapter 3

Bohmian mechanics

3.1 Introduction

This chapter provides a description of Bohmian mechanics. It is divided into three sections. The first section is a historical overview about Bohmian mechanics. We develop the history of quantum mechanics in order to explain the election of the Copenhagen interpretation of quantum mechanics becomes the successful explanation of quantum phenomena in front of others theories as Bohmian mechanics. In the next sections, Sec. 3.3 and Sec. 3.4, we present the theoretical basis that describes Bohmian mechanics for both single and many-particle quantum systems, respectively. At the end of each of both sections we summarize the main ideas and equations in the form of few postulates. Finally, we explain the process of measurement of the current in a nanoelectronic system. The measure is one of the points of the quantum theory where the Bohmian mechanics has more advantages. The contents of this chapter follows [4].

3.2 Historical development of Bohmian mechanics

In general, the history of quantum mechanics is explained in textbooks as a history where each step follows naturally from the one preceding it. However, it was exactly the opposite. The beginning of the twentieth century were a time where new routes to understand the quantum phenomena were proposed. Most of the new routes, were nowhere and others were simply abandoned. Some of the routes were successful in providing new mathematical formalism capable of predicting quantum phenomena. In this section we explain the history of one of this routes: Bohmian mechanics.

In 1900, Max Planck suggested [50] that black bodies emit electromagnetic radiation in discrete energies $h\nu$, where ν is the frequency of the emitted radiation and h is the (now called) Plank constant. Five years later, Albert Einstein used this discovery in his explanation of the photoelectric effect [51], suggesting that the energy transfer between light and matter was done in terms of *light quanta* or *photons*[1] of energy $h\nu$. Even though this theory solved the black body radiation problem, the fact that the absorption and the emission

[1]In fact, the word *photon* was not coined until 1926, by Gilbert Lewis [52].The word *quantum* referred as the minimum unit of any physical entity (for example, the energy) involved in an interaction.

of light by atoms is discontinuous was still in conflict with the classical description of the light-matter interaction. In 1913, Niels Bohr [53–55] wrote a revolutionary paper on the hydrogen atom where he solved the (erroneously predicted) instability by postulating that electrons can only orbit around atoms in some particular *non-radiating* orbits. Thus, atom radiation occurs when electrons *jump* from one orbit to another of lower energy. His *imaginative* postulates were in full agreement with the experiments on spectral lines. Werner Heisenberg wrote his first paper on quantum mechanics in 1925 [57] and two years later stated his uncertainty principle [59]. It was him, with the help of Max Born and Pascual Jordan, who developed the first version of quantum mechanics based on a matrix formulation [57, 58, 60, 61]. On the other hand, in 1923, Louis de Broglie proposed in his PhD dissertation, that all particles (as electrons) exhibit wave-like phenomena such as diffraction or interference [56].

In 1926, Erwin Schrödinger published *An undulatory theory of the mechanics of atoms and molecules* [63] where, inspired by de Broglie's work [56, 62, 64], he described particles (such as electrons or protons) with a wave, solution of a (wave) equation, the Schrödinger equation. In this equation, we find a potential energy, $V(\vec{r},t)$, that represents the potential *felt* by the electron, and also we find the wave(field) $\psi(\vec{r},t)$ that was called the wavefunction. Schrödinger, at first, interpreted his wavefunction as a description of electron charge density $q\left|\psi(\vec{r},t)\right|^2$ with q the electron charge. Later, Max Born refined the interpretation of Schrödinger and defined $\left|\psi(\vec{r},t)\right|^2$ as the probability density of finding the electron in a particular position $\vec{r}$ at time t [65]. Schrödinger's wave version of quantum mechanics and Heisenberg's matrix mechanics were apparently incompatible, but they were eventually shown to be equivalent [65, 66] by Wolfgang Ernst Pauli and Carl Eckart, independently.

Physicist stored to develop successful theories for understanding quantum phenomena. To explain the physics behind quantum systems, the concepts of wave and particle should be merged in some way. Two different routes appeared:

1. **Wave or particle?**: The concept of trajectory was, consciously or unconsciously, abandoned by most the young scientists (Heisenberg, Pauli, Dirac, Jordan, ...). The main idea behind this route is that depending of the experimental situation one has to choose between a wave or a particle behavior. Electrons are associated basically to probability (amplitude) waves. The particle nature of the electron appears when we measure the position of the electron. In Bohr's words, an object cannot be both a wave and a particle at the same time; it must be either one or the other, depending upon the situation. This approach is the Copenhagen, or *orthodox* interpretation of quantum mechanics.

2. **Wave and particle**: Louis de Broglie, on the other hand, presented an explanation of quantum phenomena were the wave and particle concepts merge at the atomic scale by assuming that a pilot-wave solution of Schrödinger equation guides the electron trajectory, as the electron is guided by the electromagnetic field. This is what we call Bohmian mechanics. An object cannot be a wave and a particle at the same time, but two can.

Perhaps the most relevant event for the historical development of the quantum theory was the fifth Solvay Conference, that took place from 24 to 29 October 1927 in Brussels [67]. There, de Broglie, presented his recently developed pilot-wave theory and how it could

account for quantum interference phenomena in electrons [67]. He did not receive an enthusiastic reaction from the illustrious audience gathered for the occasion. In the following months, it seems that he had some difficulties on interpreting quantum measurement within his theory, and decided to avoid it.

Let us mention that the elements of the pilot-wave theory (electrons guided by waves) were already in place in de Broglie's thesis in 1924 [56], before either matrix or wave mechanics existed. In fact, Schrödinger used the de Broglie phases to develop its famous equation. In addition, it is important to remark that de Broglie himself developed a single-particle and a many-particle description of his pilot-waves visualizing also the *non-locality* of the latter [67]. Perhaps, his remarkable contribution and influence on Bohmian mechanics has not been fairly recognized by scientists and historians because he abandoned his own ideas rapidly without defending them [67, 68].

David Bohm's formulation of quantum mechanics appeared in 1952 after the *orthodox* formalism was fully established. He was, perhaps, the first person to genuinely understand the significance and fundamental implications of the description of quantum phenomena by trajectories guided by waves.

The original papers by Bohm [69, 71] provide a formal justification of the guidance equation developed 25 years before by de Broglie. David Bohm completed the work of Louis de Broglie in two fundamental aspects. First, as explained before, he demonstrated that Bohmian mechanics leads to exactly the same predictions as the ones obtained by *orthodox* quantum mechanics. Second, he provided a theory of measurement. He developed an explanation of the measurement problem without invoking the *wavefunction collapse*.

Nowadays, the theory developed by de Broglie and Bohm that we called Bohmian mechanics is quite marginal among scientific community. After the Solvay conference, Bohr, Heisenberg and their colleagues spread the *orthodox* interpretation around the world and convinced the vast majority of the physics community that both quantum mechanics and their interpretation worked with extraordinary precision. A lot of young physicists were attracted to European institutes to study with the *fathers* of this new theory, and during the second quarter of the twentieth century, that as good disciples, they spread the Copenhagen interpretation over the entire globe. Among others, the goal of this thesis is to show that Bohmian mechanics is in fact, a very useful theory for computing quantum phenomena.

3.3 Bohmian Mechanics for a single-particle

In this section we show how to describe a quantum system associated to only one particle (or one degree of freedom) in terms of trajectories. We will derive such trajectories from two different procedures. First, as a direct consequence of the local conservation of particles extracted from the Schrödinger equation and, second, directly following the work presented by Bohm in his original paper [69].

3.3.1 Single-particle continuity equation

The single-particle Schrödinger equation in a $1D$ system subjected to a scalar time-dependent potential energy, $V(x,t)$, is:

$$i\hbar\frac{\partial\psi(x,t)}{\partial t} = -\frac{\hbar^2}{2m}\frac{\partial^2\psi(x,t)}{\partial x^2} + V(x,t)\psi(x,t). \tag{3.1}$$

It is important to emphasize that in the *orthodox* interpretation of $\psi(x,t)$, equation Eq. (3.1) does not describe a single-experiment, but an ensemble of identical (single-particle) experiments. The *orthodox* meaning of the square modulus of the wavefunction $|\psi(x,t)|^2$ is the probability density of finding a particle at the position x at time t when a measurement is done.

It is interesting to look for a *local* continuity equation inside Eq. (3.1). In order to find it, let us work with $\psi(x,t)$ and its complex conjugate $\psi^*(x,t)$. In particular, we can rewrite Eq. (3.1) as:

$$\psi^*(x,t)i\hbar\frac{\partial\psi(x,t)}{\partial t} = -\psi^*(x,t)\frac{\hbar^2}{2m}\frac{\partial^2\psi(x,t)}{\partial x^2} + \psi^*(x,t)V(x,t)\psi(x,t), \tag{3.2}$$

$$-\psi(x,t)i\hbar\frac{\partial\psi^*(x,t)}{\partial t} = -\psi(x,t)\frac{\hbar^2}{2m}\frac{\partial^2\psi^*(x,t)}{\partial x^2} + \psi(x,t)V(x,t)\psi^*(x,t). \tag{3.3}$$

From the rest of Eq. (3.2) and Eq. (3.3), we see:

$$\frac{\partial|\psi(x,t)|^2}{\partial t} = i\frac{\hbar}{2m}\frac{\partial}{\partial x}\left(\psi^*(x,t)\frac{\partial\psi(x,t)}{\partial x} - \psi(x,t)\frac{\partial\psi^*(x,t)}{\partial x}\right). \tag{3.4}$$

We can easily identify Eq. (3.4) as the local conservation of particles when $\rho(x,t) = |\psi(x,t)|^2$ and we define the current density, $J(x,t)$, as:

$$J(x,t) = i\frac{\hbar}{2m}\left(\psi(x,t)\frac{\partial\psi^*(x,t)}{\partial x} - \psi^*(x,t)\frac{\partial\psi(x,t)}{\partial x}\right). \tag{3.5}$$

Unlike most wave equations, the Schrödinger equation is compatible with a local conservation of particles due to the fact that $V(x,t)$ is a real function. We have noticed above that we can interpret $\rho(x,t) = |\psi(x,t)|^2$ as a spatial distribution of an ensemble of trajectories. Such ensemble of particles can be obtained by repeating a single-particle experiment and measuring, at each time t, the number of particles at each position x. The presence of the local conservation of particles is very relevant because, then, we can justify our starting point for looking for an ensemble of continuous trajectories describing $\rho(x,t) = |\psi(x,t)|^2$.

Now, if we want to find the quantum trajectories supported by the local conservation law Eq. (3.4), we just have to search for a definition of the particle velocity. From the knowledge that $|\psi(x,t)|^2$ is the distribution of the ensemble of particles in the configuration space, we can easily conclude that the particle velocity compatible with the local conservation of particles is:

$$v(x,t) = \frac{J(x,t)}{|\psi(x,t)|^2}, \tag{3.6}$$

when $J(x,t)$ is defined from Eq. (3.5). Due to the continuity equation, an ensemble of well-defined trajectories whose initial positions are all selected according to the distribution $|\psi(x_o,t_o)|^2$ will reproduce $|\psi(x,t)|^2$ at all times.

3.3.2 Single-particle quantum Hamilton–Jacobi equation

Alternatively, we can look for a definition of particle velocity (i.e. trajectory) from a *quantum* Hamilton-Jacobi equation. This is exactly the path followed by Bohm in his original paper. We write the quantum (complex) wavefunction, $\psi(x,t) = \psi_r(x,t) + i\psi_i(x,t)$, in a polar form:

$$R^2(x,t) = \psi_r^2(x,t) + \psi_i^2(x,t), \tag{3.7}$$

$$S(x,t) = \hbar \arctan\left(\frac{\psi_i(x,t)}{\psi_r(x,t)}\right). \tag{3.8}$$

In principle, $S(x,t)$ is not well defined when $\psi_r(x,t) = \psi_i(x,t) = 0$. At those points, $R(x,t) = 0$, meaning that no electrons will reach them[2].

The quantum Hamilton-Jacobi equation can be found by introducing into Eq. (3.1) $\psi(x,t) = R(x,t)\exp(iS(x,t)/\hbar)$. On the one hand, the imaginary part of the resulting equation gives the *local* conservation law:

$$\frac{\partial R^2(x,t)}{\partial t} + \frac{\partial}{\partial x}\left(\frac{1}{m}\frac{\partial S(x,t)}{\partial x}R^2(x,t)\right) = 0. \tag{3.9}$$

On the other hand, the real part gives a *quantum* Hamilton-Jacobi equation:

$$\frac{\partial S(x,t)}{\partial t} + \frac{1}{2m}\left(\frac{\partial S(x,t)}{\partial x}\right)^2 + V(x,t) + Q(x,t) = 0. \tag{3.10}$$

An additional term appears in the quantum Hamilton-Jacobi equation, the so-called quantum potential, this is defined as:

$$Q(x,t) = -\frac{\hbar^2}{2m}\frac{\partial^2 R(x,t)/\partial x^2}{R(x,t)}. \tag{3.11}$$

In conclusion, we obtain an interpretation of the wavefunction solution of the Schrödinger equation as an ensemble of *quantum* trajectories, with different initial positions and velocities. The velocity of each trajectory $x[t]$ is defined as:

$$v[t] = \left[\frac{1}{m}\frac{\partial S(x,t)}{\partial x}\right]_{x=x[t]}. \tag{3.12}$$

Interestingly, it can be easily shown that this new expression of quantum velocity is identical to that mentioned in expression Eq. (3.6):

$$v(x,t) = \frac{1}{m}\frac{\partial S(x,t)}{\partial x} = \frac{J(x,t)}{|\psi(x,t)|^2}, \tag{3.13}$$

where $J(x,t)$ is defined by expression Eq. (3.5).

[2]We assume that the wavefunction is single-valued so that $R(x,t)$ is also single-valued. However, the definition of $S(x,t)$ has some practical difficulties. In principle, $S(x,t)$ is a multi-valued function because of the function $\arctan(x)$ itself is a multi-valued function. If we want to use Eq. (3.7) and Eq. (3.8) to reconstruct the wavefunction, then, the multi-valued problem can be eliminated by imposing an (arbitrary) additional restriction on the definition of S. [70, 72, 73]

3.3.3 The basic postulates for a single-particle system

In this subsection we present the basic postulates of the Bohmian theory. They synthesize in few sentences all the discussions done up to here. In general, the postulates of any physical theory can be presented in different compatible ways. We follow here the standard presentation of Bohmian mechanics that provides the smaller number of ingredients [70, 72, 74, 75].

FIRST POSTULATE: *The dynamics of a single-particle in a quantum system is defined by a trajectory $x[t]$ that moves continuously under the guidance of a wavefunction $\psi(x,t)$. The wavefunction $\psi(x,t)$ is a solution of the Schrödinger equation:*

$$i\hbar\frac{\partial\psi(x,t)}{\partial t} = -\frac{\hbar^2}{2m}\frac{\partial^2\psi(x,t)}{\partial x^2} + V(x,t)\psi(x,t). \tag{3.14}$$

The trajectory $x[t]$ is obtained by time-integrating the particle velocity $v[t]$ defined from expression Eq. (3.6):

$$v(x,t) = \frac{J(x,t)}{|\psi(x,t)|^2}, \tag{3.15}$$

where $J(x,t)$ is the current density defined as:

$$J(x,t) = i\frac{\hbar}{2m}\left(\psi(x,t)\frac{\partial\psi^*(x,t)}{\partial x} - \psi^*(x,t)\frac{\partial\psi(x,t)}{\partial x}\right). \tag{3.16}$$

The initial position $x[t_o] = x_o$ and velocity $v[t_o] = v_o$ have to be specified to completely determine the trajectory $x[t]$.

SECOND POSTULATE (quantum equilibrium hypothesis): *The initial position and velocity of a particular trajectory cannot be known with certainty. When the experiment is repeated many times, the initial positions $\{x_o^j\}$ of an ensemble of trajectories $\{x^j[t]\}$, associated to the same $\psi(x,t)$, have to be generated so that the number of particles of the ensemble that lies between x and $x+dx$ at the initial time t_o is proportional to $R^2(x,t_o) = |\psi(x,t_o)|^2$. The initial velocity of each trajectory is determined by $v_o = J(x_o^j,t_o)/|\psi(x_o^j,t_o)|^2$.*

The condition on the initial position can be written mathematically as:

$$R^2(x,t_o) = \lim_{M\to\infty}\frac{1}{M}\left(\sum_{j=1}^{M}\delta(x - x^j[t_o])\right) \quad \text{for } t = t_o, \tag{3.17}$$

where $j = 1, ..., M$ is the number of different trajectories of the ensemble.

We want to discuss some points about these two postulates: First, these postulates represent a minimalist explanation of the causal interpretation without mentioning neither the Hamilton–Jacobi equation Eq. (3.10) nor the quantum potential Eq. (3.11). Certainly, we can formulate Bohmian mechanics without them, however, the quantum Hamilton–Jacobi (and the quantum potential) allow us to improve our understanding of Bohmian mechanics and provides clear arguments for discussing the similarities and differences between classical and quantum theories.

Second, according the second postulate and the continuity law, Eq. (3.4), an ensemble of Bohmian trajectories will reproduce $R(x,t)^2 = |\psi(x,t)|^2$ at any time:

$$R^2(x,t) = \lim_{M\to\infty} \frac{1}{M} \left(\sum_{i=1}^{M} \delta(x - x_i[t]) \right) \quad \text{for } \textit{any } t. \tag{3.18}$$

This is exactly the reason why it is claimed that Bohmian mechanics exactly reproduces the position measurement of *orthodox* quantum mechanics.

Finally, since an ensemble of Bohmian trajectories reproduces $\psi(x,t)$ at any time, the ensemble of trajectories will also reproduce the mean values of observables that can be written in the position representation. Furthermore, no postulate about measuring is needed. For a more detailed explanation about Bohmian measurement, please refer to Ref. [70, 72, 74, 75] and Sec. 3.5.

3.4 Bohmian Mechanics for many-particle systems

Most of our knowledge about the behavior of a quantum system has been understood from a simple system composed of just one particle, the so-called single-particle system discussed in the previous section. However, a single quantum particle system is some kind of rude idealization of natural systems. A macroscopic object is composed of a very large number of particles. This is true for an apple or even for an atom. The ultimate reason why we compute single-particle, while the reality is many-particle, is just a practical limitation in our computational capabilities. Hereafter, let us explain this point with detail.

3.4.1 The many-body problem

It is important to specify the meaning of the term *many-particle* in Bohmian mechanics, as it can easily be misinterpreted. We need an infinite ensemble $j = 1, \ldots, M \to \infty$ of trajectories to describe the statistics of a single-particle quantum system. However, this ensemble of trajectories cannot be defined with the adjective *many-particle* that we discuss here, since they all refer to different realizations of a quantum system with one degree of freedom.

Here, we will discuss quantum systems with N degrees of freedom, i.e. a N body quantum systems. We will keep a particular variable x_i for each degree of freedom $i = 1, \ldots, N$. The wavefunction, itself, is an explicit functions of all $\{x_1, \ldots, x_N\}$ variables. Now, a many-particle Bohmian trajectory involves N interacting particles $\{x_1[t], \ldots, x_N[t]\}$. Along this section, in order to simplify our notation, we will use either $\vec{x}[t] = \{x_1[t], \ldots, x_N[t]\}$ or $\vec{x} = \{x_1, \ldots, x_N\}$. The relevant point that allows us to use the adjective *many-particle* is that the N particles interact among them, i.e., the potential energy that appears in the many-particle Schrödinger equation depends on all particle positions $\{x_1, \ldots, x_N\}$.

An ensemble average of the many-particle system will require $j = 1, \ldots, M \to \infty$ many-particle Bohmian trajectories $\vec{x}^j[t]$. When needed, we will use the superscript j to refer to the statistical index $j = 1, \ldots, M$ and the subscript i to the N interacting particles, i.e. $\vec{x}^j[t] = \{x_1^j[t], \ldots, x_N^j[t]\}$.

For the non-relativistic systems discussed here, the dynamics of the many-particle quantum system is obtained from the following Schrödinger equation:

$$i\hbar\frac{\partial\psi(x_1,\ldots,x_N,t)}{\partial t}=\left(\sum_{k=1}^{N}-\frac{\hbar^2}{2m}\frac{\partial^2}{\partial x^2}+U(x_1,\ldots,x_N,t)\right)\psi(x_1,\ldots,x_N,t). \tag{3.19}$$

The solution $\psi(x_1,\ldots,x_N,t)$ of this equation is the so-called *many-particle wavefunction*, that is defined in a N-dimensional space (plus time) [3].

Due to the computational burden associated with this equation Eq. (3.19), it is unsolvable most of the times. The computational problem is that we have to evaluate the wavefunction $\psi(x_1,\ldots,x_N,t)$ and the potential $V(x_1,\ldots,x_N,t)$ in the configuration space $x_1,x_2,\ldots,x_N$ plus time. Let us put numbers to understand the problem. Let us count the number of hard discs that we have to use to save the information contained in $\psi(x_1,\ldots,x_N,t)$. We consider, for example, a system with $N=10$ particles in a $1D$ space $0\ nm\leq x\leq 10\ nm$. Let us assume that equation Eq. (3.19) is solved with a finite-difference method[4] with a spatial-step $\Delta x=1\mathring{A}$ (a much larger Δx would imply a bad accuracy in the solution of Schrödinger equation). Therefore, the number of discrete (complex) points for each x_i axis is about 100. Then, the total number of points in the configuration space for the 10 particles is $100^{10}=10^{20}$. If we use 16 bits for each real variable, we will need 32 bits for saving the complex value of the wavefunction in each grid point. Let us assume that each hard disk is able to keep 1 Terabyte of information (1 Terabyte=8×1024^4 bits). Finally, the number of hard disks needed for saving the information contained in $\psi(x_1,\ldots,x_N,t)$ would be more than 3×10^8 computers for 10 particles (more than 3×10^{28} computers for 20 particles). Impossible with today computers.

In the scientific literature, there are many attempts to provide reasonable approximations to the *many-body quantum problem*. The Density Functional Theory [37, 38] and quantum Monte-Carlo are some of the most popular techniques among the scientific community for dealing with the *many-body problem*. In the next chapter, in Sec. 5.2, we will discuss how Bohmian trajectories can help us in solving the *many-body problem*. First, in the next section, we present the basic developments of the many-particle Bohmian trajectories, from the continuity equation and also from the quantum Hamilton-Jacobi equation.

3.4.2 Many-particle continuity equation

We start by considering (non-relativistic) spinless particles. Later in section Sec. 3.4.4 we will introduce spin. As we did for the single-particle version, we can look for a *local* continuity

[3] The variable N can be defined as the number of particles in a $1D$ space or it can be related to the number of particles in a $3D$ space. For example, we can assume $\vec{r}_1=(x_1,x_2,x_3)$ as the $3D$ position for first particle and $\vec{r}_2=(x_4,x_5,x_6)$ for the second. In simple words, $\psi(x_1,x_2,x_3,t)$ can be interpreted as 3 particles in a $1D$ space or just one particle in a $3D$ space. From a physical point of view, one particle in a $3D$ space is a *single-particle* system. However, from the computational point of view, it is equivalent to a 3 particle system in $1D$. Here, we will use the notation $\vec{x}=x_1,x_2,\ldots,x_N$ to write compactly the degrees of freedom (without specifying if the real space is $3D$ or $1D$)

[4] we truncate the continuous variable x_i into a discrete number of points that are called the grid.

equation inside the Eq. (3.19). In particular, we found:

$$\frac{\partial|\psi(\vec{x},t)|^2}{\partial t}+\sum_{k=1}^{N} i\frac{\hbar}{2m}\frac{\partial}{\partial x_k}\left(\psi(\vec{x},t)\frac{\partial\psi^*(\vec{x},t)}{\partial x_k}-\psi^*(\vec{x},t)\frac{\partial\psi(\vec{x},t)}{\partial x_k}\right)=0. \tag{3.20}$$

We can easily identify Eq. (3.20) as the local conservation of particles discussed in the previous section when we define the k-th component of the N-vector current density as:

$$J_k(\vec{x},t)=i\frac{\hbar}{2m}\left(\psi(\vec{x},t)\frac{\partial\psi^*(\vec{x},t)}{\partial x_k}-\psi^*(\vec{x},t)\frac{\partial\psi(\vec{x},t)}{\partial x_k}\right). \tag{3.21}$$

Since the many-particle Schrödinger equation is also compatible with a local conservation of particles, therefore, we can interpret $|\psi(x_1,\ldots,x_N,t)|^2$ as a distribution of an ensemble of N trajectories in configuration space. The velocity of the k-th trajectory is:

$$v_k(x_1,\ldots,x_N,t)=\frac{J_k(x_1,\ldots,x_N,t)}{|\psi(x_1,\ldots,x_N,t)|^2}, \tag{3.22}$$

In fact, the strategy followed here to develop Bohmian mechanics from non-relativistic Schrödinger equation can be extended to any quantum theory where a continuity equations holds: first, look for a continuity equation for the presence probability and, then, define a velocity for the Bohmian trajectories as the current density divided by the previous presence probability.

3.4.3 Many-particle quantum Hamilton Jacobi equation

Alternatively, we can obtain Bohmian mechanics from a quantum Hamilton–Jacobi equation. We start by introducing the polar form of the many-particle wavefunction $\psi(x_1,\ldots,x_N,t)=R(x_1,\ldots,x_N,t)e^{iS(x_1,\ldots,x_N,t)/\hbar}$ into the (non-relativistic) many-particle Schrödinger equation Eq. (3.19). Then, after a quite simple manipulation, one obtains from the imaginary part:

$$\frac{\partial R^2(x_1,\ldots,x_N,t)}{\partial t}+\sum_{k=1}^{N}\frac{\partial}{\partial x_k}\left(\frac{1}{m}\frac{\partial S(x_1,\ldots,x_N,t)}{\partial x_k}R^2(x_1,\ldots,x_N,t)\right)=0, \tag{3.23}$$

where we recognize a local conservation of particles and the velocity of the x_i particle as:

$$v_k(x_1,\ldots,x_N,t)=\frac{1}{m}\frac{\partial S(x_1,\ldots,x_N,t)}{\partial x_k}. \tag{3.24}$$

Equations Eq. (3.22) and Eq. (3.24) are identical. The real part of the Schrödinger equation, leads to a many-particle version of the quantum Hamilton–Jacobi equation:

$$\frac{\partial S(x_1,\ldots,x_N,t)}{\partial t}+\sum_{k=1}^{N}\frac{1}{2m}\frac{\partial^2 S(x_1,\ldots,x_N,t)}{\partial x_k^2}+V(x_1,\ldots,x_N,t)+Q(x_1,\ldots,x_N,t)=0. \tag{3.25}$$

where the kinetic energy provides an additional justification of our definition of velocity. We have defined the quantum potential:

$$Q(x_1, \ldots, x_N, t) = \sum_{k=1}^{N} Q_k(x_1, \ldots, x_N, t), \tag{3.26}$$

with:

$$Q_k(x_1, \ldots, x_N, t) = -\frac{\hbar^2}{2m} \frac{\partial^2 R(x_1, \ldots, x_N, t)/\partial x_k^2}{R(x_1, \ldots, x_N, t)}. \tag{3.27}$$

3.4.4 Spin and identical particles

Up to here, we have only discussed particles without spin, i.e. spinless particles. However, elementary particles have spin, which is an additional discrete degree of freedom of particles (different from its position). In this subsection we will briefly explain the extension of Bohmian mechanics to include spin.

In the *orthodox* interpretation of quantum mechanics, a non-relativistic particle with spin s is described by means of a vector of wavefunctions with $(2s + 1)$ components:

$$\psi_1(\vec{r}, t), \psi_2(\vec{r}, t), \ldots, \psi_{2s+1}(\vec{r}, t). \tag{3.28}$$

In principle, the time evolution of each component is not a solution of the Schrödinger equation, but of more involved wave equations such as the Pauli, Klein-Gordon or Dirac equations [79–81]. In this subsection, we will use the vector $\vec{r}$ to represent the $3D$ position of each particle $\vec{r} = (x_1, x_2, x_3)$.

As mentioned before, the strategy to find Bohmian trajectories inside these *new* quantum wave equation is the following: first, look for a continuity equation of the probability presence in the modified equation. Second, from the current density of the continuity equation, define the Bohmian velocity as indicated in expression $\frac{d\vec{r}(t)}{dt} = \vec{v}(\vec{r}, t) = \frac{\vec{j}(\vec{r},t)}{\rho(\vec{r},t)}$. The idea is quite simple, but the mathematical development for the Pauli equation can be much more complicated.

3.4.5 Single-particle system for $s = 1/2$ particles

For an electron with $s = 1/2$, the vector of wavefunctions has two components $2s + 1 = 2$. See practical examples of the particle trajectories for spin-1/2 eigenstate for the two slit experiment in [82] and spin-1/2 particle trajectories for hydrogen eigenstates [81].

Fortunately, the fact that single and many-particle Schrödinger equations discussed along this chapter do not take into account the spin of the particles does not invalidate them. Because of the properties of the Pauli matrices, if the magnetic field can be neglected, then the Pauli equation reduces to the familiar Schrödinger equation for a particle in a purely electric potential[5], except that it operates on a two component spinor. Hence Schrödinger equation is actually satisfied by each component of the spinor $\Psi(\vec{r}, t) = \{\psi_0(\vec{r}, t), \psi_1(\vec{r}, t)\}$.

[5]The electric field depends on $\vec{\nabla} V(\vec{r}, t)$ and $\partial \vec{A}(\vec{r}, t)/\partial t$. Thus, we are not assuming that $\vec{A}(\vec{r}, t) = 0$.

In many practical situations, when the total Hamiltonian is separable into a part depending only on the positions plus a part only on the discrete spin degree of freedom, and the initial state is $\psi_0(\vec{r},0) = \psi(\vec{r},0)\alpha_1(0)$ and $\psi_1(\vec{r},0) = \psi(\vec{r},0)\alpha_2(0)$. Then, in later times, one can write the spinor evolution in a simpler form as:

$$\vec{\Psi}(\vec{r},t) = \psi(\vec{r},t)\cdot\vec{\chi}(t) = \psi(\vec{r},t)\cdot\begin{pmatrix}\alpha_0(t)\\ \alpha_1(t)\end{pmatrix} = \psi(\vec{r},t)\cdot\begin{pmatrix}\uparrow(t)\\ \downarrow(t)\end{pmatrix}, \tag{3.29}$$

where the function $\psi(\vec{r},t)$ depends only on the coordinate of the particles and the function $\vec{\chi}(t)$ is a vector function that depends only on the spins and time. We call the former the *coordinate* or *orbital* wavefunction, and the latter *spin* wavefunction. Schrödinger equation essentially determines the coordinate function $\psi(\vec{r},t)$. The evolution of the spin wavefunction evolves independently of $\psi(\vec{r},t)$. In any instance where we are not interested in the actual spin of the particles, we can use Schrödinger equation and regard as the wavefunction the coordinate function alone, $\psi(\vec{r},t)$, as we have done hitherto. On the contrary, if we are only interested in spin, we can look for the time-evolution of $\vec{\chi}(t)$ alone.

3.4.5.1 Many-particle system for $s = 1/2$ particles

For a non-relativistic system of many-particles without magnetic field (when the orbital and spin contributions of the Hamiltonian are separable) and the initial wavefunction can be written as a product of the orbital part $\psi(\vec{r}_1,\vec{r}_2,\dots\vec{r}_N,0)$ multiplied by the vector wavefunction of spin $\vec{\chi}(0)$, then, we can write the many-particle wavefunction as:

$$\Psi(\vec{r}_1,\dots\vec{r}_N,t) = \phi(\vec{r}_1,\vec{r}_2,\dots\vec{r}_N,t)\vec{\chi}(t), \tag{3.30}$$

where $\vec{\chi}(t) = \{\alpha_1(t),\alpha_2(t),\dots,\alpha_W(t)\}$. The subindex W refers to the number of possible values of the measurement of the spin in one direction for the whole many-particle system. You can determine W by looking on the possibilities that arise when combining the spin projections of each individual particle, i.e. $\alpha_1(t) = \{\uparrow_1\uparrow_2\dots\uparrow_N\}(t)$[6]. Then we can write:

$$\vec{\chi}(t) = \begin{pmatrix}\uparrow_1\uparrow_2\dots\uparrow_N(t)\\ \uparrow_1\uparrow_2\dots\downarrow_N(t)\\ \dots\\ \downarrow_1\downarrow_2\dots\downarrow_N(t)\end{pmatrix}, \tag{3.31}$$

Let us emphasize that, even without magnetic field, when the initial many-particle wavefunction cannot be written as a product of the orbital and spin wavefunctions:

$$\{\psi_1(\vec{r}_1,\dots,\vec{r}_N,0),\psi_2(\vec{r}_1,\dots,\vec{r}_N,0),\dots,\psi_W(\vec{r}_1,\dots,\vec{r}_N,0)\}, \tag{3.32}$$

[6]Additionally, you can look also for the projection of the spin of the total system. Both, procedures are connected by the Clebsch-Gordon coefficients [79]

then, we have to look for a global non-factorizable wavefunction:

$$\vec{\Psi}(\vec{r}_1,\dots\vec{r}_N,t)=\begin{pmatrix}\psi_1(\vec{r}_1,\dots,\vec{r}_N,t)\\ \psi_2(\vec{r}_1,\dots,\vec{r}_N,0)\\ \dots\\ \psi_W(\vec{r}_1,\dots,\vec{r}_N,t)\end{pmatrix}=$$
$$=\psi_1(\vec{r}_1,\dots,\vec{r}_N,t)\begin{pmatrix}\uparrow_1\uparrow_2\dots\uparrow_N(t)\\ 0\\ \dots\\ 0\end{pmatrix}+\dots+\psi_W(\vec{r}_1,\dots,\vec{r}_N,t)\begin{pmatrix}0\\ 0\\ \dots\\ \downarrow_1\downarrow_2\dots\downarrow_N(t)\end{pmatrix}. \tag{3.33}$$

Again, each $\psi_j(\vec{r}_1,\dots,\vec{r}_N,t)$ is just a solution of the many-particle Schrödinger equation.

3.4.5.2 Bohmian mechanics for identical particles

In Bohmian mechanics for identical particles, one uses the same type of wavefunction as in *orthodox* quantum mechanics. In addition, the same expression for the Bohmian velocity Eq. (3.22) is used for identical or non-identical particles. Therefore, we have to include the symmetrization postulate of the wavefunction among the postulates of Bohmian mechanics.

It is a traditional claim in many textbooks on quantum mechanics that the identical particles defined here (i.e. two electrons with an anti-symmetrical wavefunction) are indistinguishable. If the particles had trajectories, it is suggested, then they would automatically be distinguishable. From Bohmian mechanics with the symmetrization postulate we see that the adjective *indistinguishable* is inappropriate because we can perfectly label one particle as $\vec{r}_1[t]$ and another as $\vec{r}_2[t]$ and distinguish their trajectories perfectly.

In fact, the Bohmian trajectories actually enhance our understanding of the symmetrization postulate. Let us assume a two-electron system, with an anti-symmetrical orbital wavefunction $\psi(\vec{r}_1,\vec{r}_2,t)$. We assume that an electron labeled as 1 with initial position $\vec{r_1}[0]=a$ evolves into $\vec{r_1}[t]$ and $\vec{r_2}[0]=b$ evolves into $\vec{r_2}[t]$. Then, it can be easily understood that $\vec{r_1'}[0]=b$ evolves into $\vec{r_1'}[t]=\vec{r_2}[t]$ and $\vec{r_2'}[0]=a$ evolves into $\vec{r_2'}[t]=\vec{r_1}[t]$. We use primes to notice that $\vec{r_1}[t]$ and $\vec{r_1'}[t]$ correspond to trajectories of the same degree of freedom r_1 with different initial positions (a or b). This condition follows from the symmetry of the velocity Eq. (3.22) (i.e. the symmetry of the current density and modulus) when positions of the two electrons are interchanged. Then, the ensamble computed from $\vec{r_1}[t]$ and $\vec{r_2}[t]$ are identical to those computed from $\vec{r_1'}[t]$ and $\vec{r_2'}[t]$. This is the exact requirement for identical particles.

3.4.6 The basic Postulates for many-particle system

The basic postulates of Bohmian mechanics for many-particle are exactly the same that we have developed for single-particles, plus the new symmetrization postulate.

In order to simplify our presentation, we assume that the simpler many-particle wave-

function, written as:

$$\vec{\Psi}(\vec{r}_1,\ldots,\vec{r}_N,t)=\psi(\vec{r}_1,\ldots,\vec{r}_N,t)\begin{pmatrix}\uparrow_1\uparrow_2\ldots\uparrow_N(t)\\0\\\ldots\\0\end{pmatrix}. \tag{3.34}$$

The generalization of the present postulates to include the more general wavefunctions Eq. (3.33) or Eq. (3.30) follows straightforwardly from what we have done. However, it will imply writing W-different wavefunctions in the postulates.

FIRST POSTULATE: *The dynamics of a many-particle quantum system comprises a wavefunction Eq. (3.34) whose orbital part $\psi(\vec{r}_1,\vec{r}_2,\ldots,\vec{r}_N,t)$ is defined everywhere in the configuration space $(x_1,x_2,\ldots,x_N)$ and in every time, plus a many-particle trajectory $\vec{x}[t]=(x_1[t],x_2[t],\ldots,x_N[t])$ that moves continuously under the guidance of the wavefunction.*

The orbital part of the wavefunction $\psi(\vec{r}_1,\vec{r}_2,\ldots,\vec{r}_N,t)$ is solution of the many-particle Schrödinger equation:

$$i\hbar\frac{\partial\psi(x_1,\ldots,x_N,t)}{\partial t}=\left(\sum_{k=1}^{N}-\frac{\hbar^2}{2m}\frac{\partial^2}{\partial x^2}+V(x_1,\ldots,x_N,t)\right)\psi(x_1,\ldots,x_N,t).$$

Each component $x_k[t]$ of the many-particle trajectory $\vec{x}[t]=\{x_1[t],\ldots,x_N[t]\}$ is obtained by time-integrating the particle velocity $v_k[t]$ defined from:

$$v_k(x_1,\ldots,x_N,t)=\frac{J_k(x_1,\ldots,x_N,t)}{|\psi(x_1,\ldots,x_N,t)|^2},$$

where $|\psi(x_1,\ldots,x_N,t)|^2=\psi(x_1,\ldots,x_N,t)\psi^*(x_1,\ldots,x_N,t)$ is the square modulus of the wavefunction and $J_i(x_1,\ldots,x_N,t)$ is the mean value of the current density:

$$J_k(x_1,\ldots,x_N,t)=\frac{\partial\psi(x_1,..,x_N,t)}{\partial x_k}\psi^*(x_1,..,x_N,t)-\frac{\partial\psi^*(x_1,..,x_N,t)}{\partial x_k}\psi(x_1,..,x_N,t).$$

The initial positions $\vec{x}_o[t_o]=\{x_{1o},x_{2o},\ldots,x_{No}\}$ and velocities $\vec{v}_o[t_o]=\{v_{1o},v_{2o},\ldots,v_{No}\}$ have to be specified in order to completely determine the many-particle trajectory.

SECOND POSTULATE (quantum equilibrium hypothesis): *The initial positions $\vec{x}_o[t_o]=\{x_{1o},x_{2o},\ldots,x_{No}\}$ and velocities $\vec{v}_o[t_o]=\{v_{1o},v_{2o},\ldots,v_{No}\}$ of a particular many-particle j-trajectory cannot be known with certainty. When the experiment is repeated many times, the initial positions $\vec{x}^j_o[t_o]=\{x^j_{1o},\ldots,x^j_{No}\}$ of an ensemble of trajectories $\vec{x}^j[t]=\{x^j_1[t],\ldots,x^j_N[t]\}$, associated to the same $\psi(x_1,\ldots,x_N,t)$, have to be generated so that the number of particles of the ensemble that lies between $\{x_1,\ldots,x_N\}$ and $\{x_1+dx_1,\ldots,x_N+dx_N\}$ at the initial time t_o is proportional to $R^2(x_{1o},\ldots,x_{No})=|\psi(x_{1o},\ldots,x_{No},t_o)|^2$. The initial velocity is determined by $v^j_o=J_i(x_{1o},\ldots,x_{No},t_o)/|\psi(x_{1o},\ldots,x_{No},t_o)|^2$*

The condition on the initial position can be written mathematically as:

$$R^2(x_1,\ldots,x_N,t_o)=\lim_{M\to\infty}\frac{1}{M}\left(\sum_{j=1}^{M}\prod_{k=1}^{N}\delta(x-x_k^j[t_o])\right)\quad\text{for } t=t_o. \tag{3.35}$$

Notice the presence of two indices, the $j=1,\ldots,M$ for the infinite ensemble and the $k=1,\ldots,N$ for the N degrees of freedom.

THIRD POSTULATE (symmetrization postulate of quantum mechanics): *If the variables $\vec{r}_i,\uparrow_i$ and $\vec{r}_j,\uparrow_j$ that refer to two identical particles (i.e. two particles of the same species, such as two electrons) then the wavefunction Eq. (3.34) is either symmetric:*

$$\psi(.,\vec{r}_i,.,\vec{r}_j,.,t)\begin{pmatrix}\uparrow_i\ldots\uparrow_j\ldots\\0\\\ldots\\0\end{pmatrix}=\psi(.,\vec{r}_j,.,\vec{r}_i,.,t)\begin{pmatrix}\uparrow_j\ldots\uparrow_i\ldots\\0\\\ldots\\0\end{pmatrix}, \tag{3.36}$$

if the species is bosonic (every species with integer spin 0, 1, 2, . . . is bosonic), or anti-symmetric:

$$\psi(.,\vec{r}_i,.,\vec{r}_j,.,t)\begin{pmatrix}\uparrow_i\ldots\uparrow_j\ldots\\0\\\ldots\\0\end{pmatrix}=-\psi(.,\vec{r}_j,.,\vec{r}_i,.,t)\begin{pmatrix}\uparrow_j\ldots\uparrow_i\ldots\\0\\\ldots\\0\end{pmatrix}, \tag{3.37}$$

if the species is fermionic (every species with half-odd spin 1/2 , 3/2 , . . is fermionic). In Eq. (3.36) and Eq. (3.37) it is understood that all other degrees of freedom of the other particles remain unchanged[7]. Again, no postulate about measuring is needed, since in Bohmian mechanics measurement is treated as a particular case of the interaction between particles in next section.

3.5 Bohmian measurement

The Bohmian explanation of a quantum measurement is, perhaps, the most attractive (and also ignored) feature of the Bohmian explanation of the quantum nature. In this section we explain the measurement process from the point of view of Bohmian mechanics.

3.5.1 Differences between *orthodox* and Bohmian measurements

According to Bohmian postulates, the evolution of the wavefunction is uniquely determined by the Schrödinger equation with the appropriate Hamiltonian. Surprisingly, this is not true for the *orthodox* interpretation of the quantum theory.

[7]This simple spin vector wavefunction is clearly symmetrical, so that the orbital wavefunction has to be either symmetrical or anti-symmetrical. For a general wavefunctions Eq. (3.33) or Eq. (3.30), this postulate implies much more complicated restrictions on the possible orbital and spin wavefunctions.

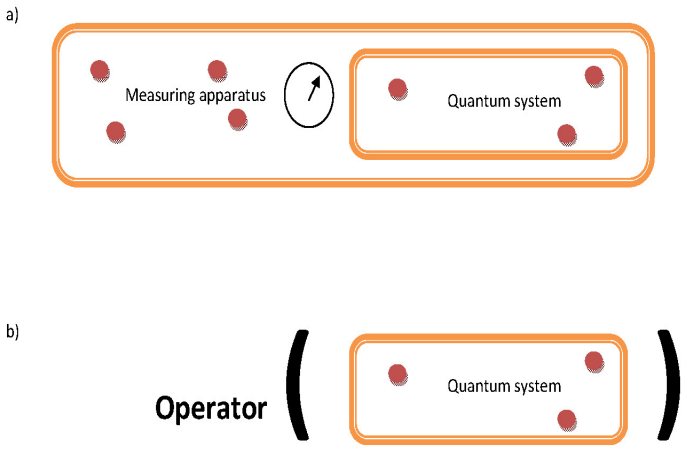

Figure 3.1: (a) The Bohmian measurement assumes that the *quantum system* and the *measuring apparatus* are explicitly simulated. (b) The *Orthodox* measurement assumes that only the *quantum system* is explicitly simulated, but the *measuring apparatus* is substituted by a proper operator acting of the wavefunction of the system.

In the measurement process, one usually separates the *quantum system* and the *measuring apparatus*. See Fig. 3.1. The *orthodox* theoretical prediction of some experimental property of the *quantum system* is described through the use of a proper operator $\hat{A}$ that is related, somehow, to the *measuring apparatus*, and whose eigenvalues give the possible outcomes of the measurement. Thus, the time-evolution of the wavefunction of the *quantum system* is governed by two (quite) different laws[8]:

1. The first dynamical evolution is the Schrödinger equation. This dynamical law is deterministic in the sense that the final wavefunction of the *quantum system* is perfectly determined when we know the initial wavefunction and the Hamiltonian of the *quantum system*.

2. The second dynamical law is called the *collapse* of the wavefunction. The collapse is a process that occurs when the wavefunction interacts with a *measuring apparatus*. The wavefunction before the measurement is substituted by one of the eigenstates of the particular operator $\hat{A}$ related to the *measuring apparatus*. Contrarily to the dynamical law given by the Schrödinger equation, the collapse law is not deterministic. The final wavefunction is selected randomly from the list of the operator's eigenstates.

The duality in the time-evolution of quantum systems in the *orthodox* interpretation is certainly a persistent controversial issue, the so-called *measurement problem* or *collapse of the wavefunction* [84, 85].

[8]Here we describe the van Neumman measurement. Other types less *invasive* measurements are also possible [83]

In the Bohmian theory, the measurement process is treated just as any other quantum process and the previous measurement difficulties of the *orthodox* interpretation simply disappear. There is no need to introduce operators [70, 86] although is posible to define operators in Bohmian mechanics, see Sec. 3.5.1.2. Here, the whole quantum system is described by a particle plus a wavefunction (rather than a wavefunction alone). The wavefunction and the trajectories are both, associated to the *quantum system* plus the *measuring apparatus*. See Figure 3.1. The whole quantum system includes the pointer of the apparatus. In fact, what we measure is not a property of the quantum system, but a position of the pointer. Then, there is one dynamical law for the evolution of the wavefunction and another dynamical law for the evolution of the trajectory:

1. The Schrödinger equation (with the appropriate Hamiltonian of the *quantum system* plus the *measuring apparatus*) determines the time-evolution of the wavefunction, independently of the fact that a measurement process takes place or not.

2. The time-evolution of the particle is determined by the time-integration of the Bohmian velocity, independently of the fact that a measurement process takes place or not.

The Bohmian and the *orthodox* explanations of a measurement produce the same predictions. This important fact is clearly manifested in the excellent work of Goldstein and co-workers [87]. However, the mathematical implementation of the equations of motion in each case are quite different. The *orthodox* quantum theory requires an operator to describe the effect of the *measuring apparatus*, but this operator is not needed in the Bohmian explanation.

Therefore, a proper modeling of a Bohmian measurement just needs the explicit consideration of the degrees of freedom of the *pointer* in the many-particle wavefunction and many-particle Bohmian trajectories that define the whole system. The back-reaction of the measurement process on the wavefunction is trivially considered. Certainly, a Hamiltonian with or without the *measuring apparatus* will provide a different evolution of the *quantum system* wavefunction.

3.5.1.1 The evaluation of sequential measurement with Bohmian trajectories

Here, we provide a didactic explanation on how Bohmian mechanics explains the unitary and non-unitary evolution of a quantum system. The wavepackets in Fig. 3.2 represent the solution of the (unitary) Schrödinger equation for a wavepacket incident upon a tunneling barrier, at three different times. The initial wavepacket (with norm equal to one) is divided into a transmitted plus a reflected wavepackets. According to Copenhagen explanation, when the system is measured at time t_1, a non-unitary evolution appears in the wavefunction and, randomly, the reflected wavepacket disappears. Only the transmitted wavepacket describes the electron at time t_1. Then, when the system is measured again at t_2, the electron is still represented by the transmitted wavepacket. Alternatively, the same unitary and non-unitary evolution can be explained with Bohmian mechanics. The initial position of the Bohmian trajectory is selected randomly at the initial time. Then, at times t_1 and t_2 the evolution of the trajectory is only determined by the transmitted wavepacket. The reflected wavepacket is an empty wave that has no effect on the evolution of the trajectory.

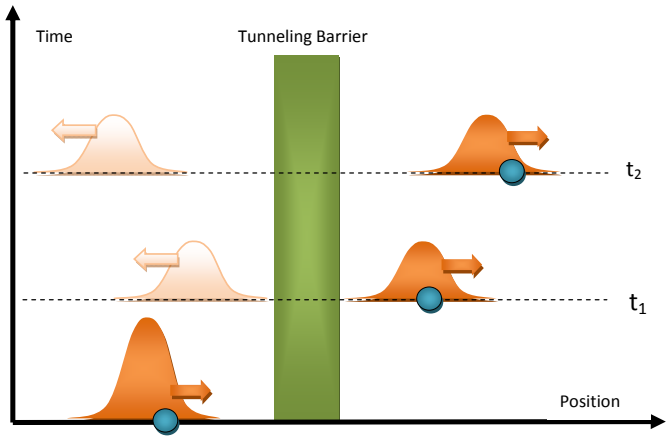

Figure 3.2: Schematic explanation of the ability of Bohmian mechanics to discuss unitary and non-unitary evolution of a wavepacket incident upon a tunneling barrier.

3.5.1.2 The evaluation of a mean value in terms of hermitian operators with Bohmian trajectories

The operators, which are an indispensable tool in the orthodox formulation of quantum mechanics to define the measurement process, become unnecessary in Bohmian formulation. However, to be fair, the Bohmian measurement process explained in the previous subsection has a quite limited practical utility. The inclusion of the measuring apparatus into the whole Hamiltonian is not an easy task because it implies increasing enormously the number of degrees of freedom that one has to simulate. In these circumstances, the use of an Hermitian operator acting only on the wavefunction of the quantum system with the ability of providing the outcomes of the measurement process without the explicit simulation of the measuring apparatus is very welcomed. Let us emphasize that we are talking only about advantages and desencantases at a computational level.

In simple words, operators are not needed in Bohmian mechanics, but they are a very helpful mathematical trick in practical computational issues. This ideas are emphasized by Goldstein, Dürr, Teufel and coworkers when they refer to the *Naive realism about operators* [70, 78, 87].

We can always write the hermitian operator $\hat{A}$ an the mean value $\left\langle \hat{A} \right\rangle_{\psi}$ in the position representation. Then, the mean value of this operator over the wavefunction $\psi(x,t)$ is given by:

$$\left\langle \hat{A} \right\rangle_{\psi} = \int_{-\infty}^{\infty} \psi^*(x,t) \hat{A} \left(x, -i\hbar \frac{\partial}{\partial x} \right) \psi(x,t) dx. \tag{3.38}$$

Alternatively, the same mean value can be computed from Bohmian mechanics by defining an spatial average of a local magnitude $A_B(x)$ weighted by $R^2(x,t)$:

$$\left\langle \hat{A} \right\rangle_{\psi} = \int_{-\infty}^{\infty} R^2(x,t) A_B(x) dx. \tag{3.39}$$

In order to obtain the same value with Eq. (3.38) and Eq. (3.39), we can easily identify the local mean value[9] $A_B(x)$ as:

$$A_B(x) = Real\left(\left[\frac{\psi^*(x,t)\hat{A}\left(x, -i\hbar\frac{\partial}{\partial x}\right)\psi(x,t)}{\psi^*(x,t)\psi(x,t)}\right]_{\psi(x,t)=R(x,t)e^{i\frac{S(x,t)}{\hbar}}}\right). \tag{3.40}$$

For practical computations, we will compute the mean value using Eq. (3.39) with an large $j = 1, \ldots, M$ number of Bohmian trajectories with different initial positions. Finally, we obtain:

$$\left\langle \hat{A} \right\rangle_{\psi} = \lim_{M\to\infty} \frac{1}{M} \sum_{j=1}^{M} A_B(x_j[t]). \tag{3.41}$$

By construction, in the limit $M \to \infty$, the value of Eq. (3.41) is identical to the value of Eq. (3.39). We have done a single-particle explanation its generalization to many-particle systems is quite easy.

From last equations, we compute the mean value of the current density operator. First, let us notice that probability density operator can be written as $|x\rangle\langle x|$ and its expected mean value is $\langle\psi|\, x\rangle\langle x|\,\psi\rangle = |\psi(x,t)|^2$ or, in the Bohmian language, $\langle\psi|\, x\rangle\langle x|\,\psi\rangle = R^2(x,t)$. The (hermitian) current operator can be written as $\hat{J} = 1/(2m)(|x\rangle\langle x|\,\hat{p} + \hat{p}\,|x\rangle\langle x|)$. It can be easily demonstrated that:

$$\langle J\rangle_{\psi} = J(x,t) = v(x,t)R^2(x,t) = \lim_{M\to\infty} \frac{1}{M} \sum_{j=1}^{M} v(x_j[t])\delta(x - x_j[t]). \tag{3.42}$$

The average value of the current density depends on the position and it is equal to the average Bohmian velocity multiplied by the square modulus of $R(x,t)$. At a particular position x, this current is just the sum of all particles that reside around this position $x = x_i[t]$ at time t. More details about Bohmian measurement in [4].

[9] We take only the real part, *Real*(), of an expression because we know that mean value is real, but Eq. (3.40) without *Real*() can take complex (real and imaginary) values. In any case, it is clear that the integration of the imaginary part in Eq. (3.39) would give zero.

Chapter 4

Exchange interaction among electrons

4.1 Introduction

The exchange interaction is a pure quantum effect, without classical counterpart. The exchange interaction have the effect of imposing important restrictions on the type of many-particle wavefunctions that are valid for describing a system of identical particles. Therefore it has also some effect on determining the total current crossing an electron device. In Sec. 4.2, we present a preliminary discussion on how the exchange interaction determines the maximum number of electrons in the device active region. This result arise from the huge energy needed to put two electrons very close. Next, in Sec. 4.3, we present a new approximation to study many-particle system with spin of different orientations. A numerical example to test the mentioned approximation is presented.

4.2 Exchange interaction for spinless electrons

Electrons are fermions (spin 1/2) and, therefore, suffer from exchange interaction. In a very simple picture, on can say that electrons with identical spin repel each other when they try to occupy the same regions of the phase-space. This interaction is not classical and we cannot find a term in the potential energies of the many-particle Schrödinger equation that accounts for it. Alternatively, this new interaction is introduced in the *shape* of the wavefunction, through the requirement of providing anti-symmetrical wavefunctions. See the third postulate of the many-particle Bohmian formulation for identical particles, Eq. (3.37). We say that a many-particle wavefunction is anti-symmetrical when the interchange of the degrees of freedom associated to two different electrons (positions and spin) provides a global change of the sign of the wavefunction.

First of all, let us discuss what we understand by spinless electrons. If we consider that all electrons have the same spin, then, the interchange of spins is irrelevant and we know for sure that the orbital wavefunction must be anti-symmetrical when we interchange the positions of the electrons. The orbital wavefunction will be identical to the one constructed by considering that electrons have no spin (i.e. spinless electrons). In summary, when we talk about spinless electrons, we can understand that all electrons have identical spin.

4.2.1 Density of states and exchange interaction

4.2.1.1 Preliminary discussions

As explained in the literature, the standard procedure to compute the density of states of an electron device is assuming that its geometry is a rectangular box of size: $\triangle L_x$, $\triangle L_y$ and $\triangle L_z$. Then, we can use Born Von Karman boundary conditions for determining the wavevectors in the three dimensions: $k_x = \frac{2\pi}{L_x} n_x$, $k_y = \frac{2\pi}{L_y} n_y$ and $k_z = \frac{2\pi}{L_z} n_z$, where n_x, n_y and n_z are integers [14]. Then, in a $1D$ system, the number of allowed states, $N(k)$, in the phase-space $\triangle L \triangle k$ is:

$$N(k) = \frac{\triangle L \triangle k}{2\pi}, \tag{4.1}$$

where the phase-space region $\triangle L \triangle k$ is defined from:

- a spatial region of length, $\triangle L = L_2 - L_1$, (i.e., the electron positions are restricted to the values $L_1 \leq x \leq L_2$). For the $1D$ system commented here this means that $\triangle L = \triangle L_x$.

- a wavevector region, $\triangle k = k_2 - k_1$, (i.e., the wavevectors of the electrons are restricted to the values $k_1 \leq k \leq k_2$). For example, we have $k_1 = 2\pi / L_x$ for $n_x = 1$. This means that we need a phase-space of $2\pi = k_1 L_x$ to put an electron there.

Alternatively the previous result can be understand from the exchange interaction without invoking the Born Von Karman Boundary conditions. The exchange interaction have the effect of imposing restrictions on the number of electrons in the device active region. This theme is an important issue on the modeling of electron devices because of the maximum number of electrons in the device active region is the responsible for determining the total current across the system.

In reference [88], Dr. Oriols presents a *many-particle wavepacket formalism* to study a system formed by two electrons where each electron is represented by a wavepacket. In this formalism, it is demonstrated that the area a in the phase-space occupied by the first wavepacket (and not allowed for the second wavepacket) is $a = 2\pi$. This result, is an universal value independent of any wavepacket parameter. It represents that each electron forms around it a region in the phase-space equal to 2π forbidden for other electrons[1].

Then, when the entire phase-space is occupied (i.e., $\rho = \frac{\triangle L \triangle k}{N(k)} = 2\pi$) we consider that we arribe at a number maximum of electrons in this region. Therefore, one might think that no more electrons can be injected into the device active region. But, what ultimately governs the injection of electrons into the device active region is the amount of energy that we need to inject a new electron into this region. Therefore, we need add more and more kinetic energy into the system to inject a new electron overcoming the natural $\rho = 2\pi$ density.

[1]We mention that if $\rho = 2\pi$ is the phase-space density, the computation of the conductance $G = \frac{q^2}{\hbar}\rho$, where q is the electron charge and $\hbar$ is the reduced Plank constant, leads to the Landauer conductance, $G = \frac{2q^2}{h}$, where the factor two is for the electron spin degeneracy.

4.2.1.2 Exchange interaction and total energy

We can study the influence of the total energy with a numerical example. We consider a *three-electron* system, all with spin up orientation, represented by the next Gaussian wavepackets:

$$\begin{aligned}
\psi_1(x_1) &= \frac{1}{\left(\pi\sigma_{x_1}^2\right)^{1/4}} \exp\left(ik_{o1}x_1\right) \exp\left(-\frac{\left(x_1 - x_{o1}\right)^2}{2\sigma_{x_1}^2}\right), \\
\psi_2(x_2) &= \frac{1}{\left(\pi\sigma_{x_2}^2\right)^{1/4}} \exp\left(ik_{o2}x_2\right) \exp\left(-\frac{\left(x_2 - x_{o2}\right)^2}{2\sigma_{x_2}^2}\right), \\
\psi_3(x_3) &= \frac{1}{\left(\pi\sigma_{x_3}^2\right)^{1/4}} \exp\left(ik_{o3}x_3\right) \exp\left(-\frac{\left(x_3 - x_{o3}\right)^2}{2\sigma_{x_3}^2}\right),
\end{aligned} \tag{4.2}$$

where $\sigma_{x1} = \frac{1}{\sigma_{k1}}$, $\sigma_{x2} = \frac{1}{\sigma_{k2}}$, $\sigma_{x3} = \frac{1}{\sigma_{k3}}$, are the wavepacket spatial dispersions, x_{o1}, x_{o2} and x_{o3}, are the central positions for each wavepacket, $k_{o1} = \left(\frac{2mE_{o1}}{\hbar^2}\right)^{1/2}$, $k_{o2} = \left(\frac{2mE_{o2}}{\hbar^2}\right)^{1/2}$ and $k_{o3} = \left(\frac{2mE_{o3}}{\hbar^2}\right)^{1/2}$, are the central wavevector values for each wavepacket and E_{o1}, E_{o2} and E_{o3}, are the kinetic energies of each of the three electrons. To simplify the notation we have considered a system $1D$ in the x direction. No Coulomb interaction is present in this simple system, then, the total energy is only due to the kinetic energy.

The wavefunction of this system is defined as a Slater determinant:

$$\Psi(x_1, x_2, x_3) = C \sum_{j=1}^{N!} \psi_1(x_{p(j)_1})\psi_2(x_{p(j)_2})\psi_3(x_{p(j)_3})(s(\vec{p}_j)), \tag{4.3}$$

where, the sum is over all $N!$ permutations $\vec{p}_j = \{p(j)_1, p(j)_2, p(j)_3\}$ and $s(\vec{p}_j) = \pm 1$ is the sign of the permutations and C is a constant of normalization[2].

Then, we can compute the mean (average) value of the kinetic energy for the *three-electron* system as follows:

$$\langle T \rangle = \frac{\int_{-\infty}^{\infty}\int_{-\infty}^{\infty}\int_{-\infty}^{\infty} \Psi^*(x_1, x_2, x_3)\hat{T}\Psi(x_1, x_2, x_3)dx_1dx_2dx_3}{\int_{-\infty}^{\infty}\int_{-\infty}^{\infty}\int_{-\infty}^{\infty} |\Psi(x_1, x_2, x_3)|^2 dx_1dx_2dx_3}, \tag{4.4}$$

where the operator kinetic energy is $\hat{T} = -\frac{\hbar^2}{2m}\frac{\partial^2}{\partial x^2}$. We do not specify x_1, x_2 and x_3 because $\langle T_1 \rangle = \langle T_2 \rangle = \langle T_3 \rangle = \langle T \rangle$. Now, we define the normalized phase-space distance between the central positions of two wavepackets, as [88]:

$$d(1,i)^2 = \frac{(k_1 - k_i)^2}{2\sigma_k^2} + \frac{(x_{o1} - x_{oi})^2}{2\sigma_x^2}; \;\; i = 2, 3. \tag{4.5}$$

To measure the relevance of the kinetic energy we compute the mean value of the kinetic energy as we decrease the distance d between one of the electrons, that we named electron 1,

[2]The constant of normalization C is irrelevant to the computation of Bohmian velocity and so from now we will not account with it. In Sec. 4.2.2 we treat the computational difficulties for the computation of the Bohmian velocity in many particle scenarios because we do not know the wavefunction.

and the other two electrons, 2 and 3 respectively. For simplicity, we study $d(1,2) = d(1,3)$[3]. In Fig. 4.1, we plot in the square black line the mean value of the kinetic energy of the *three-electron* system as we decrease the value of the distance d among electrons. In principle the total kinetic energy of a system of identical particles, as electrons, is the sum of the kinetic energies of the individual components. For this reason, in order to make a comparison with the previous plot, in the circle red line of Fig. 4.1 we plot the theoretical kinetic energy as a sum of the individuals kinetics energies of the three electrons that conforms the system.

In Fig. 4.1, we show that for large values of d the mean value of the kinetic energy of the *three-electron* system is equal to the value of the sum of the kinetic energies from its individuals components. In this context all of the electrons are place in a separate area of the phase-space equal of 2π. But, this is not true for small values of d. This difference between the two values represents the amount of kinetic energy that we have to add into the system in order to place inside the phase-space area of the independent electron 1 the others two electrons.

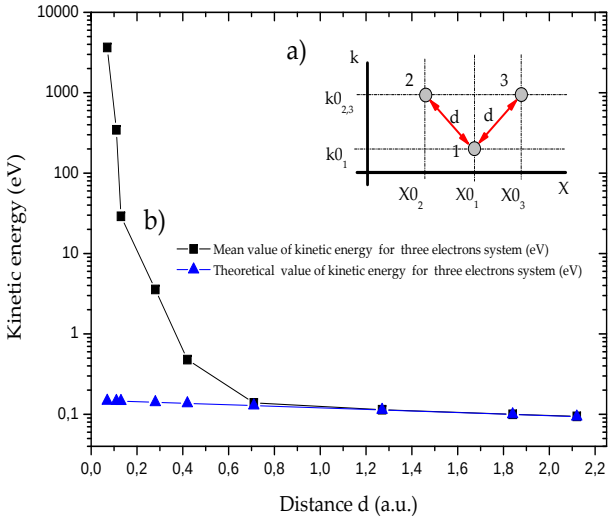

Figure 4.1: a) Schematic representation of three electron system. b) Variation of the mean value of the kinetic energy (square solid line) and theoretical kinetic energy as a sum of the individuals kinetics energies (up triangle solid line) as we decrease the distance d for a three electron system. The quantity of kinetic energy increases as we decrease the valor of d.

In summary, the reason why we cannot put another electron in a region with a density $\rho = 2\pi$ is not because it is imposible, but because it requieres a lot of energy.

4.2.2 Bohmian velocities for spinless electrons

Here, we generalize the expression of Eq. (4.3) for N particles and we comment a set of rules to compute numerically this wavefunction and the Bohmian velocity. The many-particle

[3]This scheme is completely equivalent to inject a new electron when the phase-space is completely occupied by other two electrons.

antisymmetrical wavefunction for N spinless electrons is:

$$\Psi(x_1, x_2, x_3, \ldots, x_N) = \sum_{j=1}^{N!} \prod_{i=1}^{N} \psi_N(x_{p(j)_N})(s(\vec{p}_j)). \tag{4.6}$$

For the practical computation of Bohmian velocity, we follow the next steps:

1. First, we represent the wavefunction, Eq. (4.6), in a matrix where its terms are the particular wavefunctions for each electron with their positions permuted:

$$\begin{pmatrix} \psi_1(x_{p(j)_1}) & \psi_1(x_{p(j)_2}) & \ldots & \psi_1(x_{p(j)_N}) \\ \psi_2(x_{p(j)_1}) & \ldots & \ldots & \ldots \\ \ldots & \ldots & \ldots & \ldots \\ \psi_N(x_{p(j)_1}) & \ldots & \ldots & \psi_N(x_{p(j)_N}) \end{pmatrix} \tag{4.7}$$

2. the practical computation of the previous matrix is impossible. Thus, we can simplify the matrix using the *Gauss method*. The result is a matrix with all of zero under the mean diagonal. Then, $\Psi(x_1, x_2, x_3, \ldots, x_N)$ of Eq. (4.6) (which is the determinant of Eq. (4.7)) is equal to the product of the diagonal elements of such matrix.

3. Then, from Eq. (4.6) we can compute the Bohmian velocity:

$$v_i\left(x_1, x_2, x_3..., x_N\right) = \frac{J_i\left(x_1, x_2, x_3..., x_N\right)}{|\Psi\left(x_1, x_2, x_3..., x_N\right)|^2}, \tag{4.8}$$

where , $J_i\left(x_1, x_2, x_3..., x_N\right)$, is the mean value of the quantum current for a particular electron i and $|\Psi\left(x_1, x_2, x_3..., x_N\right)|^2$ is the total norm of the many - particle wavefunction.

If instead of study N fermions we study a system of N bosons we also can compute the wavefunction Eq. (4.6) as:

$$\Psi(x_1, x_2, x_3, \ldots, x_N) = \sum_{j=1}^{N!} \prod_{i=1}^{N} \psi_N(x_{p(j)_N}). \tag{4.9}$$

Equation (4.9), have difficulties to be solved because of the $N!$ factorial terms have to be computed explicitly (because of the absence of sign in Eq. (4.9) is not possible build a determinant as in Eq. (4.7), and then, there is no Gauss method available). Finally, we comment that expression Eq. (4.6), is the determinant of Eq. (4.7) and expression Eq. (4.9), is the permanent of Eq. (4.7).

4.3 Exchange interaction for electrons with different spin

In the previous section, we have neglected the electron spin to study many-particle systems with spinless electrons. However, even if we are not interested in the evaluation of the spinor, we cannot neglect the degrees of freedom of electron with arbitrary spins because the exchange of particles must interexchange the particle coordinates and the spins. Thus, the symmetry of the function of spins is very relevant to determine the exchange properties of the orbital part.

4.3.1 Bohmian velocities with arbitrary spin-orientation

Following reference [89] we compute the Bohmian velocities associated to N-electron wavefunctions with arbitrarily spin orientations. To understand the complexity on computing the antisymmetrize wavefunction taking into account the $N!N!$ products of permutations with spins with different directions, we present an example for three electrons, one with spin up ($\uparrow_i$) and the others two with spin down ($\downarrow_i$). For simplicity, we assume that electrons have no Coulomb interaction. We define the orbital wavefunctions of these electrons as the Gaussian wavepackets of Eq. (4.3). Thus,the antisymmetric wavefunction of the total system is:

$$\begin{aligned}\Psi(x_1,x_2,x_3\uparrow_1,\downarrow_2,\downarrow_3) = &+\psi_1(x_1)\psi_2(x_2)\psi_3(x_3)(\uparrow_1\downarrow_2\downarrow_3)-\psi_1(x_1)\psi_2(x_3)\psi_3(x_2)(\uparrow_1\downarrow_3\downarrow_2)\\ &-\psi_1(x_2)\psi_2(x_1)\psi_3(x_3)(\downarrow_2\uparrow_1\downarrow_3)+\psi_1(x_3)\psi_2(x_1)\psi_3(x2)(\downarrow_3\uparrow_1\downarrow_2)\\ &+\psi_1(x_2)\psi_2(x_3)\psi_3(x_1)(\downarrow_2\downarrow_3\uparrow_1)-\psi_1(x_3)\psi_2(x_2)\psi_3(x_1)(\downarrow_3\downarrow_2\uparrow_1).\end{aligned} \tag{4.10}$$

The previous equation has 3! terms composed of the product of an orbital function by a spin function. Next, we compute the total norm taking into account the 3!3! products of permutations. For this purpose we have to multiply the orbital parts and the spin parts separately. The product of the spin part can be either 0 and 1. The final result is:

$$\begin{aligned}&|\Psi(x_1,x_2,x_3;\uparrow_1,\downarrow_2,\downarrow_3)|^2 =\\ &+\left[\psi_1^*(x_1)\psi_2^*(x_2)\psi_3^*(x_3)\right]\psi_1(x_1)\psi_2(x_2)\psi_3(x_3)-\left[\psi_1^*(x_1)\psi_2^*(x_2)\psi_3^*(x_3)\right]\psi_1(x_1)\psi_2(x_3)\psi_3(x_2)\\ &-\left[\psi_1^*(x_1)\psi_2^*(x_3)\psi_3^*(x_2)\right]\psi_1(x_1)\psi_2(x_2)\psi_3(x_3)+\left[\psi_1^*(x_1)\psi_2^*(x_3)\psi_3^*(x_2)\right]\psi_1(x_1)\psi_2(x_3)\psi_3(x_2)\\ &+\left[\psi_1^*(x_2)\psi_2^*(x_1)\psi_3^*(x_3)\right]\psi_1(x_2)\psi_2(x_1)\psi_3(x_3)-\left[\psi_1^*(x_2)\psi_2^*(x_1)\psi_3^*(x_3)\right]\psi_1(x_3)\psi_2(x_1)\psi_3(x_2)\\ &-\left[\psi_1^*(x_3)\psi_2^*(x_1)\psi_3^*(x_2)\right]\psi_1(x_2)\psi_2(x_1)\psi_3(x_3)+\left[\psi_1^*(x_3)\psi_2^*(x_1)\psi_3^*(x_2)\right]\psi_1(x_3)\psi_2(x_1)\psi_3(x_2)\\ &+\left[\psi_1^*(x_2)\psi_2^*(x_3)\psi_3^*(x_1)\right]\psi_1(x_2)\psi_2(x_3)\psi_3(x_1)-\left[\psi_1^*(x_2)\psi_2^*(x_3)\psi_3^*(x_1)\right]\psi_1(x_3)\psi_2(x_2)\psi_3(x_1)\\ &-\left[\psi_1^*(x_3)\psi_2^*(x_2)\psi_3^*(x_1)\right]\psi_1(x_2)\psi_2(x_3)\psi_3(x_1)+\left[\psi_1^*(x_3)\psi_2^*(x_2)\psi_3^*(x_1)\right]\psi_1(x_3)\psi_2(x_2)\psi_3(x_1).\end{aligned}$$

Let us notice that $3!3! = 36$ terms. However, we have only keep alive these terms whose spin part is 1. Then, the computation of the Bohmian velocity of each electron i in a system of N electrons has to be computed directly from the many-particle wavefunction as follows:

$$v_i\left(x_1,x_2,x_3...\uparrow_1,\downarrow_2,\downarrow_3,...\right)=\frac{J_i\left(x_1,x_2,x_3...\uparrow_1,\downarrow_2,\downarrow_3\ ...\right)}{\left|\Psi\left(x_1,x_2,x_3...\uparrow_1,\downarrow_2,\downarrow_3\ ...\right)\right|^2}, \tag{4.11}$$

where $J_i\left(x_1, x_2, x_3... \uparrow_1, \downarrow_2, \downarrow_3 ...\right)$ is the mean value of the quantum current for a particular electron i and $|\Psi\left(\vec{r}_1, \vec{r}_2, \vec{r}_3... \uparrow_1, \downarrow_2, \downarrow_3 ...,\right)|^2$ is the total norm of the many - particle wavefunction. If we increase the number of electrons the computation of the previous equation for $N!N!$ products of permutations is computationally inaccesible. In Sec. 4.3.2 we provide a approximation to treat wavefunctions with spin of different orientations.

4.3.2 An approximation for the Bohmian velocities

As we have mentioned above, the main difficulty to treat N different electron spin orientations with time-dependent wavepackets is that one must study all possible $N!N!$ products of permutations among spin states in the construction of the antisymmetrical wavefunction. Therefore, for N electrons, the explicit evaluation of $N!N!$ products of permutations is intractable for more than very few electrons [4].

To overcome this computationally inaccessible problem, the total wavefunction can be treated as a separated product of two many-particle wavefunctions, the first with spin up and the second with spin down. Then, we assume that the many-particle wavefunction can be separated into a product of spin up ($\uparrow$) and spin down ($\downarrow$) many-particle wavefunctions:

$$\begin{aligned} \Psi\left(x_1, x_2, x_3, x_4... \uparrow_1, \downarrow_2, \downarrow_3, \uparrow_4 ...\right) \approx \\ \phi_\uparrow\left(x_1, x_4... \uparrow_1, \uparrow_4 ...\right) \cdot \phi_\downarrow\left(x_2, x_3... \downarrow_2, \downarrow_3 ...\right), \end{aligned} \tag{4.12}$$

where the wavefunctions Ψ, $\phi_\uparrow$, $\phi_\downarrow$ are antisymmetrize wavefunctions and therefore are composed by a sum of different interchanged components [89].

Using the approximation written in the right hand side of Eq. (4.12), the numerical difficulties in the computation of the many-particle wavefunction disappear because it can be computed from a complex matrix (Slater) determinant of equation Eq. (4.6).

Now, in order to numerically verify the correctness of Eq. (4.12), we compute the Bohmian velocity associated to electron 1 (see Fig. 4.2) in three different situations keeping the antisymmetry of the total wavefunction: First, when the electron 1 is alone. Next, in other two situations, where we compute the velocity of electron 1 when it is surrounded by four and two additional exchange-interacting electrons[5] respectively.

In the first situation, represented by Fig. 4.2, we show the computation of the Bohmian velocity (with an approximate value of $6 \cdot 10^4 m/s$) for one independent (spin-up) electron along different positions.

In Figure 4.3, we plot the exact computation of Bohmian velocity for a system of 5 electrons (the left hand side of Eq. (4.12)) studying the electron 1 (see inset) when other 4 exchange-interacting electrons are present. We use the parameter d defined in Eq. (4.5), (see insets in Figs. 4.2, 4.3, and 4.4). Then, we compute the Bohmian velocity for four different values of distance d among electrons:*1.41,2.83,5.65* and *7.07*. For large d (left triangle line) the velocity of the electron 1 is not changed by the position of the other 4 electrons. But when we decrease d (cross line), the Bohmian velocity becomes very different from the result of Fig. 4.2 as a consequence of the Pauli (Exclusion) principle.

[4] Note that $8!^2 = 40320^2$

[5] We use the expression *exchange-interacting electrons* in reference only at the interaction among electrons

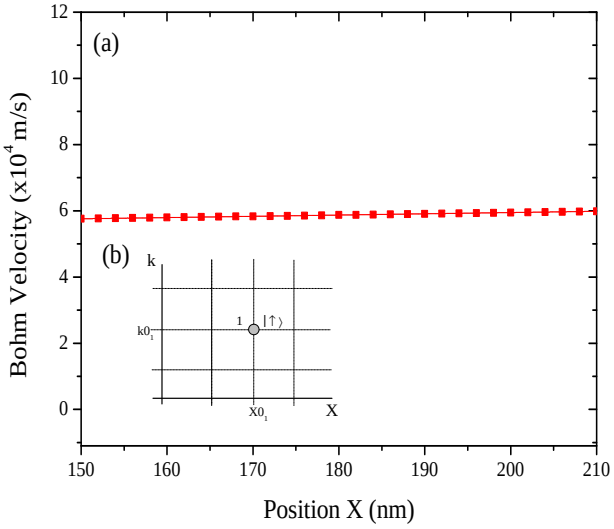

Figure 4.2: (a) Bohmian velocity for an independent electron. (b) Schematic representation of the system for an electron where we indicate the central value of the X_0 and wavevector K_0 of initial wavepacket.

In Figure 4.4, we consider the same system as in Fig. 4.3, but we compute the Bohmian velocity using the right hand side of Eq. (4.12). Thus, when we compute the Bohmian velocity Eq. (4.11) of the particle 1 we observe that only the many - particle wave function with spin up $\phi_{\uparrow}(x_1, x_4... \uparrow_1, \uparrow_4 ...,)$ will contribute to the computation of Bohmian velocity.

The strong resemblance between the Bohmian velocities of Figs. 4.3 and 4.4 from different values of d provides a numerical justification of the approximation mentioned in Eq. (4.12) for the computation of many-particle Bohmian velocities. Similar results are obtained for many other spin schemes.

---

as results of Pauli's exclusion principle.

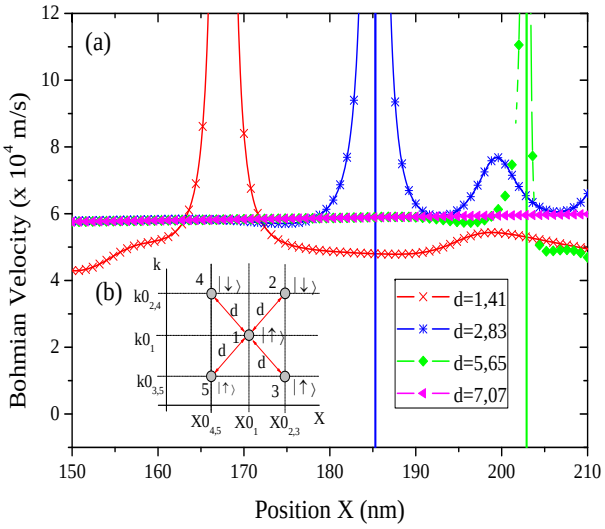

Figure 4.3: (a) Bohmian velocities for 1-electron using different values of d for a system of 5 electrons (3 spin-up and 2 spin-down). (b) In this scheme we indicate the central value of the X_0 and wavevector K_0 of initial wavepacket.

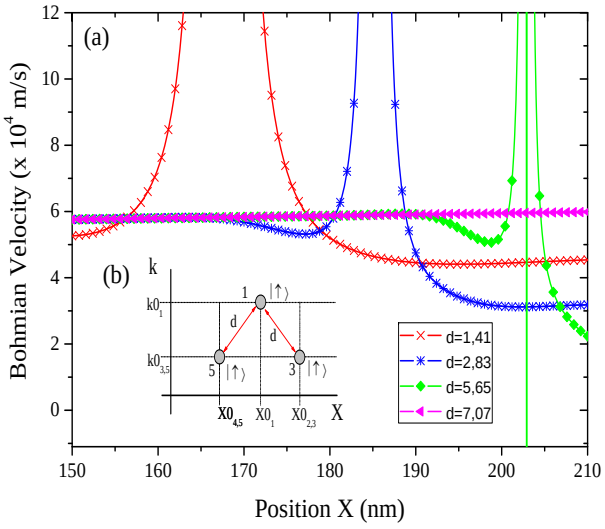

Figure 4.4: (a) Bohmian velocities for 1-electron using different values of d for a system of 3 electrons (spin-up). (b) In this scheme we indicate the central value of the X_0 and wavevector K_0 of initial wavepacket.

Despite the similitude between the two previous schemes (see Figs. 4.3 and 4.4), we find some differences in the plotted Bohmian velocities. We explain these differences in Fig. 4.5.

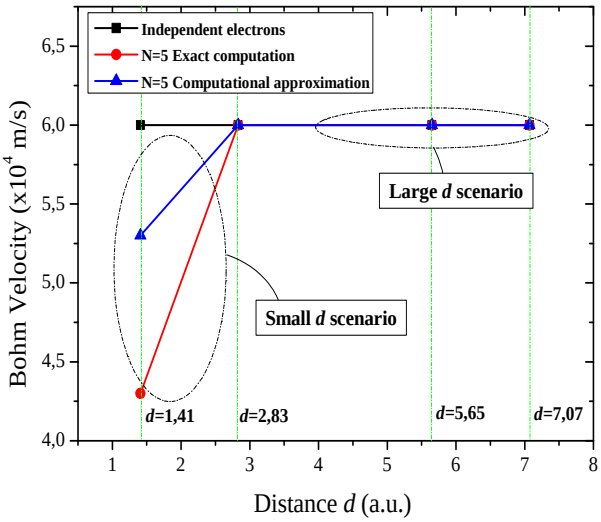

Figure 4.5: For a particular position ($X_0 = 150nm$) of Bohmian velocity of Figs 4.3 and 4.4. We plot the Bohmian velocity in function distance d among electrons for three different electron scenarios: independent electron, exact computation and computational. Lines are a guide to the eye.

We choose a particular position ($X_0 = 150nm$ in Figs. 4.3 and 4.4) and we plot the Bohmian velocity as a function of the distance d for independent electron (square black solid line), the exact computation (circle red solid line) and our computational approximation (up triangle blue solid line). In Fig. 4.5 we observe two different regions (circle dotted lines): region with for small d and region with large d.

Finally, we make a clarification, in figures 4.3 and 4.4, we have shown that the Bohmian velocity of electrons that are close to each other tends to infinity. This is because the total norm of Eq. (4.11) is zero when the electrons of the system are very close position among them (note that for two electrons, when $x_1 = x_2 = x$, then,$\Psi(x_1, x_2) = +\psi_a(x)\psi_b(x) - \psi_a(x)\psi_b(x) = 0$). So, one can understand that the electrons with different wavevector but with a very close position interact. Thus, one can think, that there is a contradiction with the results explained in Sec. 4.2 where we have commented that two electrons with different wavevector but with the same position do not interact. We can observe this by means of the Eq. (4.5) simply when $x_1 = x_2$. In fact, the effects explained in Sec. 4.2 are related to mean values and not to Bohmian velocities. A proper representation of $\Psi(x_1, x_2)$ shows that there is no contradiction. Bohmian trajectories do only accomplisher the conditions $|\Psi(x_1, x_2)|^2 = 0$, even for electrons with opposite wavevectors.

Chapter 5

The *BITLLES* simulator

5.1 introduction

Based on the Bohmian mechanics developed in chapter 3, here, we explain the main characteristics of a general, versatile and time-dependent $3D$ electron transport simulator for nanoelectronic devices. As indicated in the title of this chapter, the name of this simulator is *BITLLES*[1]. This thesis has done an important contribution to the development of the *BITLLES* simulator. This chapter is divided into other three sections.

In Sec. 5.2 we present a novel algorithm developed by Dr. Oriols to solve the many-particle time-dependent Schrödinger equation using Bohmian mechanics that explicitly includes the Coulomb and exchange correlations.

In Sec. 5.3 we define each of the potential terms that we find in the single-particle time-dependent Schrödinger equation presented in Sec. 5.2 giving special attention to Coulomb interaction. In Sec. 5.3.2, we present an algorithm to compute the Bohmian trajectories from the solution of the many-particle time-dependent Schrödinger equation taking into account only the Coulomb interaction. Next, in Sec. 5.3.3, we extend the previous algorithm to take into account both Coulomb and exchange interactions.

In Sec. 5.4 we explain the measurement of the current in an electron device under the point of view of Bohmian mechanics. Next, in Sec. 5.4.2, we explain the computation of the high-frequency current by means of the Ramo-Shockley-Pellegrini theorems.

5.2 Solving many-particle systems with Bohmian trajectories

In chapter 3, in particular in Sec. 3.4.1, we have introduced the concept of many-particle system, and also, we have discussed the computational problem associated to the solution of the many-particle Schrödinger equation of Eq. (3.19). Problem that can only be directly solved for very few degrees of freedom.

[1]The acronym *BITLLES* (Bohmian Interacting Transport for non-equiLibrium eLEctronic Structures) is also the catalan name of the bowling pins, which are solid pieces of plastic or wood situated in a *periodic* structure (similar to a solid-state structure) waiting for a ball (an electron) to impinge on them.

To surpass the computational problem associated to many-body problem, in this section, we present a novel algorithm to solve the many-particle Schrödinger of Eq. (3.19) using Bohmian trajectories. In this conditions, in order to explain the mentioned algorithm we summarize the work developed in [1] by Dr. Oriols. Following this reference a many-particle Bohmian trajectory $\vec{r}_a[t]$ associated to an a-electron can be computed from the following single-particle wavefunction, $\Psi_a(\vec{r}_a,t)$, solution of the single-particle Schrödinger equation[2]:

$$i\hbar\frac{\partial\Psi_a(\vec{r}_a,t)}{\partial t}=\{-\frac{\hbar^2}{2m}\nabla^2_{\vec{r}_a}+U_a(\vec{r}_a,\vec{R}_b[t],t)+G_a(\vec{r}_a,\vec{R}_b[t],t)+ i\cdot J_a(\vec{r}_a,\vec{R}_b[t],t)\}\Psi_a(\vec{r}_a,t), \tag{5.1}$$

where $\vec{R}_b[t]=\{\vec{r}_1[t],\vec{r}_{a-1}[t],\vec{r}_{a+1}[t],\vec{r}_N[t]\}$, at a particular time t, is a vector that contains all Bohmian trajectories except $\vec{r}_a[t]$. We mention that for the explicit computation of $\vec{r}_a[t]$ we integrate the single-particle velocity, Eq. (3.15), using the single-particle wavefunction $\Psi_a(\vec{r}_a,t)$.

The explicit definition and computation of the potentials $U_a(\vec{r}_a,\vec{R}_b[t],t)$, $G_a(\vec{r}_a,\vec{R}_b[t],t)$ and $J_a(\vec{r}_b,\vec{R}_b[t],t)$ that appear in Eq. (5.1) will be discussed in Sec. 5.3.1.

The relevant point of our quantum trajectory model is that, in order to find $\vec{r}_a[t]$ from Eq. (5.1), we do not have to evaluate the wavefunction and potential energies everywhere in the configuration space, $\{\vec{r}_1,\vec{r}_{a-1},\vec{r}_a,\vec{r}_{a+1},\vec{r}_N\}$, but only over a smaller number of configurations points, $\{\vec{r}_a,\vec{R}_b[t]\}=\{\vec{r}_1[t],\vec{r}_{a-1}[t],\vec{r}_a,\vec{r}_{a+1}[t],\vec{r}_N[t]\}$, because of all positions of the rest of electrons are fixed at $\vec{R}_b[t]$ in Eq. (5.1).

In summary, from the work of reference [1], we have been able to decompose an irresolvable single N-particle Schrödinger equation into a set of N single-particle Schrödinger equation with time-dependent potentials. It is precisely in the time-dependence of the potentials of Eq. (5.1) where the correlations with other electrons appears. From a practical point of view, all Bohmian trajectories $\vec{r}_a[t]$ have to be computed simultaneously.

5.3 Coulomb and exchange interactions

5.3.1 Coulomb interaction among electrons

Here, we define the different potential terms that we find in Eq. (5.1). Although we begin with the definition of the terms $G_a(\vec{r}_a,\vec{R}_b[t],t)$ and $J_a(\vec{r}_a,\vec{R}_b[t],t)$ the fundamental part of this subsection is dedicated to the treatment of the term of the Coulomb interaction, $U_a(\vec{r}_a,\vec{R}_b[t],t)$.

[2]We rewrite the N electrons vector-positions of the time-dependent many-particle Schrödinger equation, Eq. (3.19), for a $3D$ system as, $\{\vec{r}_1,\vec{r}_2,\cdots,\vec{r}_N\}=\{\vec{r}_a,\vec{R}_b\}$, where $\vec{r}_a$ are the positions of a particular a-electron and $\vec{R}_b$ is a vector with the rest of the electrons positions except $\vec{r}_a$.

5.3.1.1 Terms $G_a(\vec{r}_a, \vec{R}_b[t], t)$ and $J_a(\vec{r}_a, \vec{R}_b[t], t)$

$G_a(\vec{r}_a, \vec{R}_b[t], t)$ is defined as a real-valued potential energy. It takes into account, for example, the exchange interaction among particles. According to [1] we can write $G_a(\vec{r}_a, \vec{R}_b[t], t)$ as

$$G_a(\vec{r}_a, \vec{R}_b[t], t) = U_b(\vec{R}_b[t], t) + \sum_{k=1;k\neq a}^{N} \left(K_a(\vec{r}_a, t) + Q_a(\vec{r}_a, t) - \frac{\partial S(\vec{r}_a, t)}{\partial r_k} v_k(\vec{r}_a[t], t) \right). \quad (5.2)$$

$J_a(\vec{r}_a, \vec{R}_b[t], t)$ is defined as an imaginary-valued potential energy. It takes into account that the norm of $\Psi_a(\vec{r}_a, t)$ is not directly conserved (because in a many-particle system only the norm of the many-particle wavefunction is conserved). We can write $J_a(\vec{r}_a, \vec{R}_b[t], t)$ as:

$$J_a(\vec{r}_a, \vec{R}_b[t], t) = \sum_{k=1;k\neq a}^{N} \frac{\hbar}{2R^2(\vec{r}_a, t)} \left(\frac{\partial R^2(\vec{r}_a, t)}{\partial r_k} v_k(\vec{r}_a[t], t) - \frac{\partial}{\partial r_k} \left(\frac{R^2(\vec{r}_a, t)}{m} \frac{\partial S(\vec{r}_a, t)}{\partial r_k} \right) \right). \quad (5.3)$$

The solution of Eq. (5.1) needs educated guesses for the terms $G_a(\vec{r}_a, \vec{R}_b[t], t)$ of Eq. (5.2), and $J_a(\vec{r}_a, \vec{R}_b[t], t)$ of Eq. (5.3). In this subsection we provide a simple approximation. We consider a system of N electrons with Coulomb interaction, but without exchange interaction. Since no exchange interaction is considered, the correlation between the a-electron and the rest is mainly contained in the term $U_a(\vec{r}_a, \vec{R}_b[t], t)$. Thus, we can assume a Taylor expansion of the other two terms, Eq. (5.2) and Eq. (5.3), in the variable $\vec{r}_a$ around the point $\vec{r}_a[t]$:

$$G_a(\vec{r}_a, t) = G_a(\vec{r}_a[t], t) + \left[\frac{\partial G_a(\vec{r}_a, t)}{\partial \vec{r}_a} \right]_{\vec{r}_a = \vec{r}_a[t]} (\vec{r}_a - \vec{r}_a[t]) + \dots \quad (5.4)$$

and

$$J_a(\vec{r}_a, t) = J_a(\vec{r}_a[t], t) + \left[\frac{\partial J_a(\vec{r}_a, t)}{\partial \vec{r}_a} \right]_{\vec{r}_a = \vec{r}_a[t]} (\vec{r}_a - \vec{r}_a[t]) + \dots \quad (5.5)$$

The simplest approximation is just a zero-order Taylor term $G_a(\vec{r}_a, t) \approx G_a(\vec{r}_a[t], t)$ and $J_a(\vec{r}_a, t) \approx J_a(\vec{r}_a[t], t)$. Since, they are pure time-dependent terms (without spatial dependencies), they have no influence in the Bohmian velocity computed as the spatial derivative of the angle of Eq. (3.12).

5.3.1.2 Term $U_a(\vec{r}_a, \vec{R}_b[t], t)$

$U(\vec{r}_a, \vec{R}_b[t], t)$ is the potential energy that takes into account the Coulomb interaction that appears in Eq. (3.19). It can be divided into two parts:

$$U(\vec{r}_a, \vec{R}_b[t], t) = U_a(\vec{r}_a, \vec{R}_b[t], t) + U_b(\vec{R}_b[t], t). \quad (5.6)$$

To model Coulomb interaction, we consider a first ensamble $\{1, \dots, N\}$ of electrons that are inside the device active region and a second ensamble $\{N+1, \dots, M_T\}$ outside. Only the dynamics of the N electrons of the first ensamble will be directly simulated using Bohmian trajectories.

The evaluation of the term $U_a(\vec{r}_a, \vec{R}_b[t], t)$ can be simplified as:

$$U_a(\vec{r}_a, \vec{R}_b[t], t) = \sum_{\substack{j=1 \\ j\neq a}}^{N} \frac{q^2}{4\pi\varepsilon|\vec{r}_a - \vec{r}_j[t]|} + \sum_{j=N+1}^{M_T} \frac{q^2}{4\pi\varepsilon|\vec{r}_a - \vec{r}_j[t]|}. \tag{5.7}$$

The term $U_b(\vec{R}_b[t], t)$, that appears in the definition of the potential $G_a(\vec{r}_a, \vec{R}_b[t], t)$, has no role in the single-particle wavefunction $\Psi_a(\vec{r}_a, t)$ because $U_b(\vec{R}_b[t], t)$ has no dependance on $\vec{r}_a$ and it only introduces an irrelevant global phase on $\Psi_a(\vec{r}_a, t)$. Interestingly, since we deal with well-defined trajectories, instead of using Eq. (5.7), the term $U_a(\vec{r}_a, \vec{R}_b[t], t)$ can be alternatively computed from the following $3D$ Poisson equation:

$$\nabla^2_{\vec{r}_a}\left(\varepsilon(\vec{r_a})U_a(\vec{r_a}, \vec{R}_b[t], t)\right) = \rho_a(\vec{r}_a, \vec{R}_b[t], t), \tag{5.8}$$

with the appropriate boundary conditions determined by the second term of the right-hand side of Eq. (5.7) (i.e. the interaction of the first ensamble $\{1, \ldots, N\}$ with the second $\{N+1, \ldots, M_T\}$). Thus, the charge density that appears in Eq. (5.8) only considers the first ensamble of N electrons:

$$\rho_a(\vec{r}_a, \vec{R}_b[t], t) = \sum_{\substack{j=1 \\ j\neq a}}^{N} -q\delta(\vec{r}_a - \vec{r}_j[t]). \tag{5.9}$$

We notice the restriction $j \neq a$ in Eq. (5.9) that eliminates the Coulomb self-interaction. This implies that we compute on electrostatic potential for each electron. Thus, we are beyond the standard mean-field approximation. Next, we discuss the explicit boundary conditions of $U_a(\vec{r}_a, \vec{R}_b[t], t)$ in the development of the *BITLLES* simulator.

5.3.1.3 Time-dependent (Coulomb Correlated) Boundary Conditions of the Poisson equation

Since we cannot simulate all electrons in an experimental set-up including the batteries, the cable, the ammeter, etc..., we have to treat with accuracy the boundary conditions of the Poisson equation, Eq. (5.8), to model correctly the effect of the Coulomb interaction with other electrons outside the simulation box, which are responsible of the overall charge neutrality.

Here, we discuss the explicit boundary conditions of the potential $U_a(\vec{r}_a, \vec{R}_b[t], t)$ on the borders of the simulation box and also how we determine the electron charge on those boundaries. The latter is what we call the injection model.

All boundary condition of electron transport simulators are based on specifying the value of the scalar potential (or the electric field) and the charge density on the borders of the simulating box. However, it is very difficult to anticipate an educated guess for such quantities on the borders of a small simulation box that excludes the leads and the reservoirs mainly because of the far from equilibrium conditions present there [90]. Nonetheless, in order to avoid such a complexity, we can develop analytical expressions for the charge density, the electric field and the scalar potential along the leads and reservoirs [90] letting us to transfer the specification of the boundary conditions at the borders of the small simulating box into a

much simpler ones deep inside the reservoirs [90]. In particular, the two boundary conditions are:

1. Noticing that the total charge in a large volume, including the device active region, the leads and the reservoirs, tends to zero within the dielectric relaxation time, $\tau_c = \varepsilon/\sigma$, it can be easily demonstrate that the electric field deep inside the reservoirs, $E^C_{S/D}(t)$, tends to its drift value $E^C_{S/D}(t) \to E^{\rm drift}_{S/D}(t)$ within the same time $\tau_c = \varepsilon/\sigma$;

2. The scalar potentials deep inside the reservoir are fixed by the external bias $V^C_S(t) = 0$ and $V^C_D(t) = V_{\rm external}(t)$.

The temporal and spatial relations for the charge density, the electric field and the scalar potential must be, however, ultimately coupled to the injection model [90] controlling the amount of charge on the borders of the simulating box. Such a coupling process constitutes the last piece of the puzzle providing *overall charge neutrality* and *current conservation* without any fitting parameter. See reference [90, 91] for a detailed explanation of this algorithm. In reference [91] we present a method of injection of electrons which are described in terms of a binomial statistics, where the probability that N electrons are injected from one contact during the time interval τ is:

$$P(N,\tau) = \frac{M_\tau!}{N!(M_\tau - N)!} f(E)^N (1 - f(E))^{(M_\tau - N)}, \tag{5.10}$$

where M_τ is the number of attempts of injecting electrons during this time interval and $f(E)$ is the Fermi function evaluated at the energy E of the electron. This definition of the rate of injection of electrons has an important role in the definition of average current and fluctuations for $1D$, $2D$ and $3D$ devices. However, the final value of the average current and noise id determined by the dynamics inside the simulation box.

5.3.2 Explicit algorithm for Coulomb interaction

At this point, we summarize the theoretical concepts mentioned from here only taken into account Coulomb interaction. The only approximation of this trajectory-based quantum algorithm is in the potentials $G_a(\vec{r}_a, \vec{R}_b[t], t)$ and $J_a(\vec{r}_a, \vec{R}_b[t], t)$ that appears in Eq. (5.1) that are unknown and need some educated guessed. In contrast, the term $U_a(\vec{r}_a, \vec{R}_b[t], t)$ takes into account (short and long) range Coulomb interaction without approximation. Interestingly, our quantum trajectory algorithm can also be applied to systems with a space-dependent permittivity $\varepsilon(\vec{r})$ where the Poisson equation Eq. (5.8) can be directly applicable.

The steps of the algorithm to solve Eq. (5.1) are the following:

1. At the initial time t_0, we fix the initial position of all a-particles and their associated single-particle wavefunction $\Psi_a(\vec{r}_a, t_0)$.

2. From all particle positions, we compute the exact value of the potential $U_a(\vec{r}_a, \vec{R}_b[t_0], t)$ for each particle.

   A Taylor approximation for the other terms $G_a(\vec{r}_a, \vec{R}_b[t_0], t_0)$ and $J_a(\vec{r}_a, \vec{R}_b[t_0], t_o)$ of equations Eq. (5.2) and Eq. (5.3) is needed.

3. We use a finite-difference numerical method to solve each single-particle Schrödinger equation, Eq. (5.1), from t_0 till $t_0 + dt$.

4. From the knowledge of the single-particle wavefunction $\Psi_a(\vec{r}_a, t_0 + dt)$ of Eq. (5.1), we can compute the new Bohmian velocity $\vec{v}_a(t_0 + dt)$ of each a-particles and consider the injection of additional electrons.

5. From the velocity, we compute the new position of each a-particle as $\vec{r}_a[t_0 + dt] = \vec{r}_a[t_0] + \vec{v}_a(t_0 + dt)dt$ from the expression Eq. (3.6).

6. Finally, with the set of new positions and wavefunctions, we repeat the whole procedure [steps (1) to (5)] for another infinitesimal time dt till the simulation time is finished.

The algorithm explained above, can be applied to many different many-particle quantum problems (not only to study quantum electrons transport in nanoelectronics). More details and numerical results discussing the accuracy and numerical viability of this *many-particle* procedure can be found in Sec. 6 and in refs. [1, 3].

5.3.3 Exchange and Coulomb interaction among electrons

In the previous section we have showing that the wavefunction $\Psi_a(\vec{r}_a, t)$ solution of Eq. (5.1) can be constructed in two steps. First, solving Eq. (5.1) without considering the purely time-dependent potential terms, $G_a(\vec{r}_a[t], t)$ and $J_a(\vec{r}_a[t], t)$, to find $\tilde{\psi}_a(\vec{r}_a, t)$:

$$i\hbar\frac{\partial\tilde{\psi}_a(\vec{r}_a,t)}{\partial t} = \left(-\frac{\hbar^2}{2m}\frac{\partial^2}{\partial^2\vec{r}_a} + U_a(\vec{r}_a, \vec{R}_b[t], t)\right)\tilde{\psi}_a(\vec{r}_a, t), \tag{5.11}$$

where the term $U_a(\vec{r}_a, \vec{R}_b[t], t)$ is defined in Sec. 5.3.1.2. Second, multiplying the wavefunction $\tilde{\psi}_a(\vec{r}_a, t)$ by a time-dependent (real or imaginary) values (without any spatial dependence) for the final solution:

$$\Psi_a(\vec{r}_a, t) \approx \tilde{\psi}_a(\vec{r}_a, t)\exp(z_a(t)), \tag{5.12}$$

where $z_a(t)$ is a time-dependent term related with $G_a(\vec{r}_a, \vec{R}_b[t], t)$ and $J_a(\vec{r}_a, \vec{R}_b[t], t)$ defined in Eq. (5.4) and Eq. (5.5).

Here, we propose a solution of the equation Eq. (5.1), with the purpose of extending the previous algorithm to take into account the Coulomb and exchange interactions together.

For spinless electrons, the exchange interaction is effectively introduced into Eq. (5.1) through the terms $G_a(\vec{r}_a, \vec{R}_b[t], t)$ and $J_a(\vec{r}_a, \vec{R}_b[t], t)$. Due to the Pauli exclusion principle, the modulus of the wavefunction tends to zero, $R(\vec{r}_a, \vec{R}_b[t], t) \to 0$, whenever the position $\vec{r}_a \to \vec{r}_k[t]$ at a particular time t. Thus, the term $G_a(\vec{r}_a, \vec{R}_b[t], t)$ and $J_a(\vec{r}_a, \vec{R}_b[t], t)$ has asymptotes at $\vec{r}_a \to \vec{r}_k[t]$, at a particular time t, that *repel* other electrons. Then when we take into account Coulomb and exchange correlations together the approximation of Sec. 5.3.1.1 is no longer valid. The terms $G_a(\vec{r}_a, \vec{R}_b[t], t)$ and $J_a(\vec{r}_a, \vec{R}_b[t], t)$ are no longer negligible. Then, *how we can approximate* $G_a(\vec{r}_a, \vec{R}_b[t], t)$ *and* $J_a(\vec{r}_a, \vec{R}_b[t], t)$ *terms when the exchange interaction is present?* The strategy is assuming that an anti-symmetric wavefunction,

$\Psi(\vec{r},t)$, can be constructed from permutations of a many-particle wavefunction without any symmetry $\Psi_{no-sym}(\vec{r},t)$:

$$\Psi(\vec{r},t) = C\sum_{l=1}^{N!}\Psi_{no-sym}(\vec{r}_{p(l)_1},\vec{r}_{p(l)_2},...,\vec{r}_{p(l)_N},t)\ s\left(\vec{p}(l)\right). \tag{5.13}$$

The constant C is a normalization constant that will become irrelevant for the computation of the Bohmian velocity. The sum is over all $N!$ permutations $\vec{p}(l) = \{p(l)_1, p(l)_2, \ldots, p(l)_N\}$ and $s\left(\vec{p}(l)\right) = \pm 1$ is the sign of the permutations. Here, we are considering spinless electrons. Then, each wavefunction:

$$\Psi_{no-sym}(\vec{r}_{p(l)_1},\vec{r}_{p(l)_2},...,\vec{r}_{p(l)_N},t), \tag{5.14}$$

evaluated at $\vec{r} = \{\vec{r}_a, \vec{R}_b[t]\}$, can be computed following the previous (no-exchange) algorithm, Eq. (5.11) and Eq. (5.12). In particular,

$$\Psi_{no-sym}(\vec{r}_{p(l)_1}[t],...,\vec{r}_{p(l)_j}[t],...,\vec{r}_{p(l)_N}[t],t) = \tilde{\psi}_{a,p(l)_j}(\vec{r}_a,t)\exp\left(z_{a,\vec{p}(l)}(t)\right), \tag{5.15}$$

where the permutation $\vec{p}(l)$ gives $\vec{r}_{p(l)_j} = \vec{r}_a$, i.e. $p(l)_j = a$. Now, we have to use two labels in the subindex of $\tilde{\psi}_{a,h}(\vec{r}_a,t)$ to specify the solution of Eq. (5.11). The first label a accounts for the degree of freedom, i.e. the particular trajectory, that we are computing and it also fixes the potential energy $U_a(\vec{r}_a,\vec{R}_b[t],t)$ in Eq. (5.11). The second label h fixes the initial wavefunction that we will consider. If the initial many-particle wavefunction can be defined, in a region without interactions, as:

$$\Psi_{no-sym}(\vec{r}_1,...,\vec{r}_N,0) = \psi_1(\vec{r}_1,0),.....,\psi_N(\vec{r}_N,0). \tag{5.16}$$

Then, $\tilde{\psi}_{a,p(l)_j}(\vec{r}_a,0) = \psi_{p(l)_j}(\vec{r}_a,0)$. In other words, identical initial wavefunctions $\Psi_{i,j}(\vec{r}_i,t_0) = \Psi_{k,j}(\vec{r}_k,t_0)$ can evolve differently when using $U_i(\vec{r}_i,\vec{R}_i[t],t)$ or $U_k(\vec{r}_k,\vec{R}_k[t],t)$. Finally, using Eq. (5.12), the many-particle wavefunction $\Psi(\vec{r}_a,\vec{R}_b[t],t)$ can be written as:

$$\Psi_a(\vec{r}_a,\vec{R}_b[t],t) = C\sum_{l=1}^{N!}\tilde{\psi}_{a,p(l)_j}(\vec{r}_a,t)\exp\left(z_{a,\vec{p}(l)}(t)\right)\ s\left(\vec{p}(l)\right). \tag{5.17}$$

It can be easily demonstrate that using the following angles $z_{a,\vec{p}(l)}(t)$:

$$\exp\left(z_{a,\vec{p}(l)}(t)\right) = \prod_{k=1,k\neq a}^{N}\tilde{\Psi}_{k,p(l)_k}(\vec{r}_k[t],t), \tag{5.18}$$

the symmetry requirements of the Bohmian trajectories are fulfilled. Finally, putting Eq. (5.18) into Eq. (5.17), we obtain the final wave-function:

$$\Psi_a(\vec{r}_a,t) = C\sum_{l=1}^{N!}\tilde{\Psi}_{1,p(l)_1}(\vec{r}_1[t],t)\ldots\tilde{\Psi}_{a,p(l)_a}(\vec{r}_a,t)\ldots\tilde{\Psi}_{N,p(l)_N}(\vec{r}_N[t],t)s(\vec{p}(l)), \tag{5.19}$$

The algorithm needs NxN wavefunctions. It can be computed from the determinant Eq. (4.7). The generalization to electrons with arbitrarily spin can be easily constructed from the approximation Eq. (4.12).

5.4 Time-dependent electron current

5.4.1 Preliminary discussion

The functionality of any electronic device is determined by the relationship between the current measured by an ammeter and the voltage imposed at the external battery. See Figure 5.1 for a description of a typical electric circuit. The device active region is connected to a real battery (modeled by an ideal voltage source plus an internal resistance R_{IN}) and to the ground by metallic wires. The ammeter located far from the device active region measures the current. A load resistance R_L is also depicted in Fig. 5.1. In the present section, we comment on the measurement of the current in nanoelectronic devices in terms of Bohmian trajectories.

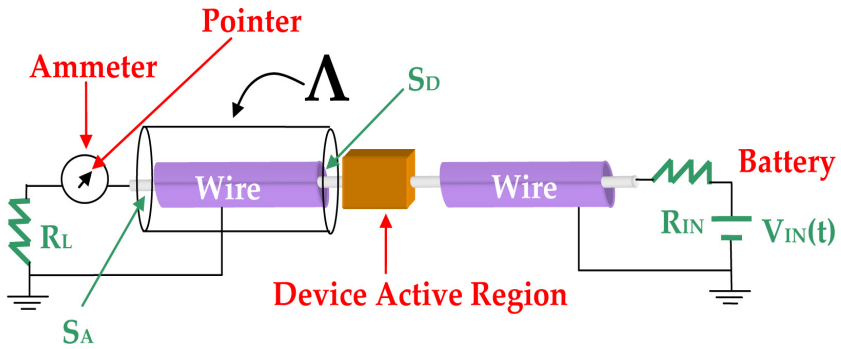

Figure 5.1: Schematic representation of the current measurement in an electron device. Device simulators compute the current on the surface, S_D, of the device active region, while the ammeter measures it on the surface, S_A.

The ammeter of Fig. 5.1 provides a relationship between the value of the *measured* current and the *observed* position of a pointer inside the ammeter [3]. The Bohmian explanation of the *measurement* process described in Sec. 3.5 tell us that what we have ultimately *measured* is the position of the ammeter pointer, not the current itself. Thus, the pointer (Bohmian) positions, $\{\vec{r}_{p1}[t], .., \vec{r}_{p_N}[t]\}$, at time t, determines the current value, $I(t)$ on the surface S_D. here, the subindex p is to refer the *pointer* (Bohmian) positions [4].

The ability of the Bohmian mechanics to predict measurable results without invoking the wavefunction collapse resides in the fact that the measured quantity depends, ultimately, on the distribution of positions of a set of Bohmian particles. Roughly speaking, we avoid *collapsing* the wavefunction to a particular position $\vec{r}[t]$ at the time t because we have already collapsed it at $\vec{r}[t_0]$ at the initial time t_0. For a more detailed explanation of the measurement process see Sec. 3.5 and reference [4].

[3]The relationship between the current and the pointer positions can be established, for example, by the magnetic deflection of a pointer: a current passing through a coil in a magnetic field causes the coil to move. The position of a *pointer* fixed to this coil will indicate the final value of the current.

In an electron device as the described in Fig. 5.1 is not possible to take into account all of degrees of freedom. It is necessary to neglect a large part of the degrees of freedom of the circuit. In this sense, we follow standard simplifying assumption that reduce the Hamiltonian of the total system into a solvable equation [4]. Thus, we cannot *completely* specify the initial N-particle wavefunction inside the simulation box (we do not know with certainty the number of electrons N inside the device active region, their energies...). We can only know these characteristics in a statistical manner. For example, we can assume that the mean energy of injected electrons follows a Fermi-Dirac statistics. In other words, we cannot longer deal with a single *pure* N-particle state, but with a *mixed quantum system* prepared by statistically combining different pure states. In this sense, we define two distributions g and h to deal with electron transport:

1. ***g-distribution:*** Is an infinite set of all of the initial position of Bohmian particles, $g = 1, ..., N_g$. The probability of each element of the $g-$ensemble is $1/N_g$. Where N_g is the number of the all the possible distributions g.

2. ***h-distribution:*** It takes into account our uncertainty on the number of electrons inside the simulation box, N, on the energy of the wavepackets associated to these electrons, on the injection time of each electron, etc. The probability of each element of the ensemble is $1/N_h$. Where N_h is the number of the all the possible distributions h.

In fact, the adaptation of Bohmian mechanics to study quantum electron transport by means of the *BITLLES* simulator leads to an algorithm based in the *Monte Carlo* technique where the randomness appears as a result of the uncertainties associated to these g and h distributions.

We continue this subsection showing that the current $I_{S_A,g,h}(t)$ crossing the surface of the ammeter, S_A, drawn in Fig. 5.1 can be related to the current $I_{S_D,g,h}(t)$ on the surface of the device active region, S_D. Let us assume that we deal with a particular $g-$element and $h-$element of the Bohmian trajectories of the circuit $\{\vec{r}_{1,g,h}[t], .., \vec{r}_{M_T,g,h}[t]\}$. We keep the subindex g and h to remind this point. Let us start by rewriting the current conservation in any point along the wire:

$$\vec{\nabla}\vec{j}_{c,g,h}(\vec{r},t) + \frac{\partial \rho_{g,h}(\vec{r},t)}{\partial t} = 0. \tag{5.20}$$

The first term, of Eq. (5.20), is the divergence of the conduction current density, $\vec{j}_{c,g,h}(\vec{r},t) = q\sum_{i=1}^{N} \vec{r}_1(t)\delta(\vec{r}_i(t)-\vec{r})$, while the other is the temporal variation of the electron charge density

[4] Standard approximations[4]:

1. We use the standard Born-Oppenhaimer approximation that can be justified because of the mass of atomic nuclei is much higher than the electron mass.

2. From the M_T electrons in all the system described in Fig. 5.1 , we do only consider explicitly N (free) electrons inside the $3D$ device active region.

3. The interaction of the N electrons with the (fixed) atomic nuclei in the device active region can be considered through the effective electron mass approximation.

$\rho_{g,h}(\vec{r},t)$ of Eq. (5.9). The second term can be related to the electric field, $\vec{E}_{g,h}(\vec{r},t)$, by using the Poisson (i.e. first Maxwell) equation:

$$\vec{\nabla}\left(\varepsilon(\vec{r})\vec{E}_{g,h}(\vec{r},t)\right) = \rho_{g,h}(\vec{r},t), \tag{5.21}$$

where the electric permittivity, $\varepsilon(\vec{r})$, is assumed to be a time-independent scalar function. Thus, we can rewrite Eq. (5.20) as:

$$\vec{\nabla}\vec{j}_{c,g,h}(\vec{r},t) + \vec{\nabla}\left(\varepsilon(\vec{r})\frac{\partial\vec{E}_{g,h}(\vec{r},t)}{\partial t}\right) = \vec{\nabla}\left(\vec{j}_{c,g,h}(\vec{r},t) + \vec{j}_{d,g,h}(\vec{r},t)\right) = 0, \tag{5.22}$$

where the displacement current density is $\vec{j}_{d,g,h}(\vec{r},t) = \varepsilon(\vec{r})\frac{\partial\vec{E}_{g,h}(\vec{r},t)}{\partial t}$. From Equation (5.22), we can define the total current $\vec{j}_{T,g,h}(\vec{r},t) = \vec{j}_{c,g,h}(\vec{r},t) + \vec{j}_{d,g,h}(\vec{r},t)$ as a divergence free vector. The subindex T, c and d mean *total*, *conduction* and *displacement*. Finally, by integrating Eq. (5.22) on the wire volume of Λ of Fig. 5.1, we arrive to the following identity for the total current:

$$\int_{\Lambda}\vec{\nabla}\vec{j}_{T,g,h}(\vec{r},t)dv = \int_{S}\vec{j}_{T,g,h}(\vec{r},t)d\vec{s} = 0, \tag{5.23}$$

where the first integral is evaluated inside the volume Λ and the second integral over the closed surface S limiting this volume Λ. The surface S is composed of the ammeter surface, S_A, the device surface S_D and a lateral cylindrical surface drawn in Fig. 5.1. We assume that this lateral surface is so far away from the metallic wire that the electric field there is almost zero and there are no particles crossing it[5]. Thus, the integral surface of the right hand side of expression (5.23) can be rewritten as:

$$\int_{S_D}\vec{j}_{T,g,h}(\vec{r},t)d\vec{s} + \int_{S_A}\vec{j}_{T,g,h}(\vec{r},t)d\vec{s} = 0. \tag{5.24}$$

Expression (5.24) tells us that $I_{S_A,g,h}(t) = -I(t)_{S_D,g,h}$. There is an irrelevant sign related with the direction of the vector $d\vec{s}$.

In conclusion, the current measured on the surface S_A is equal to the current measured on the surface of the simulation box S_D. We have emphasized the importance of the Coulomb interaction among electrons to assure *overall charge neutrality*. Also, we have discussed that one has to compute time-dependent variations of the electric field (i.e. the displacement current) to assure that the total time-dependent current computed in a surface of the simulating box is equal to that measured by an ammeter, i.e. *current conservation*.

5.4.2 The practical computation of $I_{g,h}(t)$

In the previous section, we have determined how to compute the current $I_{g,h}(t)$ from the Bohmian trajectories crossing the surface S_D. However, from a practical point of view,

[5]In fact, the relevant point is not only that the lateral surface is far away from the wire, but also that the difference between the relative dielectric constants in the wire and in the air tends to concentrate the electromagnetic field inside the wire

an algorithm based on the Ramo-Shockley-Pellegrini theorems [6–10] that computes the current from a volume integral is greatly preferred. These provide useful expressions for the computation of the total (conduction plus displacement) currents on a particular surface. These expressions involve a spatial integral over a volume that contains this surface, see Fig. 5.2. We develop these expressions in Sec. 5.4.2.2. In order to understand the practical advantages of Ramo-Shockley-Pellegrini theorems, we will compare it with a direct method. Theoretically, both algorithms, provide identical results, but the latter avoids some spurious numerical effects. Here we directly follow the development of ref. [3, 92]. We will use the volume Ω drawn in Fig. 5.2 which contains the whole device active region. In particular, we assume that one of the surface of the volume Ω of Fig. 5.2 is in contact with the surface S_A of the volume Λ of Fig. 5.1. We will discuss one particular element of the g and h ensembles, but we will omit the subindexes to simplify the notation.

5.4.2.1 Direct method

As we have mentioned at the beginning of this section, the total current flowing through one surface S_i (of the volume Ω of Fig. 5.2) has two different components:

Displacement current: We write the displacement current as:

$$I_d(t) = \int_{S_i} \varepsilon(\vec{r}_i) \left(\frac{d\vec{E}(\vec{r}_i, t)}{dt} \right) d\vec{s}. \tag{5.25}$$

We use the vector $\vec{r}_i$ to remind us that Eq. (5.25) is evaluated only on the surface S_i. It is important to specify that $\vec{E}(\vec{r}, t)$ is the electric field seen by an additional probe electron located at the observation position $\vec{r}$ at time t due to the presence of the rest of the electrons.

We remark that the scalar electrostatic potential used in the computation of the electric field $\vec{E}(\vec{r}, t)$ has an infinite value each time that the position $\vec{r}$ is equal to the position of any Bohmian trajectory, $\vec{r} = \vec{r}_a[t]$. Therefore, each time that a Bohmian particle crosses the surface S_i, an infinity appears in Eq. (5.25).

Particle (conduction) current: Since our algorithms deal with Bohmian trajectories $\vec{r}_a[t]$, the particle (conduction) current density on a particular point $\vec{r}_i$ of the surface S_i at time t has to be computed from:

$$I_c(t) = \int_{S_i} \vec{j}_i(\vec{r}_i, t) d\vec{s} = \lim_{dt \to 0} \sum_{i=1}^{N'(t)} \frac{-q}{dt} \mathrm{sgn(i)}. \tag{5.26}$$

In Equation (5.26) the sum $N'(t)$ is over the number of Bohmian trajectories that have crossed the surface S_i during the temporal step dt. The function $sgn(i) = 1$ when one trajectory leaves the volume Ω through the surface S_i, while we put $sgn(i) = -1$ when the trajectory enters.

In this equation the simulation time step, dt, provides the temporal resolution of our approach plays a crucial role. We observe that the current density of Eq. (5.26) tends to infinity (when dt tends to zero) each time that a Bohmian trajectory crosses S_i. In principle, this infinity of the conduction current has an opposite sign to the infinity of the displacement current and both compensates. Numerically, such compensation is not trivial.

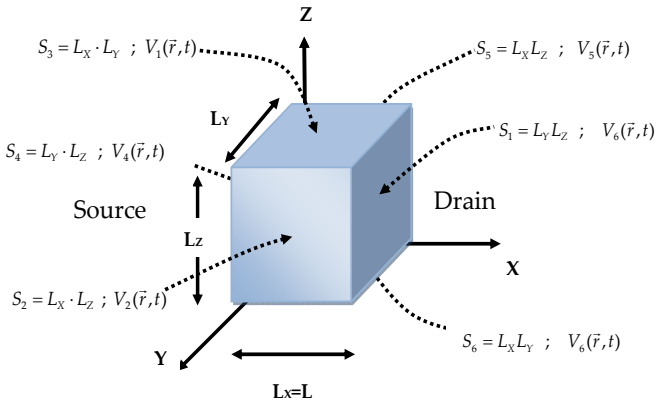

Figure 5.2: Volume Ω: this is a schematic representation of the arbitrary $3D$ geometry considered in this chapter as simulation box for the computation of quantum transport with local current conservation.

5.4.2.2 The use of the Ramo-Shockley-Pellegrini theorems

Next, we compute the total current with a second method using the Ramo-Shockley-Pellegrini theorems [3, 92, 93]. The extension of these to Bohmian mechanics provides a numerically viable algorithm to compute the time-dependent many-particle conduction and displacement currents fulfilling current conservation. A vector function $\vec{F}_i(\vec{r})$ inside the volume Ω is defined through the expression $\vec{F}_i(\vec{r}) = -\vec{\nabla}\Phi_i(\vec{r})$ where the scalar function $\Phi_i(\vec{r})$ is the solution of the Laplace equation (for the particular boundary condition at the surface S_i, $\Phi_i(\vec{r}) = 1$; $\vec{r}\epsilon S_i$ and zero elsewhere, $\Phi_i(\vec{r}) = 0$; $\vec{r}\epsilon S_{h\neq i}$):

$$\vec{\nabla}\left(\varepsilon(\vec{r})\vec{F}_i(\vec{r})\right) = -\vec{\nabla}\left(\varepsilon(\vec{r})\Phi_i(\vec{r})\right) = 0. \tag{5.27}$$

The total time-dependent current through the surface S_i can be then decomposed into three terms [92]:

$$I_i(t) = \Gamma_i^q(t) + \Gamma_i^e(t) + \Gamma_i^m(t), \tag{5.28}$$

where:

$$\Gamma_i^q(t) = -\int_\Omega \vec{F}_i(\vec{r})\vec{j}_c(\vec{r}_i,t)d^3\vec{r}, \tag{5.29}$$

$$\Gamma_i^e(t) = \int_S \vec{F}_i(\vec{r})\varepsilon(\vec{r})\frac{\partial}{\partial t}V(\vec{r},t)d\vec{s}, \tag{5.30}$$

$$\Gamma_i^m(t) = \int_\Omega \vec{F}_i(\vec{r})\varepsilon(\vec{r})\frac{\partial^2}{\partial t^2}\vec{A}(\vec{r},t)d^3\vec{r}. \tag{5.31}$$

We use the subindex, i, in Eqs. (5.28 - 5.31) because of the current through a surface different from S_i leads to a different definition of $\vec{F}_i(\vec{r})$. Let us remark that the first method provides a computation of the total current through the integration on the surface S_i. Contrarily, this second method computes the total current in a surface S_i through a volume

integral in Eq. (5.29) and an integral over all surfaces of the volume Ω in Eq. (5.30). Let us note that the evaluation of the third term $\Gamma_i^m(t)$ can be omitted because it is related to the radiation properties of the electromagnetic field generated inside Ω that are negligible for the system studied here [92].

In particular, the computation of $\Gamma_i^q(t)$ and $\Gamma_i^e(t)$ can be obtained numerically from:

Current component $\Gamma_i^q(t)$: The evaluation of Eq. (5.29) can be simplified by [3]:

$$\Gamma_i^q(t) = \sum_{i=1}^{N} \vec{F}_i(\vec{r}_i\,[t])q\vec{v}_i(\vec{r}_i\,[t]). \tag{5.32}$$

Let us mention that Eq. (5.32) not only contains the conduction current, but also contains partially the displacement current.

Current component $\Gamma_i^e(t)$: The evaluation of $\Gamma_i^e(t)$ follows directly the Eq. (5.30). We rewrite it here for convenience:

$$\Gamma_i^e(t) = \int_S \vec{F}_i(\vec{r})\varepsilon(\vec{r})\frac{\partial V(\vec{r},t)}{\partial t}d\vec{s}. \tag{5.33}$$

The time derivative is obtained with a simple finite-difference evaluation, $\partial V(\vec{r},t)/\partial t = (V(\vec{r},t) - V(\vec{r},t-dt))/dt$.

In summary, the numerical evaluation of the total current through a particular surface S_i due to a set of N Bohmian trajectories can be computed from Eqs. (5.25) and (5.26) with the direct method, and from Eqs. (5.32) and (5.33) with the Ramo-Shockley-Pellegrini theorems. In principle, both provide identical results. However, from a computational point of view, we will see in the numerical results that the latter is preferred because it is free from technical difficulties in its numerical implantations. More details in references [3, 4].

5.4.3 The practical computation of DC, AC and transient currents

We compute the time-dependent current from the Bohmian trajectories crossing the surface S_D through Eq. (5.32) and Eq. (5.33). Here, we discuss how we can determine the average value of the current at time t_1 (or the expectation value, or the mean, or the first moment). We use the following ensemble average:

$$\langle I(t_1)\rangle = \lim_{N_g,N_h\to\infty} \frac{1}{N_g N_h}\sum_{g=1}^{N_g}\sum_{h=1}^{N_h} I_{g,h}(t_1). \tag{5.34}$$

When the battery of Fig. 5.1 is fixed to a constant value, then, the whole circuit becomes stationary. For a stationary process, the mean current in Eq. (5.34) is independent of time. Then, if the process is ergodic, we can compute the mean current from the following (first-order) time average expression:

$$\overline{I_{g,h}(t)} = \lim_{T\to\infty}\frac{1}{T}\int_{-T/2}^{T/2} I_{g,h}(t)dt. \tag{5.35}$$

In this case, the practical procedure for the computation of the mean current is simpler. Before beginning the simulation, we select only one particular realization of the $h-$distribution

for an *infinite*[6] number of electrons. Simultaneously, we fix the $g-$distribution of the initial positions for the previous (infinite) realization of wavepackets.

A single sample function often provides little information about the statistics of the process. However, if the process is ergodic, that is, time averages equal ensemble averages, then all statistical information can be derived from just one sample element of the $h-$ and $g-$ distributions.

Electrical engineers are not only interested in the DC behavior of nanoelectronic devices, but also in their transient or AC performance. For these time-dependent scenarios, the circuit is no longer neither stationary nor ergodic. Then, we cannot use ergodicity and we have to compute the mean value of the current at each particular time, t_1, only from the ensemble average of Eq. (5.34).

When we measure experimentally the current, we do not found a fixed (DC) value but a randomly varying function of time. These fluctuations of the current are simply called noise [94, 97]. The characterization of the noise is an important issue in electronics in order to understand how to avoid it in practical circuit applications. On the other hand, from a physical point of view, there is a lot of useful information in the noise that is missing (because of the average) in the mean values discussed above. Roughly speaking, the noise can be characterized by the *variance* of the probability distribution of the current. The average current is known as the first moment of the current probability distribution, while the variance as the second moment. In fact, once we know all values $I_{g,h}(t)$ from the infinite $g-$ and $h-$ ensembles, one can compute the probability of each current value and, from them, any higher moments of the current distribution. In this sense, our Bohmian simulation algorithm can be compared to the *orthodox* full counting statistics technique; both, provides full information about the current distribution for quantum transport. See references [95–97] for an explanation of the latter technique.

The practical expressions for the computation of the current fluctuations within Bohmian mechanics are quite simple. In fact, once the simulations are done, we directly know all possible measurable current values $I_{g,h}(t_1)$ and their probabilities $1/(N_g N_h)$, thus, we can use standard statistical techniques to characterize the fluctuations of the current. This is another very relevant advantage of using Bohmian mechanics to study quantum electron transport in front of *orthodox* techniques [97].

The fluctuating signal of the current can be defined from $\Delta I_{g,h}(t) = I_{g,h}(t) - \langle I_{g,h}(t)\rangle$. We can obtain information of the noise from the variance (or the mean square or the second moment) defined as $\langle \Delta I(t)^2\rangle = \langle I(t)^2\rangle - \langle I(t)\rangle^2$. However, experimentalists are interested in having information on how the noise is distributed along the different frequencies[7]. Therefore, the characterization of fluctuations of the current are computed from the covariance:

$$\langle \Delta I(t_1)\Delta I(t_2)\rangle = \lim_{N_g,N_h\to\infty} \frac{1}{N_g N_h} \sum_{g=1}^{N_g}\sum_{h=1}^{N_h} \Delta I_{g,h}(t_1)\Delta I_{g,h}(t_2). \tag{5.36}$$

If the process is ergodic, i.e. $\langle \Delta I_{g,h}(t)\Delta I_{g,h}(t+\tau)\rangle = \overline{\Delta I_i(t)\Delta I_i(t+\tau)}$, we can compute the

[6]The practical procedure for the *infinite* number is selecting a number large enough so that the mean current remains practically unchanged for successive times.

[7]Most of electronic apparatuses, and the ammeter itself, have to be interpreted as low-pass filters. Therefore, they are not able to measure *all* noise of the spectrum, but only up to a maximum frequency

noise equivalently from the autocorrelations function:

$$\overline{\Delta I(t)\Delta I(t+\tau)} = \lim_{T\to\infty} \frac{1}{T} \int_{-T/2}^{T/2} \Delta I_{g,h}(t)\Delta I_{g,h}(t+\tau)dt. \tag{5.37}$$

In addition, a process is called wide-sense (or weakly) stationary if its mean value is constant and its autocorrelation function depends only on $\tau = t_2 - t_1$. Then, we define the autocorrelation function $R(\tau)$ as:

$$R(\tau) = \overline{\Delta I(t)\Delta I(t+\tau)}, \tag{5.38}$$

because depends only on $\tau = t_2 - t_1$. Wide-sense stationary processes are important because of the autocorrelation function of Eq. (5.37) and the power spectral density function $S(f)$ (measured by experimentalists) form a Fourier transform pair:

$$S(f) = \int_{-\infty}^{\infty} R(\tau)e^{-j2\pi f\tau}\, d\tau. \tag{5.39}$$

This is known as the Wiener-Khinchine theorem. In many systems, one obtains the well known Schottky's result [98] for the shot noise:

$$S_{Schot}(f) = 2q\left\langle I\right\rangle, \tag{5.40}$$

which is also referred in the literature as *Poissonian value* of shot noise. More details in reference [4].

Chapter 6

Numerical results

6.1 Introduction

We can implement the *BITLLES* simulator with different electronic devices where each device is designed with its proper electrical parameters. In this chapter we present a set of numerical results configurating the *BITLLES* simulator for three different electron devices.

The first one, Sec. 6.2, is the *Resonant Tunneling Diode* (*RTD*). *RTD's* play a crucial role to understand many of the electronic transport features belonging solely to the quantum world. These features make it ideal for testing the *BITLLES* simulator. Next, in Sec. 6.3, we present the main results of a set of applications for *RTD*. First, we present the characteristic I-V for different boundary conditions between the contacts and the device active region in a DC scenario. Later, we present a frequency multiplier using Ramo-Shockley-Pellegrini theorems and finally we model the noise characteristics of a *RTD* to obtain the Fano factor.

The second of these devices, Sec. 6.4, is a new type of devices which we have called *Driven Tunneling Device* (*DTD*)[1]. This device is specially designed to process signal at high frequency. In Sec. 6.5, we present the mean results of two high frequency applications: frequency rectifier and frequency multiplier.

In both set of results we have included a list of articles related with this applications (Sec. 6.3 and Sec. 6.5). These results have been computed with Coulomb correlation, but without exchange correlations.

Finally, in Sec. 6.6 we test the capabilities of *BITLLES* simulator to compute electrical parameters taking into account Coulomb and exchange correlations together. In particular, we present the DC and noise characteristics of a nano-resistor.

6.2 Resonant Tunneling Diode (*RTD*)

From the original electronic transport analysis of structures exploiting a finite sequence of potential barriers spaced by a distance shorter than the electron mean free path, Esaki, in 1970, introduced for the first time the RTDs [99–101]. The simple case of two barriers, useful

[1]The patent was deposited with the number of request 2005011937 with title: "Device to generate an electrical signal".

to study the relevant quantum features generally involved in superlattice, is also the basic physical picture of the *RTD* active zone, see Fig. 6.1.

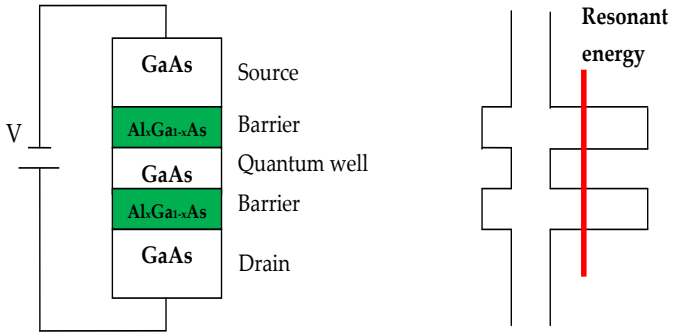

Figure 6.1: (a) Basic configuration for a typical *RTD* and (b) Related conduction and valence band structure.

To understand electronic transport in this device, it can be assumed that the only permitted energies in the well for the electrons are those very close to the resonant energies E_{R_n} [2]. If the transport is assumed ballistic, tunneling of the whole device is possible for electrons with energies close to E_{R_n} (the *resonant tunneling transport*). Varying the applied voltage V, the whole potential profile is modified. Let us assume that we keep the source contact grounded and the drain contact at V bias. Then, the resonant energies shift down when we increase bias. The electrons from the source will be able to reach the drain until the resonant energy is lower than the bottom of the source conduction band. If the resonant energy overcomes this limit, resonant tunneling is no longer permitted and the *RTD* differential conductance rapidly decreases, see Fig. 6.2. This transport behavior results in a *Negative Differential Conductance* (NDC) region of the current-voltage ($I-V$) characteristic. For more details about features of RTDs, please see [102, 103].

The resonant tunneling is of general interest in many applications of quantum mechanics (see references therein [104]), the particular case of *RTD* is very intriguing not only for its peculiar properties [102] but also for its potential applications in both analogue [105, 106] and digital [107] electronics. Nevertheless technology solutions to integrate RTDs in electronic circuits are still under investigation.

From a theoretical point of view RTDs have been widely studied. Their peculiar properties have attracted the interest either of important corporations such as IBM (with the works of Büttiker [97, 104] and Fischetti [108]) and Texas Instruments (Frensley [109] and Klimeck [110]) or leading universities like MIT (Brown [111]) and Purdue University (Datta [112]). Singular transmission coefficient shape and NDC region of the $I-V$ characteristic [102, 103], are only some of the most impacting *RTD* properties. Unfortunately single-particle theory for mesoscopic structures is not adequate to describe the totality of the typical behavior of these

[2] Roughly speaking, the value E_{R_n} are the energies of the single-particle stationary quantum states of the well with infinite thickness barriers.

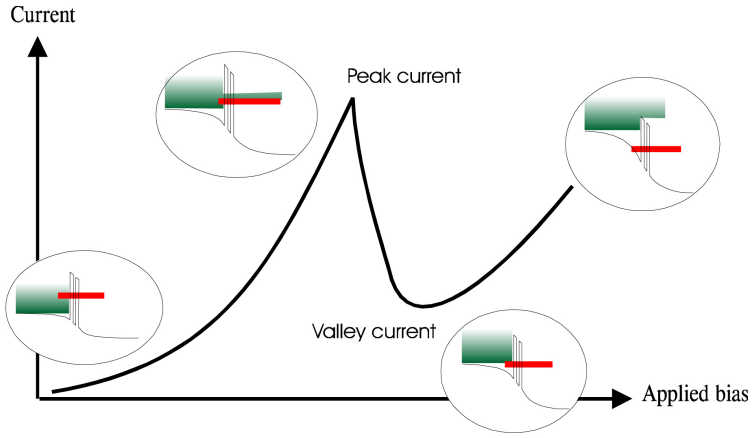

Figure 6.2: Schematic representation of the I-V curve of a typical *RTD*. The resonant energy inside the quantum well acts like an energetic filter that lets the electrons from the source to arrive at the drain.

devices. Also in the most idealized case of *RTD*, the inclusion of the Coulomb correlation between electrons is enough to spoil the results of the single-particle theory. Many-body based theories and simulations, confirmed by experimental measurements show for example, different current patterns [2, 110, 112] or very enhanced noise spectrum in NDC region [113, 114]. However theories involving the solution of the many-body Schrödinger equation are in general very hard to treat. The widely used approximation to partially overcome this problem is the Breit-Wigner formalism [115, 117]. This picture includes many of the effects arising from the quantum correlations by introducing a phenomenological scattering parameter based on the concept of decoherence [97, 118]. It furnishes a powerful tool to analyze theoretically RTDs and reproduce their characteristics in an analytical way [103]. Nevertheless, some other tools as second quantization ([113] and references therein) or Hartree approximation and Bardeen approach ([116] and references therein), must be adopted in order to treat more complicated phenomena as noise. Other approaches devoted to the numerical simulation are the non-equilibrium Green function combined with the Landauer formalism [112], Wigner distribution function [109, 110, 119]. Besides Monte Carlo methods are also used to simulate mesoscopic devices [120]. Some of these techniques have been explained in chapter 2.

6.3 *RTD* applications

In this section, we configure *BITLLES* simulator as a *RTD* and we discuss its numerical results.

6.3.1 Coulomb interaction in DC scenario

- **A.Alarcón, G.Albareda , F.L.Traversa and X.Oriols *Nanoelectronics: Quantum electron transport* in the book *"Applied Bohmian Mechanics: From Nanoscale Systems to Cosmology"*, edited by X. Oriols and J. Mompart, Panstanford Publishing, ISBN: 978-981-4316-39-2**

As a first example, we consider the importance of the Coulomb interaction in the pre-

diction of the current-voltage characteristic of a typical *RTD* using *BITLLES* simulator. It consists on two highly doped drain-source $GaAs$ regions (the leads), two $AlGaAs$ barriers of $1.2nm$, and a quantum well (the device active region) of $6nm$. Transport takes place from source to drain in the x direction. The lateral dimensions are $L_y = L_z = 48.6nm$. Room temperature is assumed. As discussed in Sec. 5.3.1, the practical quantum algorithm for the *RTD* implies solving numerically N time-dependent single-particle $1D$ Schrödinger equations. All Schrödinger equations are coupled to the Poisson equations with the boundary conditions given by our boundary condition algorithm, see Sec. 5.3.1.3. More technical details can be found in references [1] and [2].

As discussed in Sec. 5.3.1, we distinguish between (i) the Coulomb interaction among electrons inside the simulation box plus (ii) the Coulomb correlations among these electrons and those outside the simulation box. Therefore, we will compare the results obtained by means of the previously described model, with those obtained, in one hand by eliminating the Coulomb correlations among the electrons of the device active region and those of the leads (i.e. assuming standard Dirichlet external bias at the borders of the device active region of the *RTD*. Please see Sec. 5.3.1.3 for a detailed description), and on the other hand, with those obtained by switching off the Coulomb correlations (i.e. assuming the simplest single particle treatment of electrical transport). In Figure 6.3, we present the

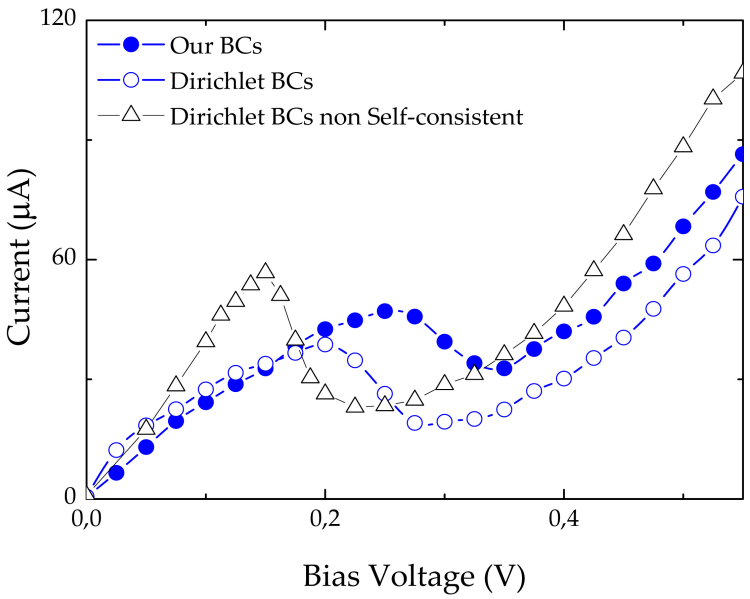

Figure 6.3: *RTD* Current-voltage characteristic. Results taking into account the Coulomb correlations between the electrons of the leads and the electrons of device active region are presented in solid circles. Open circles refer to the same results neglecting the lead-device active region interaction. Open triangles refer to a wholly non-interacting scenario, i.e. both Coulomb interaction between the leads and the device active region and Coulomb interaction among electrons within the device active region are neglected.

current-voltage curves of the simulated *RTD* using our boundary conditions algorithm (solid circles), standard Dirichlet external bias boundary conditions (open circles), and switching of Coulomb correlations (open triangles). As it can be observed, the differences between these three approaches appear not only in the magnitude of the current but also in the position of

the resonant region. More details are explained in Ref. [90].

6.3.2 Coulomb interaction in high frequency scenarios

- **Source: A.Alarcón and X.Oriols, *Computation of quantum electron transport with local current conservation using quantum trajectories*, Journal of Statistical Mechanics: Theory and Experiment. Volume: 2009(P01051), (2009).**
- **F. L. Traversa, E. Buccafurri, A. Alarcón, G. Albareda, R. Clerc, F. Calmon, A. Poncet , X. Oriols, *Time dependent many-particle simulation for Resonant Tunneling Diodes: interpretation of an analytical small signal equivalent circuit*, Transaction on electron devices (submitted) (2011).**

Next, we design *BITLLES* simulator to provide an example of the computation of the total current in time-dependent scenarios that includes a time-dependent solution of the $3D$ Poisson equation. First, we will consider a single-electron crossing a *RTD* to show the accuracy of our quantum electron transport approach in providing local current conservation, i.e. the sum of the conduction plus the displacement currents is zero when integrated on any closed surface. Second, as an enlightening example, we will compute transient currents with *BITLLES* simulator.

For the first example, we consider a *RTD* composed of two highly doped source-drain $GaAs$ regions, two $AlGaAs$ barriers with the length of $1.6nm$ and height $0.5eV$, and a quantum well with a length of $2.4nm$. We assume a constant effective mass $m^*_{AsGa} = 0.067m_0$ with m_0 the electron free mass along the whole $3D$ structure. Transport takes place from source to drain in the x direction. The lateral dimensions y and z are small enough for considering electron confinement[3]. In the x direction, the time evolution of an initial Gaussian wavepacket with initial kinetic energy of $0.25eV$ coming from the source contact is computed. The computation of the trajectory requires the algorithm explained in the Sec. 5.3.2. At each simulation time step dt, we solve the Poisson equation (in this single-electron case we solve the Laplace equation) with the appropriate boundary conditions. From this potential profile, we solve Eq. (5.1) to find $\Psi_a(\vec{r}_a, t)$ with a temporal step $dt = 10^{-17}s$ and a spatial resolutions in the x direction of $dx = 0.2nm$. Finally, we compute the next position of the Bohmian trajectory.

In detail, the scalar electrostatic potential energy is obtained from the numerical solution of the $3D$ Poisson equation. The boundary conditions at the source and drain surfaces are equal to zero volts. In the rest of the surfaces, we assume an electric field equal to zero, but no explicit restriction is imposed on the value of the potential. For simplicity, we assume a homogeneous dielectric constant $\varepsilon = 13\varepsilon_0$ (with ε_0 the vacuum permittivity) in the whole device active region. The time-dependent electric field, $\vec{E}(\vec{r}, t) = -\vec{\nabla}V(\vec{r}, t)$, changes with time due to electron dynamics and it is different from zero even in the source and drain surfaces.

The computation of the total current following the expressions developed in Sec. 5.4.2 needs the knowledge of (i) the Bohmian trajectory depicted in Fig. 6.4, (ii) the time derivative of the potential profile (and the associated electric field) and (iii) the function $\vec{F}_i(\vec{r})$ defined as the solution of the Laplace equation, see Eq. (5.26). In Figure 6.5, we show the

[3]Then, the Bohmian velocities in the lateral directions are zero because we consider that the wavefunction involves only one quantized level.

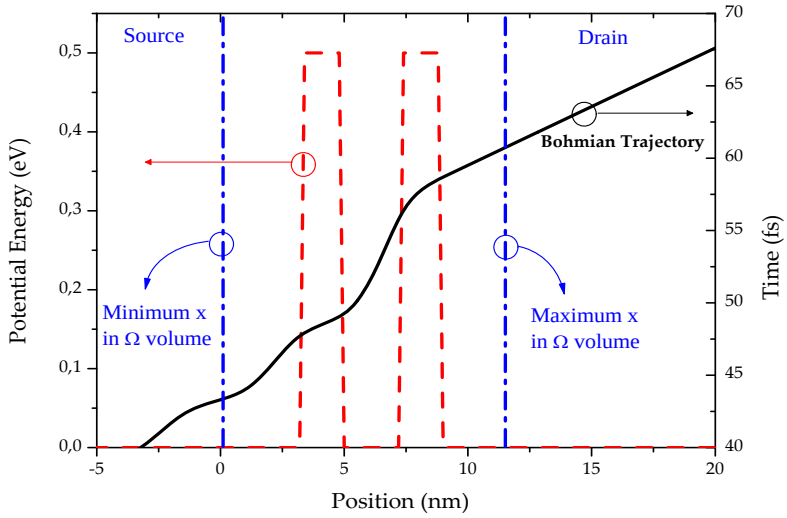

Figure 6.4: Dashed line: Potential energy profile for a double-barrier structure. Solid line: Bohmian trajectory of an electron crossing the heterostructure. Dashed dotted line: Schematic representation of the limits of the volume Ω in the x direction.

total time-dependent current on the six surfaces of volume Ω of Fig. 5.2. The numerical evaluation of the total current through each of the six surfaces is computed from the Eqs. (5.25) and (5.26) with the direct method, and from Eqs. (5.32) and (5.33) for the Ramo-Shockley-Pellegrini method. It is interesting to notice that there is a correlation between the three accelerations of the Bohmian trajectory in Fig. 6.4 and the three oscillatory behaviors of the currents in Fig. 6.5. In general, the results obtained for the total current are identical for the two methods. However, we observe in the plots of the surfaces 1 and 4 two peaks when the total current is computed from the first method. As mentioned in Sec. 5.4.2, these spurious peaks are a consequence of the infinities generated in Eqs. (5.23) and (5.25) when a Bohmian trajectory crosses these surfaces. The computation of the current using the second method is free from these spurious numerical peaks. The reason for the advantage of the second method is that Eq. (5.32) contains not only the conduction current, but also part of the displacement current.

Once we have already discussed the ability our the *BITLLES* simulator to compute time-dependent currents, we show here, the current response to the step input voltage in the NDC region. In order to capture the pure effects of the dynamic in *RTD*, we introduce some formalism.

If the input signal at the bias is the step voltage $V(t) = V_1 u(t) + V_2 [1 - u(t)]$ where $u(t)$ is the Heaviside (step function) function. The voltages V_1 and V_2 are constant. Then the current response can be expressed as $I(t) = I_{tran}(t) + I_1 u(t) + I_2 [1 - u(t)]$ where I_1 and I_2 are the stationary currents corresponding to V_1 and V_2 respectively, and I_{tran} is the *intrinsic* transient current. This formalism permits to focus on the current component carrying the dynamics involved in the *RTD* without performing any time derivative that from a numerical point of view could be very inaccurate.

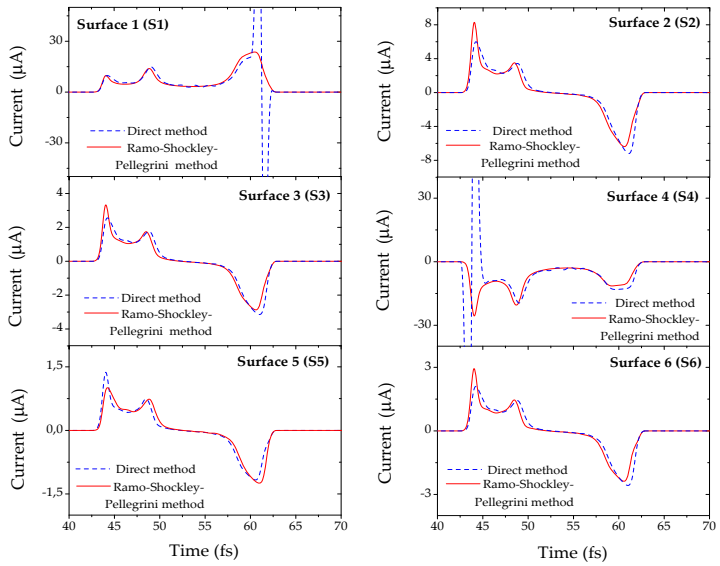

Figure 6.5: Time-dependent total current computed on the six surfaces that form the volume Ω of Fig. 5.2. The computation of the current within the first method (dashed lines) has spurious effects that are not present when the second method (solid line) is used.

The results reported in Fig. 6.6 are for a *RTD* including Coulomb correlation among the N electrons and among these electrons and those in the leads. Some behaviors can be observed. As pointed out in the inset a, $I_{tran}(t)$ manifests a delay of about $0.2ps$ with respect to the step input voltage, due to the dynamical adjustment of the electric field in the leads. After the delay, the current response becomes a RLC-like response (inset a, solid line RLC response 2) i.e. purely exponential. Performing the Fourier transform of $I_{tran}(t)$ (inset b solid line) and comparing with the single pole spectra (Fourier transform of RLC-like responses, inset b, dashed and dashed dotted lines) as depicted in the inset b, we are able to estimate the cut-off frequency (about 1.6 THz for this device) and the frequency offset (about 0.76 THz) due to the delay.

6.3.3 Current-current correlations

- **A.Alarcón, G.Albareda , F.L.Traversa and X.Oriols *Nanoelectronics: Quantum electron transport* in the book *"Applied Bohmian Mechanics: From Nanoscale Systems to Cosmology"*, edited by X. Oriols and J. Mompart, Panstanford Publishing, ISBN: 978-981-4316-39-2**

In the following example, we show how the *BITLLES* simulator can compute noise features. Each Bohmian trajectory used to evaluate the current is selected according to the $g-$ and $h-$ distribution (see Sec. 5.4.1) giving rise to the noise. Thus, in the *BITLLES* simulator the noise in the current can be easily obtained evaluating the autocorrelation function $R(\tau)$ of the current $I_{g,h}(t)$ from Eq. (5.38). Taking the Fourier transform, it gives the two-sided power spectrum $S(f)$ of the fluctuations of Eq. (5.39). In the following we will refer to the Fano factor as the ratio $\gamma = S(0)/S_{schot}$ with S_{schot} given by Eq. (5.40).

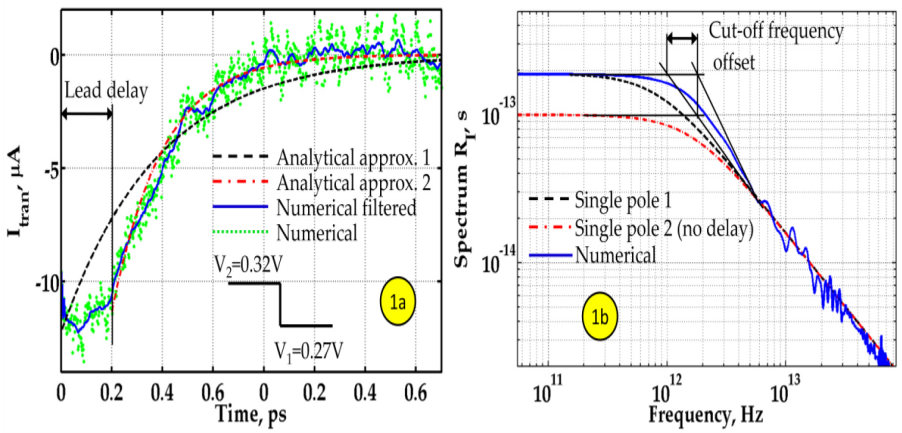

Figure 6.6: $I_{tran}(t)$ an its Fourier transform in inset a and b respectively.

We now briefly discuss on how the many-body Coulomb interaction might affect noise in RTDs. Specifically, we investigate on the correlation between an electron trapped in the resonant state during a dwell time τ_d and the ones remaining in the left reservoir. This correlation occurs essentially because of the trapped electron perturbs the potential energy felt by the electrons in the reservoir. In the limit of non-interacting electrons and mean field approximation, the Fano factor will be essentially proportional to the partition noise (see Fig. 6.7). However if the Coulomb correlation is self-consistently included in the simulations

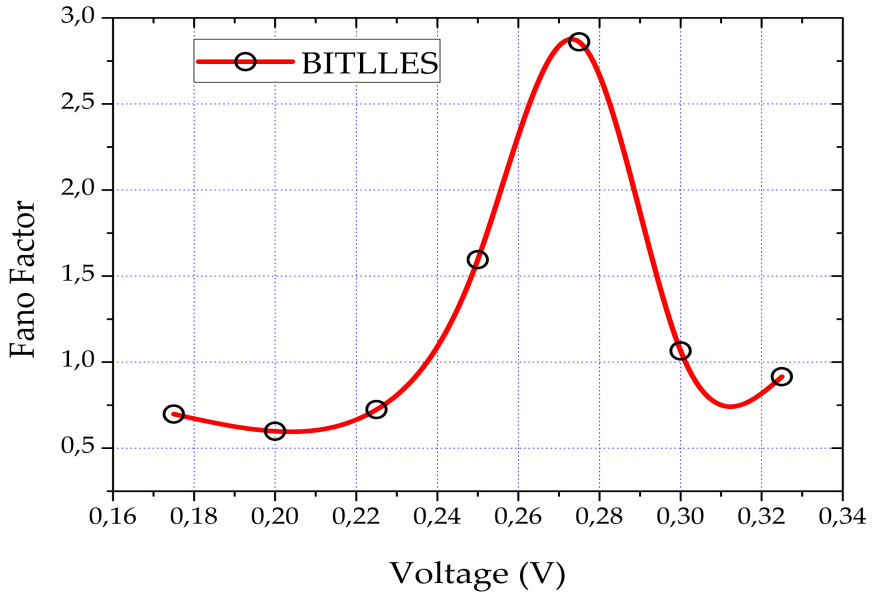

Figure 6.7: Fano Factor evaluated using the current fluctuations directly available from *BITLLES*

(see Sec. 5) this result is no longer reached. Roughly speaking, as depicted in Fig. 6.8, an electron tunneling into the well from the source, raises the potential energy of the well by an amount of e/C_{equ}, where e is the electron charge and C_{eq} the structure equivalent

capacitance. As a consequence, the density of state in the well is shifted upwards by the same amount. This can affect the noise in the following ways: If the resonant energy E_{R_1} is

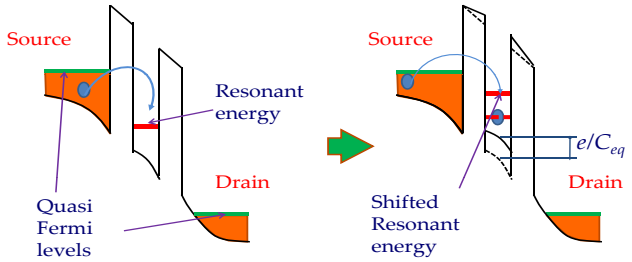

Figure 6.8: *RTD* Band diagram deformation caused by particle tunneling in the well

over the bottom of the conduction band in the source, when an electron enters into the well, the density of state inside the well is raised but it does not change much the transmittance of the sample for other electrons. The noise remains in the sub-poissonian regime ($\gamma < 1$) already present in the limit of partition noise only. Conversely if the resonant energy is under the conduction band at the source, the raised density of state because of the presence of an electron in the well makes accessible the resonant energy to other electrons staying near the bottom of the source conduction band. Therefore, many electrons in the source can tunnel into the well thanks to the first transmitted electron. Thus the Coulomb interaction tries to regroup the electrons providing a super-poissonian noise ($\gamma > 1$) (see Fig. 6.8).

Because of the inclusion of the time dependence self-consistent solution of the potential, with *BITLLES* simulator we are not only able to reproduce Fano factor for 0 frequency as reported in Fig. 6.9, but we can also evaluate the high frequency spectrum $S(f)$ given by Eq. (5.39) revealing information about internal energy scale of RTDs not available from DC transport.

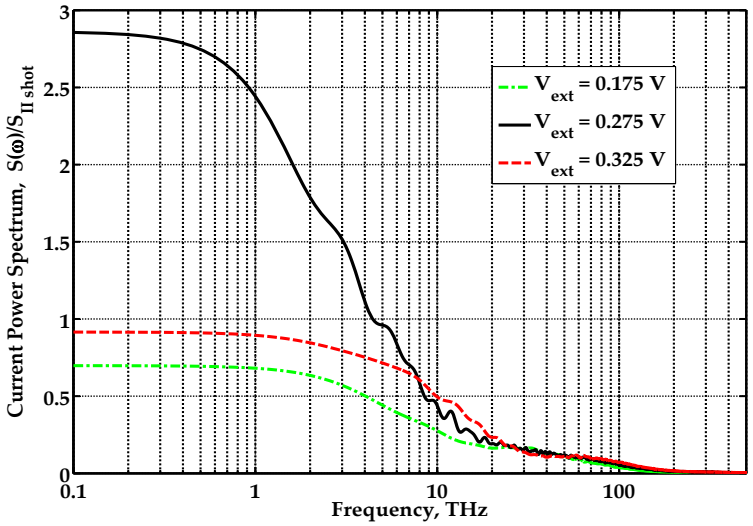

Figure 6.9: Current noise power spectrum referred to Poissonian shot noise at different biases.

6.4 Driven Tunneling Device (*DTD*)

The lack of devices capable of generating, detecting and processing signals at frequencies of Terahertz (THz) is currently one of the main difficulties for the progress of new technologies for communications. Nowadays, solid-state devices with nanometric dimensions can also generate output currents at THz frequencies (for example, some prototype transistors [121, 122] have been reaching gate lengths below 10 nm and frequencies working close to THz). Since the conduction current is directly related to the electron dynamics, electron transit times of few picoseconds [123] lead to output currents with THz frequencies.

In general, quantum electron transport in nanoscale systems is studied with static scenarios because of the electron transit time is much shorter than the inverse of any external frequency affecting the device active region. However, in quantum systems driven by THz signals the previous approximation is not valid and the electron transport cannot rely on (stationary) Hamiltonian eigenstates (i.e. the electron energy along the device active region is no longer a constant of motion). Several driven tunneling phenomena, such as control of tunneling [125], harmonic generation [124] or the manipulation of the population dynamics [130] are already discussed in the literature for different physical [126] or chemical [127] systems. However, to our knowledge, the use of driven tunneling phenomenology for developing THz electron devices remains practically unexplored, in part, because of the difficult coupling between quantum electron transport and electromagnetism [128, 129]. If electrons were neutral particles, only the Schrödinger equation determines their dynamics in nanoscale scenarios. However, electrons are charged particles and they obey Schrödinger and Maxwell equations, simultaneously[4].

[4]Interestingly, the coupling between semi-classical electron transport and electromagnetism has been already investigated [134, 135].

Here, we present a new type of nanoelectronic device designed to process signals at THz regime. We have called this device *Driven Tunneling Device* (*DTD*). It is a three terminal device where the drain-source conductance is controlled by a gate terminal that can oscillate at THz frequencies. The device active region is formed by a double barrier and a quantum well. *DTD* can operate at room temperature, as most double barrier devices, see Fig. 6.10.

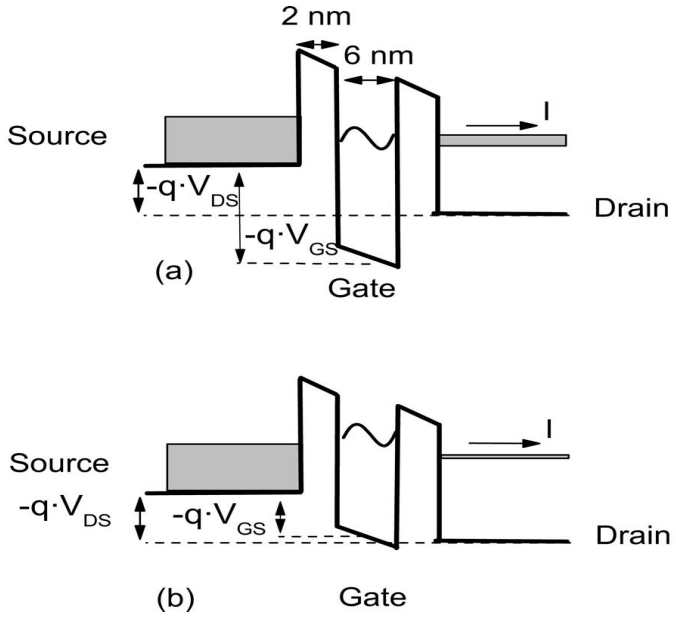

Figure 6.10: Schematic representation to explain the control on the source-drain current from the voltage applied in the gate terminal. a) From the voltage applied in the gate terminal the resonant energy in the quantum well is aligned with the energies of the bottom of the conduction band and the current increases. b) When voltage applied in the gate brokes the energetic alignment and the current source-drain decreases.

The original contribution of this proposal is the use of dynamically modulated tunneling [124, 125, 130] to control the output quantum current at THz frequencies (i.e. previous proposals [131, 132] do not exploit the capabilities of the driven tunneling phenomenology).

The essential characteristics that specify the *DTD* device are the following [133]:

1. The performance of *DTD* is based on coupling non-stationary quantum transport (i.e. quantum electron transport with Hamiltonians that vary at frequencies comparable to the inverse of the electron transit time) with electromagnetism.

2. The density of states inside the device active region of the *DTD* is designed/adapted by properly modifying the conduction or valence band (by introducing *perturbations* on the potential profile as double barrier structure).

3. The *DTD* is designed to produce an output current through the device active region of the *DTD* that is mainly due to quantum time-dependent conduction current. In other words, the *DTD* behaves as a conductor rather than as a dielectric, even at THz frequencies below.

Let us enlarge the explanation of these three basic characteristics of a *DTD* with the help of Fig. 6.11. In the inset of Fig. 6.11, we show a double barrier structure where the

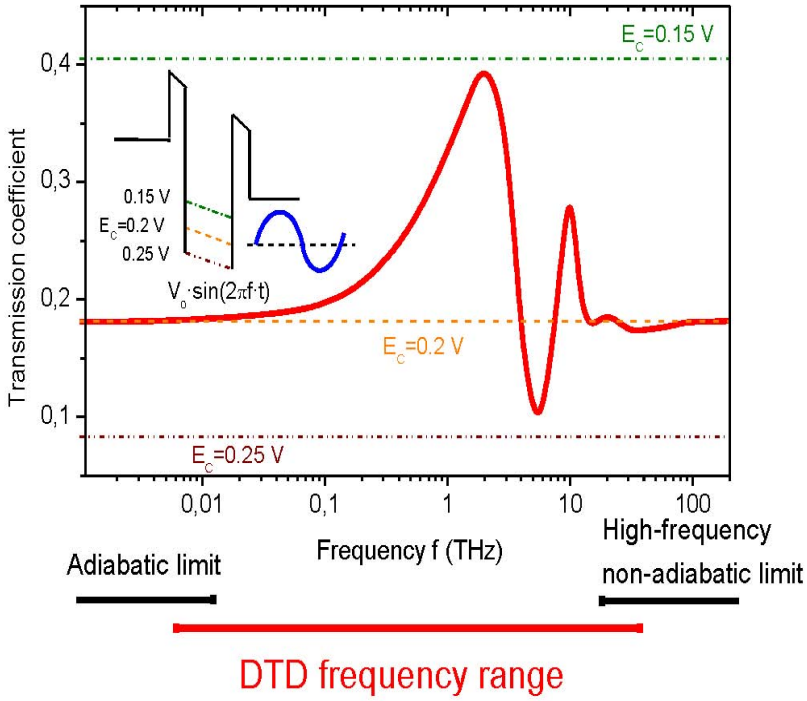

Figure 6.11: Transmission coefficient in function of the oscillating signal applied in the gate terminal. We have adiabatic limit for f $\rangle$ 100 GHz and non-adiabatic limit (high frequency) for f $\rangle$ 50 THz.

bottom of the conduction band varies sinusoidally. Figure 6.11 shows the evolution of the transmission probability of an electron in the double barrier when we vary the frequency of oscillation by means of the gate voltage. We can distinguish three different regimes by comparing the electron transit (dwell) time and the inverse of the frequency of the gate voltage [136, 137]:

1. ***Adiabatic limit***: If the potential variations that occurs at the gate are much slower than the times involved in the description of the dynamics of electrons them we are under a static or quasi-static regime and the quantum electron transport through the double barrier can be understood by quantum theories independent of time. For frequencies of few GHz can be assumed an adiabatic behavior of the system (the system varies slowly between static states) because of the dynamics of electrons in nanoscale devices involving transit times of order of picoseconds.

2. ***DTD working operation***: The *DTD* exploit the potential of quantum electron transport in non-static systems, i.e., when the adiabatic limit does not apply. For its part, the dynamic transmission coefficient varies between the maximum and the minimum of static transmission coefficient. For frequencies below 100 GHz (within the adiabatic limit) the transmission is not affected by the oscillation of the double barrier. However, when the frequency gets into the THz (comparable to the inverse of the transit time of electrons) the transmission coefficient depends of the frequency of oscillation.

3. ***Non-adiabatic limit*:** Finally, for frequencies much greater, non-adiabatic limit of very high frequency, the result is still independent of the frequency of the oscillations of the gate voltage.

As shown in Fig. 6.11, the range of frequencies where *DTD* can operate exactly focuses the THz frequencies (the limit can be extended to adiabatic or non-adiabatic high frequency for particular applications).

It is noteworthy that in *DTD*, the transit time of electrons is controlled largely by the potential barrier (height and width). On the other hand, *DTD* can be implemented with different systems containing some kind of interaction that form energy barriers (such as double or triple barriers, and even multiple barriers). Therefore, the exact range of frequencies shown in Fig. 6.11 can change with other *DTD* configurations. In particular, we have developed our proposal to double potential barrier, as described Fig. 6.11. Thus, from a manufacturing point of view, *DTD* devices allow different implementations. The only prerequisite is to have a potential profile of double / multiple barrier with a total length of few nanometers[5]. Finally, it is important mention that the habitual static (or quasi-static)

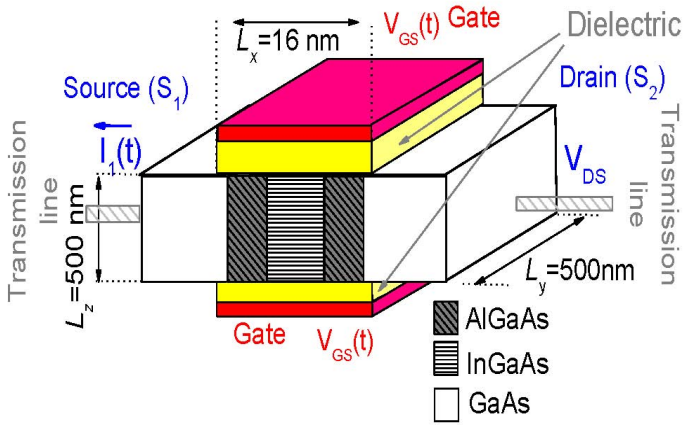

Figure 6.12: Schematic representation of a frequency multiplier *DTD* composed of a double barrier heterostructure inside the channel of a double-gate field effect transistor.

applications of tunneling devices depend on the exact value of resonant energies and these can vary of a devices to other because of small fluctuations of the barriers dimensions or imperfections of fabrication. On the contrary, the operation of *DTD* is based in the presence or not of resonant energies, without being important its exact value as this value varies with the gate voltage.

[5]In detail, one of the possible proposals for the manufacture of the devices is to use *DTD* techniques and manufacturing technologies for MOSFETs (such as double gate devices mentioned in Fig. 6.12) introducing into the canal two materials with an energy gap greater than the Si to form double barrier structure. For its part, the control of double barrier profile can be achieved through the gate voltages through of typical field effect of MOSFETs (i.e., the Coulomb interaction between electrons in the gate and channel). The configuration of double-gate MOSFET allows a robust control of the potential profile for nanoscale transistors

6.5 *DTD* applications

- **Source: X. Oriols, F. Boano, and A. Alarcón Self-consistent coupling between driven electron tunneling and electromagnetic propagation at terahertz frequencies Applied Physics letters., 92, No 22 (2008).**
- **Source: X. Oriols, A. Alarcón, L. Baella. Dynamically modulated tunneling for multipurpose electron devices: Application to THZ frequency multiplication. Solid-State Electronics, 51, 1287-1300 (2007).**

In this section we configure *BITLLES* as a *DTD* device. The results presented here, follows the reference [3][6].

In this section we present two of the possible *DTD* applications, in detail, a rectifier and a frequency generator. The computation of the total current for both applications is made exclusively by Ramo-Shockley-Pellegrini theorems explained in section Sec. 5.4.2 using Eq. (5.32) for the conduction current and Eq. (5.33) for the displacement current.

In order to compute both applications we design a *DTD* with source and drain AsGa regions and with two *AlAsGa* potentials barriers. The dimensions of the different regions of *DTD* depends of the particular application.

In all of the *DTD* $3D$ structure we apply an effective mass of $m = 0.068m_o$ where m_o electron free mass of the electrons. The Fermi energy has a value of $0.25eV$. The quantum transport takes place from source to drain in the x direction. The lateral area of *DTD* is sufficiently small to consider electron confinement. In detail, the lateral area in the y direction is $3nm$ and in the z direction is the $4.8nm$.

6.5.1 Frequency Rectifier

As a first example, we consider a *DTD* with a double barrier of $1.5nm$ with a height of $0.6eV$ and a quantum well with a value of $2.5nm$. We also apply a frequency at the gate terminal, $V_G(t)$, of $250GHz$. In Fig. 6.13, in the red line, we show the input signal voltage that we apply at the gate terminal of *DTD*. While in the black line show the rectified output signal. The rectification is carried out because of the gate negatives values. In this case the electrons find a resonant barrier that avoid the pass of current.

[6]The equations presented in reference [3] are written in a general form and are also valid for both single and many- particle systems.

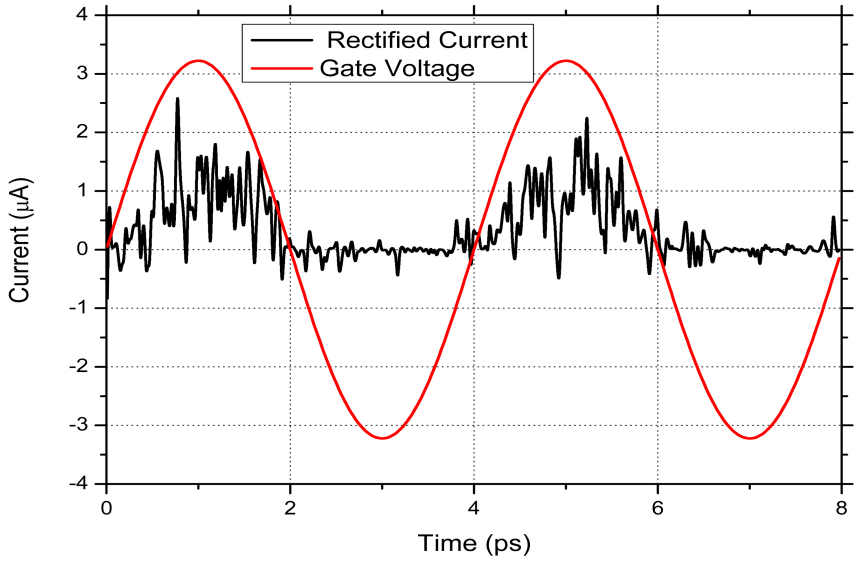

Figure 6.13: Red line: We present the *DTD* applied gate voltage that is the input signal. Black line: We present the rectified signal that corresponds at the output signal of *DTD*.

6.5.2 Frequency multiplier

Here, we consider a *DTD* with a double barrier of $1.5nm$ with a height of $0.8eV$ and a quantum well with a value of $5.1nm$. We apply a frequency at the gate terminal of $100GHz$. In Fig. 6.14 we show in the red line a period of the gate voltage and in the black line we show the generated signal with a period of $200GHz$. The multiplication appears because of the gate negative bias values, the electrons find another resonant energy different from the one used in the positive bias values.

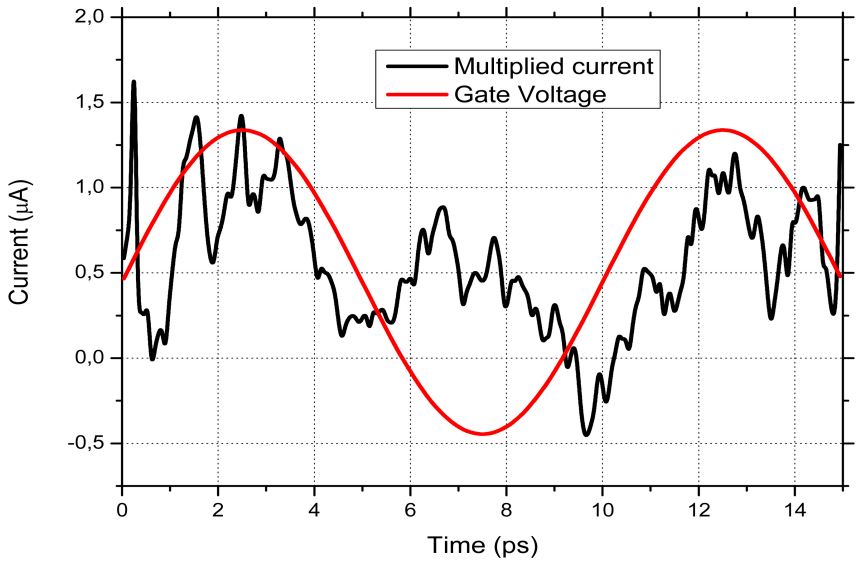

Figure 6.14: Red line: We present the *DTD* applied gate voltage that is the input signal. Black line: We present the multiplier signal that corresponds at the output signal of *DTD*.

6.6 Exchange interaction in a nano-resistor

In Sec. 4.2 we have introduced how to treat exchange interaction with Bohmian trajectories in a spinless system. This interaction has the effect of imposing restrictions at the maximum number of electrons in the device active region and, by extension, in the total current across the system. Previous results (Sec. 6.3 and Sec. 6.5) have been obtained with Coulomb correlations, but without exchange correlations. Here, we consider the importance of the exchange correlations in the prediction of the I-V characteristic of a nano-resistor, see Fig. 6.15.

6.6.1 Computation of I-V characteristic in a nano-resistor with exchange interaction

We configure the *BITLLES* simulator as the nano-resistor depicted in the Fig. 6.15, with N^+ doped source and drain AsGa regions and a device active region of $L_x = 30nm$.

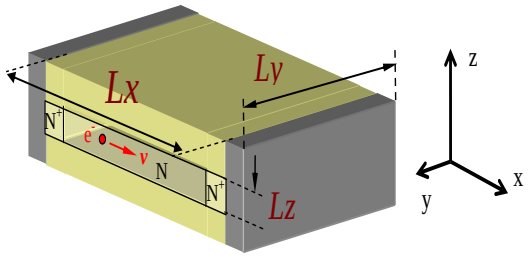

Figure 6.15: Nano-resistor designed with N^+ doped source and drain AsGa regions, a device active region of $L_x = 30nm$, an effective mass $m^*_{AsGa} = 0.067m_0$ with m_0 the electron free mass and a fermi level of $0.15eV$. The lateral dimensions are $L_y = L_z = 9nm$.

The lateral dimensions are $L_y = L_z = 9nm$. We assume a constant effective mass $m^*_{AsGa} = 0.067m_0$ with m_0 the electron free mass and we consider a fermi level of $0.15eV$. Room temperature is also considered in all simulations. We consider that the transport takes place from source to drain in the x direction. We study a $1D$ system ($L_x \gg L_y, L_z$), where we only take into account the first energy of the subband of $AsGa$ with a value of $E_1 = 0.13eV$, just below of fermi energy.

In Fig. 6.16, we present the I-V curves of the simulated system for four different scenarios under an applied source-drain bias: without correlation (square black line), with exchange correlation (circle red line),with Coulomb correlation (up triangle blue line) and with Coulomb plus exchange correlations (down triangle green line).

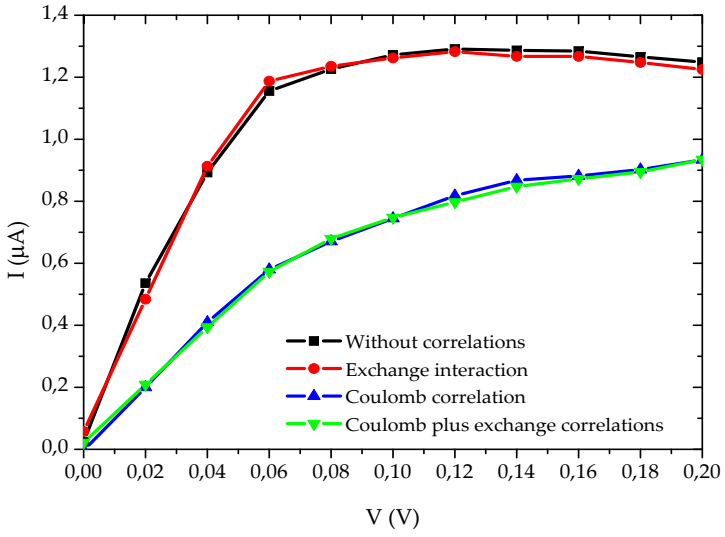

Figure 6.16: We present the I-V curves for the simulated system in four different situations: without correlation (*square black line*), with exchange correlation (*circle red line*), with Coulomb correlation (*up triangle blue* line) and Coulomb plus exchange correlations(*down triangle green line*). In this figure, we consider the importance of exchange correlations in the prediction of the I-V characteristic of a typical nano-resistor.

The differences between the current values in the different plots of Fig. 6.16 are consequence of the Coulomb and exchange interactions. We can explain this fact with the next two figures centering our explanation in the effect of the exchange interaction. The first one is the Fig. 6.17, where we plot the time-average (mean) number of electrons that travels from drain to source (square black line, red circle blue line, up triangle blue line and down triangle green line) and from source to drain (square black dotted line Circle red dotted line, up triangle blue dotted line and down triangle green dotted line). These electrons crossing the system are responsables of the DC current.

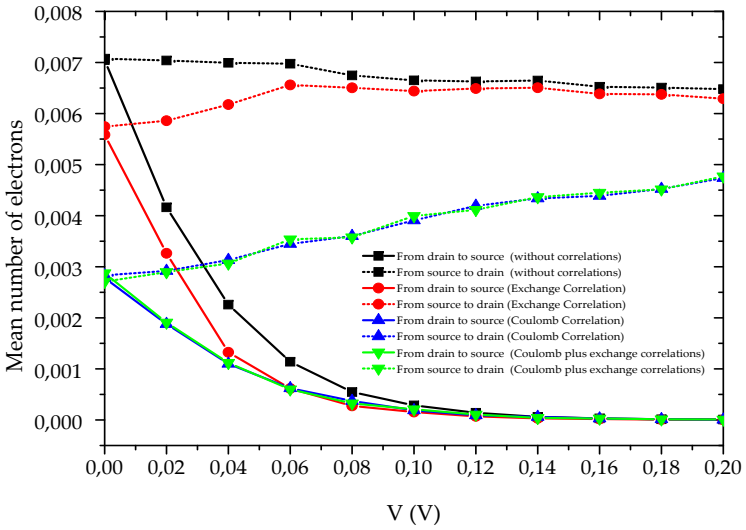

Figure 6.17: *Square black line*, *red circle blue line*, *up triangle blue line* and *down triangle green line*: we plot the main number of electrons from drain to source for the different situations showed in Fig. 6.16. *Square black dotted line*, *circle red dotted line*, *up triangle blue dotted line* and *down triangle green dotted line*: we plot the main number of electrons from source to drain for the different situations showed in Fig. 6.16.

The second is the Fig. 6.18, where we plot the time-average number of electrons injected from the drain that have been bounced (square black line, circle red line, up triangle blue line and down triangle green line) and the time-average number of electrons injected from the source that have been finally reflected (square black dotted line, circle red dotted line, up triangle blue dotted line and down triangle green dotted line).

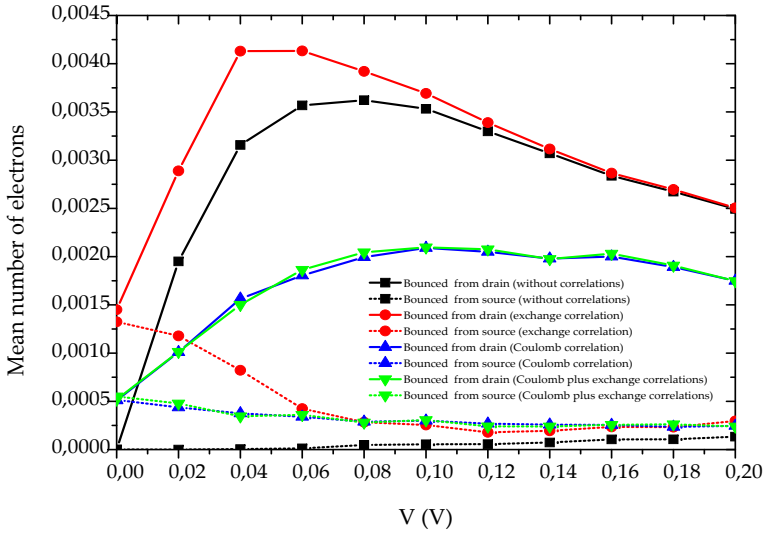

Figure 6.18: *Square black line,circle red line*, *up triangle blue line* and *down triangle green line*: we plot the main number of electrons injected from drain that have been bounced for the different situations showed in Fig. 6.16. *Square black dotted line*, *circle red dotted line*, *up triangle blue dotted line* and *down triangle green dotted line*: we plot the main number of electrons injected from source that have been bounced for the different situations showed in Fig. 6.16.

These electrons are reflected and do not cross the device active region. Therefore, these electrons do not contribute to the DC current only to the AC current.

The more interesting effect that appears in Figs. 6.17 and 6.18 is at low bias. When exchange interaction is not considered, electrons injected from the source and drain are finally transmitted. However, when exchange interaction is considered these electrons will try to occupy the same positions and the electrons will be reflected. This has been explained in the last paragraphs of Sec. 4.3.2. This explains the differences in the low bias of Fig. 6.17.

At high bias, we see that electrons are mainly coming from the source. Then, an exchange interaction with the same sign of the velocity appears. We do also see that Coulomb interaction is very strong and the effect of the exchange interaction is not appreciated when the strong Coulomb interaction is present.

6.6.2 Computation of the noise characteristic in a nano-resistor with exchange interaction

As commented in Sec. 5.4.3 one of the most relevant advantage of Bohmian mechanics is its use to compute current fluctuations. In the following example, from the time-dependent current provided by the *BITLLES* simulator, we compute noise characteristics of the nano-resistor. We design *BITLLES* simulator with the same general parameters of the nano-resistor presented in Sec. 6.6.1. The fluctuations of the current can be easily obtained from the autocorrelation function $R(\tau)$ of the current $I_{g,h}(t)$ (see Sec. 5.4.2) from Eq. (5.38). As

in Sec. 6.3.3 we define the Fano factor as the ratio $\gamma = S(0)/S_{schot}$ with S_{schot} given by Eq. (5.40).

In a system without correlations among electrons the noise are produced only by the injection of electrons from contacts into de device active region. In this case, the computation of the noise does only need the knowledge of the injection probability $P(N, \tau)$ defined in Sec. 5.3.1.3. The fluctuations of the injection produces basically a Poissonian noise. Deviations from this Poissonian value are due to the Coulomb and exchange correlations that we include inside the device active region.

In Fig. 6.19 we plot the Fano factor evaluated in four different scenarios under an applied source-drain bias: without correlation (square black line), exchange correlation (circle red line), Coulomb correlation (up triangle blue line) and Coulomb plus exchange correlations (down triangle green line). In this figure it is show that for low bias the system is super-Poissonian ($\gamma \gg 1$). We can explain this results from Eq. (5.40) where if the mean value of the current, that we show in Fig. 6.16, is small then the value of Fano factor is high. In detail, the value of the current is the result of the rest of drain and source components. On the contrary the Fano factor is the result of the sum of drain and source components of the noise. For high bias the injection of electrons is carried out principally from source and the Fano factor tends to a Poissonian value ($\gamma = 1$). For more details see reference [91].

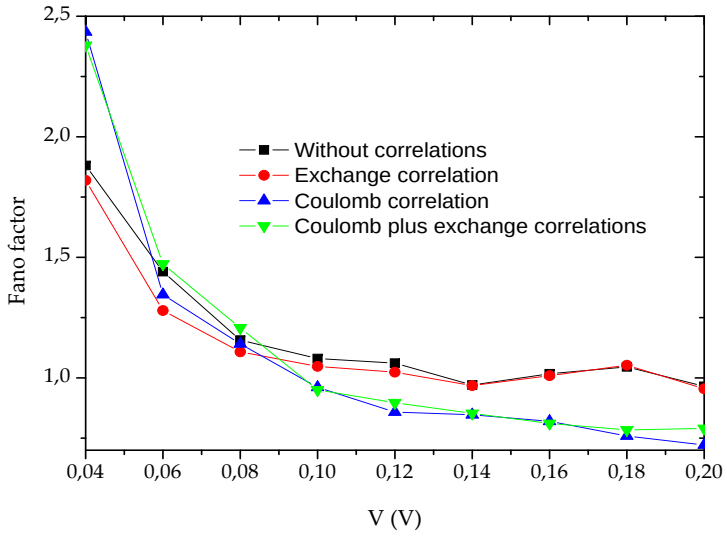

Figure 6.19: Fano factor evaluated in a nano-resistor using the current fluctuations computed from different bias computed using *BITLLES* simulator.

If we make a Fourier transform of the autocorrelation function $R(\tau)$, we obtain the current power spectrum $S(\omega)$ of Eq. (5.39). We can complete the explanation of noise characteristic of the nano-resistor computing the current power spectrum selecting three different values of V, in particular, $0,06V$, $0,10V$ and $0,20V$ as we show in Fig. 6.19. In detail, in each of the following figures we present the next simulations: without correlations (black solid line), with exchange correlation (dashed red line), with Coulomb correlation (dotted blue line) and with Coulomb plus exchange correlation (dash dotted green line).

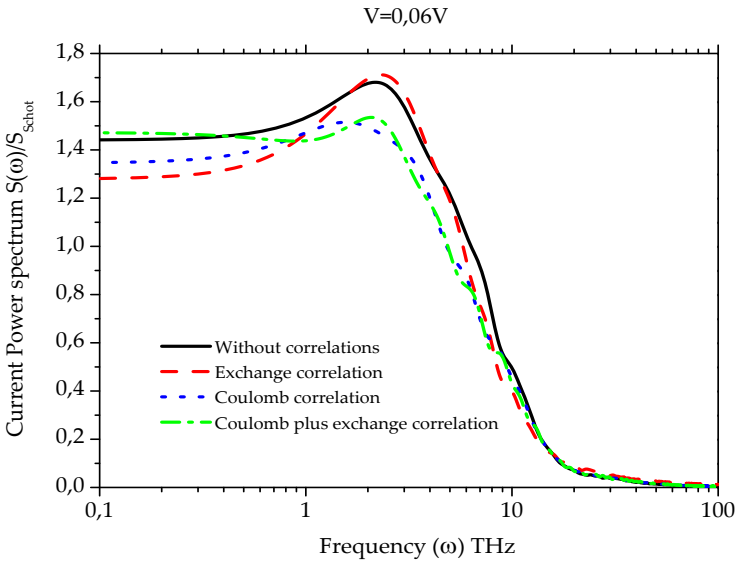

Figure 6.20: We present the current power spectrum for $V = 0,06V$. The noise has almost a Poissonian value for all cases but still super-Poissonian. The fluctuation of the current power spectrum around 1THz is because of the number of electrons bounded for low bias.

In Fig. 6.20 the fluctuations of the current has almost Poissonian value for all cases but still super-Poissonian. The fluctuation of the current power spectrum around 1THz is because of the number of electrons bounded for low bias as we can see in figure Fig. 6.18. The fluctuation is more relevant especially for exchange correlations for the reason that we have mentioned in the previous subsection: The reflected electrons do not affect the DC current, but they affect the AC value.

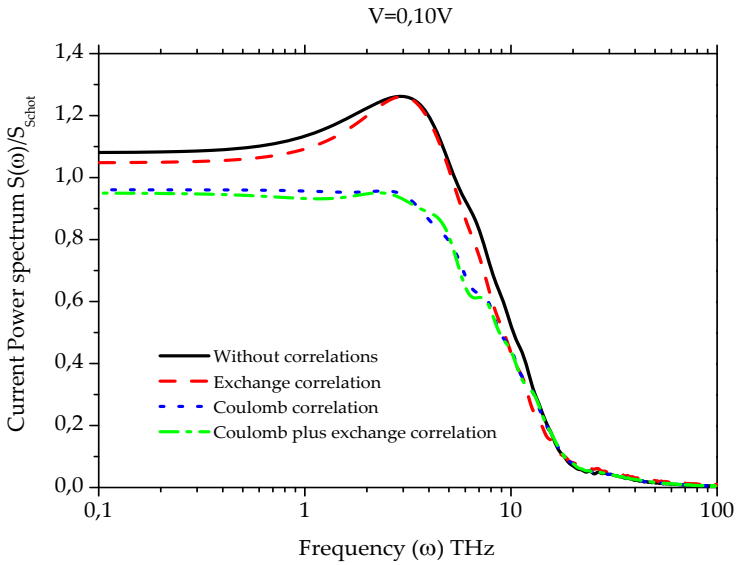

Figure 6.21: We present the current power spectrum for $V = 0, 10V$. the noise is Poissonian for simulations without correlations and with exchange correlation but is sub-Poissonian ($0 < \gamma < 1$) for simulations with Coulomb and Coulomb plus exchange correlations.

In Fig. 6.21 the system is Poissonian for simulations without correlations and with exchange correlation but is sub-Poissonian ($0 < \gamma < 1$) for simulations with Coulomb and Coulomb plus exchange correlations.

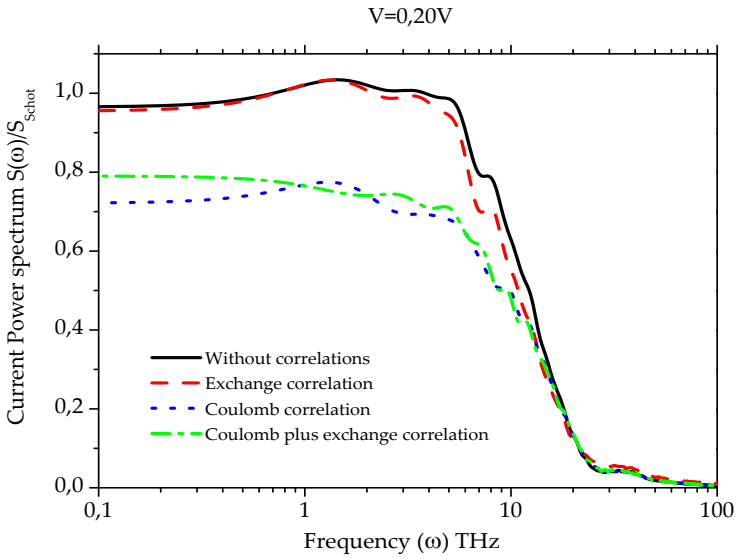

Figure 6.22: We present the current power spectrum for $V = 0, 20V$. From high bias, we realize that the electrons are not have bounced so we do not have any perturbation of the spectrum for 1THz.

In Fig. 6.22 from high bias, we realize that the electrons are not have bounced so we do not have any perturbation of the spectrum for 1THz as we have shown in Fig. 6.18.

In summary, the present results are still unpublished and more simulations are still needed to discuss as for example some differences found in Fig. 6.19 that are not mentioned here. In any case, the ability of the *BITLLES* simulator to compute higher moments and the utility of noise to characterize correlations is clearly manifested with these preliminary results.

Chapter 7

Conclusions

Nowadays, the present status of Bohmian mechanics among the scientific community is quite marginal. Most researchers do not know nothing about it or believe that is not fully correct. There are many others that know that quantum phenomena can become interpreted in terms of trajectories, but they think that this formalism cannot be useful in their daily research activity. In my opinion, the Bohmian mechanics can only leave its current marginal status and be a recognized theory, when a relevant application build from Bohmian mechanics is successfully recognized among the scientific community, see *chapter 3*. In particular, the most significative goal of this thesis is the collaboration in the development of the *BITLLES* simulator. We believe that this simulator can be, perhaps, the first revelent contribution of Bohmian theory to the field of quantum electron transport.

The two relevant features of *BITLLES* simulator are:

1. **Its ability to deal with many-particle problem with Coulomb and exchange correlations**: The many-particle Schrödinger equation can only be solved for very few degrees of freedom. This issue is at the heart of most of the unsolved problems in quantum transport (the so-called many-particle problem). Following [1], we have presented a new approximation to solve the many-particle problem based on Bohmian mechanics. This quantum electron transport model take into account the Coulomb and exchange correlations using Bohmian trajectories, see *chapter 2*. In fact, the *BITLLES* solves the many-particle correlations solving the time-dependent Poisson equation self-consistently with the time-dependent many-particle schrödinger equation.

2. **Its ability to provide a full information of the all moments current distribution**: Contrarily to the standard interpretation of quantum mechanics, the continuous measurement of the current is not a delicate issue with Bohmian mechanics because of the measured quantities depend, ultimately, on the distribution of positions of a set of Bohmian particles (i.e. no wavefunction collapse is invoked). Only a reasonable approximation of the role of the ammeter on the dynamics of simulated electrons and an ensemble averaging (or time averaging for ergodic systems) are needed. We have shown that we can compute the probabilities of all available current values. From this result, we can compute the average (first moment), the variance (second moment) and any other higher moment of the distribution of the current.

The main contributions of this thesis to the development of *BITLLES* simulator are:

1. ***Exchange interaction***: We introduce the exchange interaction to treat many-particle systems with spinless electrons. In this context, we show how exchange interaction is the final responsible for determining the total current across the system. A new approximation to study many-particle systems with spin of different orientations is present. We have developed all this ideas in *chapter 4*. Some practical examples are studied taking into account the exchange interaction.

2. ***The computation of the time-dependent total (conduction and displacement) current***: The practical implementation of the time-dependent total (conduction plus displacement) current in the *BITLLES* simulator is achieve by means of the self-consistent time-dependent solution of the Poisson equation using the Ramo-Shockley-Pellegrini theorems. Thus, the continuity of the total current is guarantied. We have developed the main ideas in *chapter 5*. Finally, in *chapter 6*, different capabilities of *BITLLES* simulator such as DC, AC and fluctuations are showed using *RTD* and *DTD* devices.

3. ***The Driven Tunneling Device***: We have presented a new type of nanoelectronic device designed to process signals at THz regime. We have named this device *Driven Tunneling Device* (*DTD*). It is a three terminal device where the drain-source conductance is controlled by a gate terminal that can oscillate at THz frequencies. We have developed the mean ideas and different examples of this device in *chapter 6*.

4. ***Tight-binding***: In order to improve the definition of the band-structure we have developed a numerical approximation to solve the Schrödinger equation using tight-binding model. Here, we develop the tight-binding Hamiltonian taking into account the Coulomb interaction among electrons. We have developed this ideas in the *appendix*.

An interesting initiative to recognize the important application of Bohmian mechanics in different field of science is summarize in the book: *Applied Bohmian Mechanics: From Nanoscale Systems to Cosmology*, [4], edited by X.Oriols and J.Mompart. We sincerely believe that the present Bohmian formulation of quantum transport has computational advantages over previous *orthodox* simulation tools. Therefore, since electron devices are present in almost every moment of our lives, we hope that the *BITLLES* simulator will be, perhaps, one of the first examples where Bohmian mechanics do really help in improving our real life.

Chapter 8

Bibliography

Bibliography

[1] X. Oriols, *Quantum trajectory approach to time dependent transport in mesoscopic systems with electron-electron interactions*, Phys. Rev. Let. **98**(6), 066803–066807 (2007).

[2] G. Albareda, J. Suñé, and X. Oriols, *Many-particle hamiltonian for open systems with full Coulomb interaction: Application to classical and quantum time-dependent simulations of nanoscale electron devices*, Phys. Rev. B, **79**(7), 075315–075331 (2009).

[3] A.Alarcón and X.Oriols, *Computation of quantum electron transport with local current conservation using quantum trajectories*, Journal of Statistical Mechanics: Theory and Experiment. **Volume: 2009(P01051)** (2009).

[4] X.Oriols and J.Mompart, *Applied Bohmian Mechanics: From Nanoscale Systems to Cosmology*, Pan Stanford Publishing (2011). **ISBN:** 978-981-4316-39-2.

[5] G. Albareda, *Classical and quantum trajectory-based approaches to electron transport with full Coulomb correlation* PhD. Thesis, Universitat Autònoma de Barcelona (2010).

[6] W. Shockley, *Currents to conductors induced by a moving point charge*, J. Appl. Phys., **9**, 635 (1938).

[7] S. Ramo, *Currents induced by electron motion*, Proc. IRE. **27**(584), 584–585 (1939).

[8] B.Pellegrini, *Electric charge motion, induced current, energy balance, and noise*, Physical Review B, 34(8), 5921 (1986).

[9] B. Pellegrini, *Elementary applications of quantum-electrokinematics theorem*, Il Nuovo Cimento D, **15**, 881 (1993).

[10] B. Pellegrini, *Extension of the electrokinematics theorem to the electromagnetic field and quantum mechanics*, Il Nuovo Cimento D, **15**, 855 (1993).

[11] A. Corbin, *The Third Element: A Brief History of Electronics*, Bloomington, IN : AuthorHouse (2006).

[12] Wangsness, *Electromagnetic fields*, John Wiley and Sons, Inc (1996).

[13] Intl. Technology Roadmap for Semiconductors.
`http://www.itrs.net/`

[14] M. Di Ventra, *Electrical transport in nanoscale systems*, Cambridge University Press, The Edinburgh Building, Cambridge CB2 8RU, UK, First edition (2008).

[15] Eckehard Schöll, *Theory of transport properties of semiconductor nanostructures*, CHAPMAN and HALL (1998).

[16] `http://www.ief.u-psud.fr`

[17] DAMOCLES: Monte Carlo simulation of semiconductor devices. `http://www.research.ibm.com/DAMOCLES/`

[18] David K. Ferry, Harold L. Grubin, Carlo Jacoboni and anti-Pekka Jauho *Quantum transport in ultrasmall devices* Plenum Pres, New York and London, Published in co-operation with NATO Scientific Affairs Division (1994).

[19] R. Landauer, *Electrical resistence of disordered one-dimensional lattices*, Philos. Mag. **21**, 863 (1970).

[20] R. Landauer, *Spatial variation of currents and fields due to localized scatterers in metallic conduction*, IBM Journal of research and development, **1**, 223 (1957).

[21] The absence of Coulomb interaction in electron systems was explained, first, by Landau in terms of the Fermi Liquid paradigm, where the real electrons were sub- stituted by quasi-electrons with a negligible Coulomb interaction among them: L. D. Landau, Soviet Physics Jetp-Ussr 8, 70 (1959); L. D. Landau, Soviet Physics Jetp-Ussr **3**, 920 (1957).

[22] M. Büttiker, A. Pretre and H. Thomas, Phys. Rev. Lett., **70**, 4114 (1993).

[23] M. Büttiker, H. Thomas and A. Pretre, Z. Phys. B, **94**, 133 (1994).

[24] M. Büttiker, J. Phys.: Condens. Matter, **5**, 9361 (1993).

[25] M. Büttiker and S. E. Nigg, Nanotechnology, **18**, 044029 (2007).

[26] M. C. Goorden and M. Büttiker M, Phys. Rev. Lett., **99**, 146801 (2007).

[27] E. Wigner, *On the quantum correction for thermodynamic equilibrium, Physical Review*, **40**, 5, 749 (1932).

[28] V. Sverdlov, E. Ungersboek, H. Kpsina, and S. Selberherr, *Current transport models for nanoscale semiconductor devices*, Materials Science and Engineering: Reports, **58**, 228 (2008).

[29] L. V. Keldysh, Zh. Eksp. Teor. Fiz., **47**, 1515 (1964).

[30] L. V. Keldysh, Sov. Phys. JETP, **47**, 804 (1978)

[31] S. Datta, *Electronic transport in mesoscopic systems*, Cambridge University Press (1995).

[32] The Nanoelectronic Modeling Group. NEMO1D
https://engineering.purdue.edu/gekcogrp/software-projects/nemo1D/

[33] The Nanoelectronic Modeling Group. NEMO3D
https://engineering.purdue.edu/gekcogrp/software-projects/nemo3D/

[34] W.Kohn and L.J.Sham, Phys. Rev. A, **140**, 1163 (1965).

[35] J. Kondo, *Resistance minimum in dilute magnetic alloys*, Progress in Theoretical Physics, **32**, 37 (1964).

[36] J. M. Luttinger, *An exactly soluble model of a many fermion system*, Journal of Mathematical Physics, **4**, 1154 (1963).

[37] P. Hohenberg and W. Kohn, *Inhomogeneous electron gas*, Physisical Review, **136**, B864 (1964).

[38] W. Kohn and L. J. Sham, *Self-consistent equations including exchange and correlation effects*, Phys. Rev., **140**(4A), A1133 (1965).

[39] J. M. Soler, E. Artacho, J. D. Gale, A. Garcia, J. Junquera, P. Ordejon and D. Sanchez-Portal, *The SIESTA method for ab initio order-N materials simulation*, Journal of Physics: Condensed Matter, **14**, 2745-2779 (2002).

[40] `http://www.tcm.phy.cam.ac.uk/~mdt26/casino2.html`

[41] `http://vonbiber.iet.unipi.it/Transiestatutorial/transiesta.html`

[42] `http://www.gaussian.com/`

[43] E. Runge and E. K. U. Gross, *Density-functional theory for time-dependent systems*, Physical Review Letters, **52**, 12, 997 (1984).

[44] `http://www.tddft.org/`

[45] J.M. Thijssen, *Computational Physics*, Cambridge University Press (1999).

[46] *Quantum Monte Carlo Methods in Physics and Chemistry*, M. P. Nightingale, Cyrus J. Umrigar, Springer (1999).

[47] *Quantum Monte Carlo Methods in Condensed Matter Physics*, M. Suzuki,World Scientific (1993).

[48] G. F. Giuliani and G. Vignale, *Quantum Theory of electron Liquid*, Cambridge University Press (2005).

[49] M. Di Ventra and R. D'Agosta, *Stochastic time-dependent current-density- functional theory*, Physical Review Letters, **98**, 22, 226403 (2007).

[50] M. Planck, *On the Law of Distribution of Energy in the Normal Spectrum*, Annalen der Physik, **4**, 553 (1901).

[51] A. Einstein, *ber einen die Erzeugung und Verwandlung des Lichtes betreffenden heuristischen Gesichtspunkt*, Annalen der Physik, **17**, 132 (1905).

[52] G.N. Lewis, *The conservation of photons*, Nature **118**(2), 874 (1926); See also `http://www.nobeliefs.com/photon.htm`

[53] N. Bohr, *On the Constitution of Atoms and Molecules, Part I*, Philosophical Magazine, **26**, 1 (1913).

[54] N. Bohr, *On the Constitution of Atoms and Molecules, Part II Systems Containing Only a Single Nucleus*, Philosophical Magazine, **26**, 476 (1913).

[55] N. Bohr, *On the Constitution of Atoms and Molecules, Part III Systems containing several nuclei*, Philosophical Magazine, **26**, 857 (1913).

[56] L. De Broglie, J. Phys. Radium, **8**, (1927).

[57] W. Heisenberg, *Über quantentheoretishe Umdeutung kinematisher und mechanischer Beziehungen*, Zeitschrift für Physik, **33**, 879 (1925); English translation in Ref. [65].

[58] M. Born and P. Jordan, *Zur Quantenmechanik*, Zeitschrift für Physik, **34**, 858 (1925); English translation in Ref. [65].

[59] W. Heisenberg, *Über den anschaulichen Inhalt der quantentheoretischen Kinematik und Mechanik*, Zeitschrift für Physik, **43**(34), 172 (1927).

[60] M. Born, *Zur Quantenmechanik der Stovorgänge*, Zeitschrift für Physik **37**, 863 (1926).

[61] M. Born, W. Heisenberg, and P. Jordan, *Zur Quantenmechanik II*, Zeitschrift für Physik, **35**, 557 (1925); English translation in Ref. [65].

[62] L. de Broglie, *Recherches sur la théorie des quantas*, Ann. de Physique, **3**, 22 (1925).

[63] E. Schrödinger, *An Undulatory Theory of the Mechanics of Atoms and Molecules*, Phys. Rev., **28**, 1049 (1926).
L. de Broglie, *Recherches sur la théorie des quantas*, PhD. Thesis, University of Paris (1924); See also [62].

[64] L. de Broglie *La mécanique ondulatorie et la structure atomique de la meterie et du rayonnement*, Le Journal de Physique et le Radium, **6**(8), 225 (1927).

[65] B. L. van der Waerden, *Sources of Quantum Mechanics*, Dover Publications (1968).

[66] B. L. van der Waerden, *From Matrix Mechanics and Wave Mechanics to Unified Quantum Mechanics*, Notices of the AMS, **44**, 323 (1997).

[67] G. Bacciagaluppi and A. Valentini, *Quantum Theory at the Cross-roads: Reconsidering the 1927 Solvay Conference* (Cambridge University Press, Cambridge (2009).

[68] L. de Broglie, *Tentative dinterpretation causale et non-lineairie de la mecanique ondulatorie*, Gauthier-Villars, Paris (1956).

[69] D. Bohm, *A suggested interpretation of the quantum theory in terms of "hidden" variables I*, Phys. Rev., **85**, 166 (1952).

[70] D. Dürr and S. Teufel, *Bohmian Mechanics: The Physics and Mathematics of Quantum Theory*, Spinger, (2009).

[71] D. Bohm, *A suggested interpretation of the quantum theory in terms of "hidden" variables II*, Phys. Rev., **85**, 180 (1952).

[72] P. R. Holland, *The Quantum Theory of Motion: An account of the de Broglie-Bohm Causal Interpretation of Quantum mechanics*, Cambridge University Press, Cambridge (1993).

[73] D. Bohm and B. J. Hiley, *The Uundivided Universe: An Ontological Intepretation of Quantum Theory*, Routledge & Kegan Paul, London (1993).

[74] A. Valentini, *Pilot-Wave Theory: An Alternative Approach to Modern Physics*, Cambridge University Press, Cambridge (2006).

[75] J. T. Cushing, A. I. Fine and S. Goldstein, *Bohmian Mechanics and Quantum Theory: An Appraisal*, Kluwer, Dordrecht (1996).

[76] D. R. Hartree, *The Wave Mechanics of an Atom with a Non-Coulomb Central Field. Part I. Theory and Methods*, Mathematical Proceedings of the Cambridge Philosophical Society, **24**(01), 89 (1928).

[77] D. R. Hartree, *The Wave Mechanics of an Atom with a Non-Coulomb Central Field. Part II. Some Results and Discussion*, Mathematical Proceedings of the Cambridge Philosophical Society, **24**(01), 111 (1928).

[78] M. Daumer, D. Dürr; S. Goldstein, et al., *Naive realism about operators*, Probability, Dynamics and causality, **45**(2-3), 379 (1997).

[79] L. D. Landau and E. M. Lifschitz, *Quantum Mechanics Non-Relativistic Theory*, Pergamon Press Ltd., London (1958).

[80] W. Struyve, *The de Broglie-Bohm pilot-wave interpretation of quantum theory*, PhD. Thesis, Universiteit Gent (2004), published also online arXiv:quant-ph/0506243.

[81] C. Colijn and E. R. Vrscay, *Spin-dependent Bohm trajectories for hydrogen eigenstates*, Phys. Lett. A, **300**, 334 (2002).

[82] P. R. Holland and C. Philippidis, *Implications of Lorentz covariance for the guidance equation in two-slit quantum interference*, Phys. Rev. A, **67**, 062105 (2003).

[83] K. Jacobs and D. Steck, *A straightforward introduction to continous quantum measurement*, Contemporary Physics, **47**(5), 279 (2006).

[84] M. Genovese, *Research on hidden variable theories: A review of recent progresses*, Physics Reports - Review Section of Physics Letters, **413**, 319 (2005).

[85] J. S. Bell, *Against measurement*, Physics World, **3**, 33 (1990).

[86] M. Daumer, D. Dürr, S. Goldstein, et al., *Naive realism about operators*, Probability, Dynamics and causality, **45**,(2-3), 379 (1997).

[87] D. Dürr; S. Goldstein and N. Zanghí, *Quantum Equilibrium and the Role of Operators as Observables in Quantum Theory*, Journal of Statistical Physics, **116**, 9595 (2004).

[88] X.Oriols, *Non-universal conductance quantization for long quantum wires: the role of the exchange interaction: the role of the exchange interaction*, Nanotechnology, **15**, S167–S175 (2004).

[89] A. Alarcón, X. Cartoixa, and X. Oriols, *Towards the explicit computation of bohm velocities associated to n-electron wavefunctions with arbitrary spin-orientations*, Physica Status Solidi C, **7**, 11-12 (2010).

[90] G. Albareda, H. Lopez, X. Cartoixa, J. J. Suñé, X. Oriols, *Time-dependent boundary conditions with lead-sample Coulomb correlations:Application to classical and quantum nanoscale electron device simulators*, Phys. Rev. B, **82**, 085301 (2010).

[91] X. Oriols, E. Fernandez-Diaz, A. Alvarez, A. Alarcón, *An electron injection model for time-dependent simulators of nanascale devices with electron confinement: Application to the comparison of the intrinsic noise of 3D-, 2D, and 1D-ballistic transistors*, Solid State Electronics, **51**, 306-319 (2007).

[92] X.Oriols, A.Alarcón, and E.Fernández-Díaz, *Time dependent quantum current for independent electrons driven under non-periodic conditions*, Phys. Rev. B, **71**, 245322–1–245322–14 (2005).

[93] A.Benali, F.L.Traversa, G.Albareda, A.Alarcóon, M.Aghoutane and X.Oriols, *Ramo-Shockley-Pellegrini theorems with quantum trajectories for the self-consistent computation of time-dependent current*, Physical Review B, (Submitted).

[94] A. Van der Ziel, *Noise in Solid State Device and Circuits*, Wiley, New York (1986).

[95] L. S. Levitov and G. B. Lesovik, JETP Lett., **58**, 230 (1993).

[96] L. S. Levitov, H. W. Lee, and G. B. Lesovik, J. Math. Phys., **37**, 4845 (1996).

[97] Y. M. Blanter and M. Büttiker, *Shot noise in mesoscopic conductors*, Physics Reports, **336**(1), 1–166 (2000).

[98] W. Schottky, *Über spontane stromschwankungen in verschiedenen elektrizitätsleitern*, Ann. Phys., **57**(541) (1918).

[99] L. Esaki, R. Tsu, *Superlattice and negative differential conductivity in semiconductors*, IBM J. Res. Dev., **14**, 61 (1970).

[100] R. Tsu, L. Esaki, *Tunneling in a finite superlattice*, Appl. Phys. Lett., **22**, 562–564 (1973).

[101] L. L. Chang, R. Tsu, L. Esaki, *Resonant tunneling in semiconductor double barriers*, Appl. Phys. Lett., **24**, 593–595 (1974).

[102] J. P. Sun, G. I. Haddad, P. Mazumder, J. N. Schulman, *Resonant tunneling diodes: Models and properties*, Proceedings of the IEEE, **86**, 641–661 (1998).

[103] J. B. Ferry, S. M. Goodnick, *Transport in nanostructures*, Cambridge University Press, (2009), second edition.

[104] M. Büttiker, *Coherent and sequential tunneling in series barriers*, IBM J. Res. Dev., **32**, 63–75 (1998).

[105] H. Mizuta, T. Tanoue, *The physics and applications of resonant tunnelling diodes*, Cambridge Studies in Semiconductor Physics and Microelectronic Engineering. (1995).

[106] H. J. De Los Santos, K. K. Chui, D. H. Chow, H. L. Dunlap, *An efficient HBT/RTD oscillator for wireless applications*, IEEE Microwave And Wireless Components Letters, **11**, 193–195 (2001).

[107] P. Mazumder, S. Kulkarni, M. Bhattacharya, J. P. Sun, G. I. Haddad, *Digital circuit applications of resonant tunneling devices*, Proceedings of the IEEE, **86**,664–686 (1998).

[108] M. V. Fischetti, *Theory of electron transport in small semiconductor devices using the pauli master equation*, J. Appl. Phys., **83**(270) (1998).

[109] W. R. Frensley, *Wigner-function model of a resonant-tunneling semiconductor device*, Phys. Rev. B, **36**(3), 1570–1580 (1987).

[110] R. C. Bowen, G. Klimeck, R. K. Lake, W. R. Frensley, T. Moise, *Quantitative simulation of a resonant tunneling diode*, J. Appl. Phys, **81**(7),3207–3214 (1997).

[111] E. R. Brown and C. D. Parker, *Resonant tunnel diodes as submillimetre-wave sources*, Philosophical Transactions: Mathematical, Physical and Engineering Sciences, **354** (1717), 2365–2381 (1996).

[112] R. Lake and S. Datta, *Nonequilibrium green's-function method applied to double-barrier resonant-tunneling diodes*, Phys. Rev. B, **45**, 6670–6685 (1991).

[113] Y. M. Blanter, M. Büttiker, *Transition from sub-poissonian to super-poissonian shot noise in resonant quantum wells*, Phys. Rev. B, **59**(15),10217–10226 (1999).

[114] G. Iannaccone, G. Lombardi, M. Macucci, and B. Pellegrini, *Enhanced shot noise in resonant tunneling: Theory and experiment*, Physical Review Letters, **80**(5), 1054–1057 (1998).

[115] G. Breit, E. Wigner, *Capture of slow neutrons*, Physical Review, **49**(519) (1936).

[116] G. Iannaccone, M. Macucci, and B. Pellegrini, *Shot noise in resonant-tunneling structures*, Physical Review B, **55**(7), 4539–4550 (1997).

[117] L. D. Landau, L. M. Lifshitz, *Quantum Mechanics Non-Relativistic Theory*, Butterworth-Heinemann (1977), third edition.

[118] M. Büttiker, *Role of quantum coherence in series resistors*, Phys. Rev. B., **33**(5), 3020–3026 (1986).

[119] K. Blanks, G. Klimeck, R. Lake, R. C. Bowen, M. Leng, C. Fernando, W. R. Frensley, D. Jovanovic, *Nemo quantum device simulator*, Government microcircuit applications conference digest of papers (gomac), 218 (1998).

[120] L. Shifren, C. Ringhofer, D. K. Ferry, *A wigner function-based quantum ensemble monte carlo study of a resonant tunneling diode*, IEEE Trans. on Electron Devices, **50** (3), 769–773 (2003).

[121] International Electron Device Meeting (IDEM) in Washington DC, 2001; 2003; 2005

[122] W.Hafez and M.Feng, *Experimental demonstration of pseudomorphic heterojunction bipolar transistor with cutoff frequencies above 600 GHz* Appl. Phys. Lett., **86**, 152101 (2005).

[123] K.T. Tsen, J.G. Kiang, D.K. Ferry, H. Morkoc, *Subpicosecond timeresolved Raman studies of field-induced transient transport in an InxGa1-xAs-based pin semiconductor nanostructure*, Appl. Phys. Lett., **89**, 26, 262101 (2006).

[124] F. Grossmann, T. Dittrich , P.Jung ,P. Hanggi, *Coherent destruction of tunneling*, Phys. Rev. Lett., **67**, 4, 5169 (1991).

[125] Platero G, Aguado R, *Photon-assisted transport in semiconductor nanostructures*, Phys Rep Rev Sect Phys Lett, 395(12),1157 (2004).

[126] M. Moskalets, M. Buttiker, *Floquet scattering theory of quantum pumps* Phys. Rev. B, **66**, 20, 205320 (2002).

[127] S. Camalet, J. Lehmann, S. Kohler, P. Hanggi, *Current noise in acdriven nanoscale conductors*, Phys. Rev. Lett., **90**, 21,210602 (2003).

[128] J. Lehmann, S. Camalet, S. Kohler, P. Hanggi, *Laser controlled molecular switches and transistors*, Chem. Phys. Lett., **368**, 34, 2828 (2003).

[129] R. Landauer, *Conductance from transmission common-sense points*, Phys. Scripta, T42:1104 (1992).

[130] M. Grifoni, P. Hanggi, *Driven quantum tunneling*, Phys. Rep. Rev. Sect. Phys. Lett., **304**, 56, 229354 (1998).

[131] KJ Chen, M Yamamoto, *Frequency multipliers using InP-based resonant-tunneling high electron mobility transistors*, IEEE Electron Dev. Lett., **17**, 5, 2358 (1996).

[132] TCLG Sollner, ER Brown, WD Goodhue, CA Correa, *Harmonic multiplication using resonant tunneling* J. Appl. Phys., **64**, 8, 424850 (1988).

[133] X. Oriols, A. Alarcón, L. Baella, *Dynamically modulated tunneling for multipurpose electron devices: Application to THZ frequency multiplication* , Solid State Electronics, **51**, 1287-1300 (2007).

[134] X. Oriols, A. Alarcon, E. Fernandez-Diaz, *Time-dependent quantum current for independent electrons driven under nonperiodic conditions*, Phys. Rev. B, **71**, (24):245322 (2005).

[135] Hussein YA, El-Ghazaly SM, Goodnick SM, *An efficient electromagnetic-physics-based numerical technique for modeling and optimization of high-frequency multifinger transistors*, IEEE Trans. Microw. Theor. Tech., **51**, 12, 233446 (2003)

[136] M. Buttiker, R. Landauer, *Traversal time for tunneling*, Phys Scripta, **32**, 4, 42934 (1985).

[137] M. Buttiker, R. Landauer, *Traversal time for tunneling* Phys Rev Lett, **49**, 23, 173942, (1982).

[138] N. W. Ashcroft, N. D. Mermin, *Solid state physics*, South Melbourne, Brooks/Cole Thomson Learning (2002).

Appendix A

Tight-binding model

Tight-binding model is based on to assume that at each lattice point of a crystalline structure the total Hamiltonian of the system can be approximated by a Hamiltonian that depends of the location of each atom. Each of these *atomic* points are described by an atomic orbital (wavefunction) [138]. In this appendix we develop a numerical approximation to solve the following Schrödinger equation:

$$\imath\hbar\frac{\partial}{\partial t}|\Psi_g(t)\rangle = H|\Psi_g(t)\rangle, \tag{A.1}$$

where the wavefunction solution of Schrödinger equation can be written as:

$$|\Psi_g(t)\rangle = \sum_j C_g(j,t)|j\rangle, \tag{A.2}$$

and where C_g are coefficients and $|j\rangle$ is the orthonormal (discrete) basis that represents each molecular orbital being j the index that determines the position of the orbital.

The Hamiltonian, $H = H_0$ of Eq. (A.1), is the tight-binding Hamiltonian without Coulomb interaction under a simple first-neighbors:

$$H_0 = \sum_i [|i\rangle\varepsilon_i\langle i| + u(|i\rangle\langle i+1| + |i\rangle\langle i-1|)], \tag{A.3}$$

where ε_i is the on-site energy and u the hopping energy.

A.1 Orthogonal orbitals

In this subsection, we solve Eq. (A.1) describing the Hamiltonian of crystalline structure *without* Coulomb interaction.

A.1.1 Development of tight-binding Hamiltonian without Coulomb interaction

We use Eqs. (A.3) and (A.2) to develop the right hand of Eq. (A.1):

$$H_0|\Psi_g(t)\rangle = H_0 \sum_j C_g(j,t)|j\rangle = \sum_i [|i\rangle \varepsilon_i \langle i| \sum_j C_g(j,t)|j\rangle + u(|i\rangle\langle i+1| \sum_j C_g(j,t)|j\rangle + |i\rangle\langle i-1| \sum_j C_g(j,t)|j\rangle)]. \quad (A.4)$$

Now, we multiply the last equation by $\langle i|$:

$$\langle i|H_0|\Psi_g(t)\rangle = \sum_i [\langle i|i\rangle \varepsilon_i \langle i| \sum_j C_g(j,t)|j\rangle + u(\langle i|i\rangle\langle i+1| \sum_j C_g(j,t)|j\rangle + \langle i|i\rangle\langle i-1| \sum_j C_g(j,t)|j\rangle)], \quad (A.5)$$

In Eq. (A.5), only when $i = j$ the scalar products will have as result equal a 1 (when $i = j$, $i + 1 = j$ and $i - 1 = j$). Therefore, we eliminate the summations of j:

$$\langle i|H_0|\Psi_g(t)\rangle = \varepsilon_i C_g(j,t) + uC_g(j+1,t) + uC_g(j-1,t) \quad (A.6)$$

Now, we develop the partial derivative of left hand of Eq. (A.1). Here, we use Eq. (A.2) and the definition of first derivative to obtain:

$$\imath\hbar|\Psi_g(t)\rangle = \imath\hbar \frac{\partial}{\partial t} \sum_j C_g(j,t)|j\rangle = \imath\hbar \frac{\sum_j C_g(j,t+\triangle t)|j\rangle - \sum_j C_g(j,t-\triangle t)|j\rangle}{2\triangle t}. \quad (A.7)$$

As in the previous subsection we multiply both sides by $\langle i|$. Therefore, only $i = j$ will have the scalar products equal to 1:

$$\langle i|\frac{\partial}{\partial t}|\Psi_g(t)\rangle = \imath\hbar \frac{C_g(i,t+\triangle t) - C_g(i,t-\triangle t)}{2\triangle t}. \quad (A.8)$$

Using Eq. (A.6) and Eq. (A.8) we obtain the definitive expression of Schrödinger equation:

$$\imath\hbar\langle i|\frac{\partial}{\partial t}|\Psi_g(t)\rangle = \langle i|H|\Psi_g(t)\rangle = \frac{\imath\hbar}{2\triangle t}[C_g(i,t+\triangle t) - C_g(i,t-\triangle t)] = \varepsilon_i C_g(i,t) + uC_g(i+1,t) + uC_g(i-1,t). \quad (A.9)$$

Finally the time evolution of the system without Coulomb interaction among electrons are done by:

$$C_g(i,t+\triangle t) = C_g(i,t-\triangle t) + \frac{2\triangle t}{\imath\hbar}(\varepsilon_i C_g(i,t) + uC_g(i+1,t) + uC_g(i-1,t)). \tag{A.10}$$

Calculation of $C_g(i,t)$

In the basis $|i\rangle$ the ket $|\Psi_g(t)\rangle$ must to be represented by a set of coefficients:

$$C_g(i,t) = \langle i|\Psi_g(x_1,t)\rangle = \langle i|\sum_j C_g(j,t)|j\rangle. \tag{A.11}$$

From previous equation we obtain the expression:

$$C_g(i,t) = \int_{-\infty}^{\infty}\langle i|x_1\rangle\langle x_1|\Psi_g(x_1,t)\rangle dx_1 = \int_{-\infty}^{\infty}\Phi_i^*(x_1)\Psi_g(x_1,t)dx_1, \tag{A.12}$$

where we have used $1 = \int_{-\infty}^{\infty}|x_1\rangle\langle x_1|dx_1$.

The function Φ_i is the spatial wavefunction of the i-orbital. We need the terms $C_g(i,t)$ to find the wavepackets to be able to compute the Bohmian velocity.

A.1.2 Development of tight-binding Hamiltonian with Coulomb interaction

When the Coulomb interaction is present we have to solve the next Schrödinger equation:

$$\imath\hbar\frac{\partial}{\partial t}|\Psi_g(t)\rangle = \{H_0 + U_c\}|\Psi_g(t)\rangle, \tag{A.13}$$

where, for example, $U_c = U(x,x_2[t]) = \frac{1}{4\pi\varepsilon_0}\frac{1}{x-x_2[t]}$ and H_0 is the tight-binding Hamiltonian of Eq. (A.3). Here, we study only the part of equation corresponding to Coulomb interaction.

As we have made in the last subsection we multiply by $\langle i|$ and also we use:

$$1 = \int_{-\infty}^{\infty}|x\rangle\langle x|dx\int_{-\infty}^{\infty}|x'\rangle\langle x'|dx'. \tag{A.14}$$

Therefore:

$$\langle i|U(x,x_2[t])|\Psi_g(t)\rangle = \tag{A.15}$$

$$= \int dx\int dx'\langle i|x\rangle\langle x|U(x,x_2[t])|x'\rangle\langle x'|\Psi_g(t)\rangle$$

$$= \int dx\int dx'\langle i|x\rangle\frac{1}{4\pi\varepsilon_0}\frac{1}{x-x_2[t]}\langle x|x'\rangle\langle x'|\Psi_g(t)\rangle. \tag{A.16}$$

Now we apply the next property of Dirac's delta:

$$\int_{\infty}^{\infty} dx' f(x)\delta(x-x') = f(x') \tag{A.17}$$

$$\begin{aligned} &\int dx' \langle i|x'\rangle \frac{1}{4\pi\varepsilon_0}\frac{1}{x-x_2[t]}\langle x'|\Psi_g(t)\rangle \\ &= \int dx' \phi_i^*(x')\frac{1}{4\pi\varepsilon_0}\frac{1}{x-x_2[t]}\sum_j C_g(j,t)\phi_j(x') = \\ &= \sum_j C_g(j,t)[\int dx' \phi_i^*(x')\frac{1}{4\pi\varepsilon_0}\frac{1}{x-x_2[t]}\phi_j(x')], \end{aligned} \tag{A.18}$$

where we use $\langle x'|\Psi_g(t)\rangle = \langle x'|\sum_j C_g(j,t)|j\rangle$.

The final expression for time evolution of the system with Coulomb interaction is:

$$\begin{aligned} C_g(i,t+\triangle t) = C_g(i,t-\triangle t) + \frac{2\triangle t}{\imath\hbar}(\varepsilon_i C_g(i,t) \\ +uC_g(i+1,t) + uC_g(i-1,t) \\ +\sum_j C_g(j,t)[\int dx' \phi_i^*(x')\frac{1}{4\pi\varepsilon_0}\frac{1}{x-x_2[t]}\phi_j(x')]). \end{aligned} \tag{A.19}$$

A.2 Non-Orthogonal orbitals

Now we calculate the evolution equation taken into account that the orbitals are non-orthogonal and without Coulomb interaction.

The tight-binding Hamiltonian is done by the equation Eq. (A.3) and the dynamic of the system by the Schrödinger equation of Eq. (A.1). The wavefunction solution of Schrödinger equation is a Gaussian function, $|\Psi_g(t)\rangle = \sum_j C_g(j,t)|j\rangle$, where C_g are the coefficients and $|j\rangle$ is the orthonormal (discrete) basis que represents each molecular orbital. Finally we define, $\langle i|j\rangle = S_{i,j}$.

We use Eqs. (A.3) and (A.2) in the right hand of Schrödinger equation:

$$\begin{aligned} H|\Psi_g(t)\rangle = H\sum_j C_g(j,t)|j\rangle = \sum_i [|i\rangle\varepsilon_i\langle i|\sum_j C_g(j,t)|j\rangle \\ +u(|i\rangle\langle i+1|\sum_j C_g(j,t)|j\rangle \\ +|i\rangle\langle i-1|\sum_j C_g(j,t)|j\rangle)]. \end{aligned} \tag{A.20}$$

Now, we multiply the last equation by $\langle l|$:

$$\langle l|H|\Psi_g(t)\rangle = \sum_i [\langle l|i\rangle \varepsilon_i \langle i| \sum_j C_g(j,t)|j\rangle + u(\langle l|i\rangle\langle i+1| \sum_j C_g(j,t)|j\rangle + \langle l|i\rangle\langle i-1| \sum_j C_g(j,t)|j\rangle)] = \tag{A.21}$$

$$= \sum_i \langle l|i\rangle [\varepsilon_i \langle i|j\rangle \sum_j C_g(j,t) + u(\langle i+1|j\rangle \sum_j C_g(j,t) + \langle i-1|j\rangle \sum_j C_g(j,t))] \tag{A.22}$$

$$= \sum_i S_{l,i} [\varepsilon_i S_{i,j} \sum_j C_g(j,t) + u(S_{i+1,j} \sum_j C_g(j,t) + S_{i-1,j} \sum_j C_g(j,t))]. \tag{A.23}$$

$$\langle l|H|\Psi_g(t)\rangle = \sum_i S_{l,i} \sum_j C_g(j,t)[\varepsilon_i S_{i,j} + u(S_{i+1,j} + S_{i-1,j})].$$

Now, we develop the partial derivative of left hand of Eq. (A.1). If we use Eq. (A.2) and the definition of first derivative we obtain:

$$\imath\hbar|\Psi_g(t)\rangle = \imath\hbar \frac{\partial}{\partial t} \sum_j C_g(j,t)|j\rangle = \imath\hbar \sum_j \frac{C_g(j,t+\triangle t) - C_g(j,t-\triangle t)}{2\triangle t}|j\rangle. \tag{A.24}$$

Now we multiply the last equation by $\langle l|$:

$$= \imath\hbar \sum_j \frac{C_g(j,t+\triangle t) - C_g(j,t-\triangle t)}{2\triangle t}\langle l|j\rangle. \tag{A.25}$$

$$\langle l|\frac{\partial}{\partial t}|\Psi_g(t)\rangle = \imath\hbar \sum_j \frac{C_g(j,t+\triangle t) - C_g(j,t-\triangle t)}{2\triangle t} S_{l,j}. \tag{A.26}$$

The final expression for the time evolution of the system is:

$$\imath\hbar \sum_j \frac{C_g(j,t+\triangle t) - C_g(j,t-\triangle t)}{2\triangle t} S_{l,j} = \sum_i S_{l,i} \sum_j C_g(j,t)[\varepsilon_i S_{i,j} + u(S_{i+1,j} + S_{i-1,j})]. \tag{A.27}$$

$$\sum_j C_g(j,t+\triangle t) = \sum_j C_g(j,t-\triangle t) +$$
$$\frac{2\triangle t}{\imath\hbar} S^{-1}_{l,j} \sum_i S_{l,i} \sum_j C_g(j,t)[\varepsilon_i S_{i,j} + u(S_{i+1,j} + S_{i-1,j})]. \tag{A.28}$$

Calculation of $C_g(i,t)$

If the orbitals are non-orthogonals, then we have to define the terms:

$$D_g(i,t) = \int_{-\infty}^{\infty} \langle i|x_1\rangle\langle x_1|\Psi_g(x_1,t)\rangle dx_1 = \int_{-\infty}^{\infty} \Phi_i^*(x_1)\Psi_g(x_1,t)dx_1, \tag{A.29}$$

where $\langle i|\Psi_g(x_1,t)\rangle = \langle i|\sum_j C_g(j,t)|j\rangle$ and $\Psi_g(x_1,t) = \sum_j C_g(j,t)\phi_j(x_i)$.
So, we obtain the expression:

$$D_g(i,t) = \int_{-\infty}^{\infty} \Phi_i^*(x_1)[\sum_j C_g(j,t)\Phi_j(x_1)]dx_1, \tag{A.30}$$

where $\sum_j C_g(j,t)$ is not dependant of x_1, then:

$$D_g(i,t) = \sum_j C_g(j,t) \underbrace{\int_{-\infty}^{\infty} \Phi_i^*(x_1)\Phi_j(x_1)dx_1}_{S_{i,j}}. \tag{A.31}$$

Notice that, $D_g(i,t) = C_g(i,t)$, for orthogonals orbitals. However, this identity is not true for non-orthogonals orbitals. Finally:

$$D_g(i,t) = \sum_j C_g(j,t)S_{i,j}. \tag{A.32}$$

We can write the last expression as matrix:

$$\begin{pmatrix} D_g(1,t) \\ \vdots \\ D_g(N,t) \end{pmatrix} = \begin{pmatrix} s_{11} & s_{12} & \cdots & s_{1N} \\ s_{21} & s_{22} & \cdots & s_{2N} \\ \vdots & \cdots & \cdots & \vdots \\ s_{N1} & \cdots & \cdots & s_{NN} \end{pmatrix} \begin{pmatrix} C_g(1,t) \\ \vdots \\ C_g(N,t) \end{pmatrix} \tag{A.33}$$

And finally $C_g(j,t)$ is:

$$\begin{pmatrix} C_g(1,t) \\ \vdots \\ C_g(N,t) \end{pmatrix} = \begin{pmatrix} s_{11} & s_{12} & \cdots & s_{1N} \\ s_{21} & s_{22} & \cdots & s_{2N} \\ \vdots & \cdots & \cdots & \vdots \\ s_{N1} & \cdots & \cdots & s_{NN} \end{pmatrix}^{-1} \begin{pmatrix} D_g(1,t) \\ \vdots \\ D_g(N,t) \end{pmatrix} \tag{A.34}$$

Appendix B

List of publications, congress and conferences

B.1 Chapters in books

A.Alarcón, G.Albareda , F.L.Traversa and X.Oriols *Nanoelectronics: Quantum electron transport* in *"Applied Bohmian Mechanics: From Nanoscale Systems to Cosmology"* Editors: X. Oriols and J. Mompart, Panstanford Publishing. **ISBN:** 978-981-4316-39-2

B.2 Articles

1. F. L. Traversa, E. Buccafurri, A. Alarcón, G. Albareda, R. Clerc, F. Calmon, A. Poncet , X. Oriols,
   Time dependent many-particle simulation for Resonant Tunneling Diodes: interpretation of an analytical small signal equivalent circuit,
   Transaction on electron devices (submitted) (2011).

2. A.Benali, F.Traversa, G.Albareda, A.Alarcón, M.Aghoutane and X.Oriols,
   Bohmian formulation of time-dependent quantum currents via Ramo-Shockley-Pellegrini theorems,
   New Journal of Applied Physics (submitted) (2011).

3. G. Albareda, A. A.Alarcón and X. Oriols,
   Electric power in nanoscale devices with full Coulomb interaction,
   Int. J. Numer. Model, DOI: 10.1002/jnm.74 (2010).

4. A. Alarcón, X.Cartoixà and X.Oriols,
   Towards the explicit computation of Bohm velocities associated to N-electron wavefunctions with arbitrary spin-orientations,
   Phys. status solidi, **7**, No 11-12, 2636-2639 (2010).

5. A.Alarcón and X.Oriols,
   Computation of quantum electron transport with local current conservation using quan-

tum trajectories,
Journal of Statistical Mechanics: Theory and Experiment, **(P01051)** (2009).

6. X. Oriols, F. Boano, and A. Alarcón,
Self-consistent coupling between driven electron tunneling and electromagnetic propagation at terahertz frequencies,
Applied Physics letters, **92**, No 22 (2008).

7. X. Oriols, A. Alarcón, L. Baella,
Dynamically modulated tunnelling for multipurpose electron devices: Application to THZ frequency multiplication,
Solid-State Electronics, **51**, 1287-1300 (2007).

8. X. Oriols , E. Fernndez- Díaz, A. Álvarez, A. Alarcón,
An electron injection model for time-dependent simulators of nanoscale devices with electron confinement: Application to the comparison of the intrinsic noise of 3D, 2D and 1D ballistic transistors,
Solid-State Electronics, **51**, 306-319 (2007).

9. E.Fernandez-Díaz, A.Alarcón and X.Oriols,
Modeling quantum transport under AC conditions: application to intrinsic high frequency limits for nanoscale double - gate Si mosfets,
IEEE Transaction on Nanotechnology, **4**, No.5 (2007).

10. X.Oriols, A.Alarcón and E.Fernàndez-Díaz,
Time dependent quantum current for independent electrons driven under non-periodic conditions,
Physical Review B, **71** (2005).

11. X. Oriols, A. Alarcón and J. Mateos,
Quantum transport under high - frequency conditions: application to bound state resonant tunnelling transistors,
Semiconductor Science and Technology, **19**, L69-L73 (2005).

B.3 Congress and conferences

1. Authors: G. Albareda, A. Alarcón, F. Traversa, A. Benali, A. Padrò, and X. Oriols.
Title: *BITLLES: a quantum-trajectory simulation tool for electron transport in large electronic structures*.
Contribution: Poster.
Proceedings High performance Computing.
Congress: HPC-NN2011 (High performance Computing).
Date: April 11-14, 2011.
City: Bilbao (Spain).

2. Authors: G. Albareda, A. Alarcón, F. Traversa, A. Benali and X. Oriols.
Title: *A quantum trajectory simulator for DC, AC, and noise with explicit Coulomb*

and exchange correlations among transport electrons.
Contribution: Collaboration in the abstract.
Proceedings NanoSpain.
Congress: NanoSpain 2011, NanoSudoe, (Spain, Portugal and France).
Date: April 11-14, 2011.
City: Bilbao (Spain).

3. Authors: A.Benali, F.Traversa , G.Albareda, A.Alarcón, M.Aghoutane and X.Oriols.
Title: *On the relationship between the intrinsic cut-off frequency and the electron transit time in nanoscale devices.*
Contribution: Poster.
Proceedings of CDE 2011.
Congress: 8 th Conferencia de Dispositivos Electrónicos.
Date: February 8-11, 2011.
City: Palma de Mallorca (Spain).
Best five poster of the CDE 2011 award.

4. Authors: A. Alarcón, A.Benali, A.Padrò, G.Albareda, F.L.Traversa and X.Oriols
Title: *The BITLLES simulator for nanoscale devices.*
Contribution: Poster.
Congress: IWCE 2010.
Date: October 27-29, 2010.
City: Pisa (Italy).

5. Authors: A. Alarcón, G.Albareda, F.L.Traversa and X.Oriols.
Title: *Quantum many-particle computations with Bohmian trajectories: Application to electron transport in nanoelectronic devices.*
Contribution: Collaboration in the abstract.
Congress: CCP6 workshop 2010.
Date: July 12-14, 2010.
City: Bangor University, Wales.

6. Authors: E.Buccafurri, F.L.Traversa, X.Oriols, A.Alarcón, G.Albareda, R.Clerc, F.Calmon and A.Poncet.
Title: *High frequency resonant tunneling behavior: Testing an analytical small signal equivalent circuit with time dependent many-particle quantum simulations.*
Contribution: Collaboration in the abstract.
Congress: NanoSpain2010.
Date: March 23-26, 2010.
City: Malaga (Spain).

7. Authors: A. Alarcón and X. Oriols.
Title: *Explicit computation of Coulomb and exchange interactions for N-electrons in open quantum systems using bohm trajectories.*
Contribution: Poster.
Congress: TNT2009.

Date: September 7-10, 2009.
City: Barcelona (Spain).

8. Authors: A. Alarcón and X. Oriols.
Title: *On the computation of high frequency current in nanoelectronic ballistic devices.*
Contribution: Oral presentation and poster.
Congress: 7 th Spanish Conference on electron devices.
Date: February 11-13, 2009.
City: Santiago de Compostela (Spain).

9. Authors: A. Alarcón and X. Oriols.
Title: *Time-dependent Electron Driven Tunneling Phenomena for multipurpose Terahertz applications: self-consistent computation of conduction and displacement current in mesoscopic systems.*
Contribution: Oral presentation and poster.
Congress: TNT2008.
Date: September 1-5, 2008.
City: Oviedo (Spain).

10. Authors: E. Fernndez - Díaz, A. Alarcón, and X. Oriols.
Title: *Ultimate quantum limit for high-frequency applications of nanoscale double- gate Si MOSFET.*
Contribution: Collaboration in the abstract.
Congress: 2004 IEEE Si Nanoelectronics Workshop.
Date: Jun 13-14, 2004.
City: Hawaii (EEUU).

11. Authors: E. Fernndez - Díaz, A. Alarcón, and X. Oriols.
Title: *Classical and quantum comparison of the high - frequency transconductance of nanoscale field effect transistors.*
Contribution: Collaboration in the abstract.
Congress: TNT2004.
Date: September 13-17, 2004.
City: Segovia (Spain).

12. Authors: A. Alarcón, X. Oriols and J. Mateos.
Title: *Intrinsic Terahertz-Frequency Limit For Resonant Tunnelling Transistors.*
Contribution: Collaboration in the abstract.
Congress: 14h Workshop on Modeling and Simulation of electron Devices.

B.4 Patent

Nanoelectronic transistor.

Developed by: **Eduard Fernandez Diaz, Alfonso Alarcón and Xavier Oriols Pladevall**.

Patent of a new type of nanoelectronic device for applications in the rank of frequencies of the TeraHertzs which we have called **DRIVEN TUNNELING DEVICES (DTD).** The patent was deposited with the number of request 2005011937 with title:

"Device to generate an electrical signal"

B.5 Awards

Special prize in IV Certamen Universitario Arquímedes, which organizes the Spanish Ministry of Education and Science and that, was celebrated at Universidad de Castilla la Mancha between 30 of November and 1 December, 2005.

Awarded by: **IBM España, S.A.**

The title of work was:

"Driven Tunneling Devices (DTD): dispositivos nanoelectrónicos para aplicaciones digitales y analógicas bajo frecuencias de Terahercios".